Design, Fabrication, Processing and Testing of Micro-Electro-Mechanical Chemical Sensors

THESIS

Brian S. Freeman
Captain, USAF, PE

AFIT/GEE/ENG/95D-01

DEPARTMENT OF THE AIR FORCE
AIR UNIVERSITY
AIR FORCE INSTITUTE OF TECHNOLOGY

Wright-Patterson Air Force Base, Ohio

DISCLAIMER NOTICE

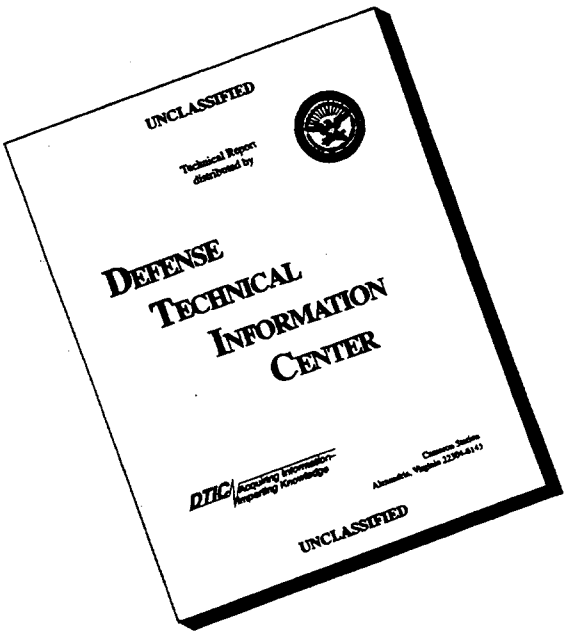

THIS DOCUMENT IS BEST QUALITY AVAILABLE. THE COPY FURNISHED TO DTIC CONTAINED A SIGNIFICANT NUMBER OF PAGES WHICH DO NOT REPRODUCE LEGIBLY.

AFIT/GEE/ENG/95D-01

Design, Fabrication, Processing and Testing of Micro-Electro-Mechanical Chemical Sensors

THESIS

Brian S. Freeman
Captain, USAF, PE

AFIT/GEE/ENG/95D-01

Approved for public release; distribution unlimited

The views expressed in this thesis are those of the author and do not reflect the official policy or position of the Department of Defense or the U. S. Government.

AFIT/GEE/ENG/95D-01

Design, Fabrication, Processing and Testing of Micro-Electro-Mechanical Chemical Sensors

THESIS

Presented to the Faculty of the School of Engineering

of the Air Force Institute of Technology

Air University

In Partial Fulfillment of the

Requirements for the Degree of

Master of Science in Engineering and Environmental Management

Brian S. Freeman, B.S. Electrical Engineering

Captain, USAF, PE

December 1995

Acknowledgements

There are many people to whom I owe a debt of gratitude for their help with this thesis. My wife Lynette and my cats, Emma and Minerva, bore the brunt of my research by spending endless evenings alone while I dallied in labs and on computer terminals. They were always there when I needed a ride in on rainy days, drafts to proof, tummies to be rubbed, and fuzzy mice to be thrown.

Dr Bright and my committee gave me the encouragement and freedom to explore many avenues, always providing advice when I had the common sense to ask.

For real expertise and help, the stalwart was Major John Comtois. His knowledge of MEMS processes, what works, what doesn't, and what might were invaluable when designing the little buggers, while his skill with the wire bonder was simply priceless. Cheers and respect to Lt Rob Reid for showing me the practical lessons of lab work and how to make masks. The other members of the MEMS thesis group also gave me ideas, advice, and support, especially during the long-night-before-submission design sessions. The Bright Boyz, I thank thee.

My research quickly became very lab-intensive and without Bill Tropp and Chris O'Brien helping me with the different processes and equipment, it would have stayed very intensive. They were always there, they were always ready to entertain my crazy ideas and take stuff out of the oven and not give too much of a hard time when I left the nitrogen on overnight or let an etch dry out. Their boss Charlie Powers, set the example; if I needed it, he could get it for me. If more people were like Mr Powers, the world would be much less stressful than it is.

I also want to thank Dr Andrew McGill from the Navy Research Labs for providing me with polymer samples that ended up being so useful, the folks at MOSIS for going all out that crazy day in September getting CMOS 6 out with end of year money.

Thank you all.

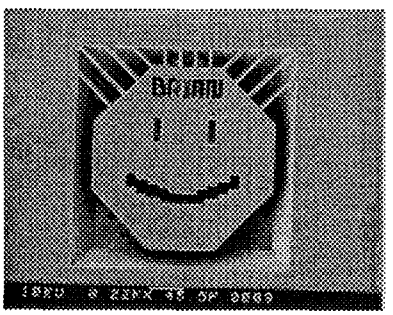

Brian S. Freeman

Table of Contents

List of Figures

List of Tables

Abstract

Chemical microsensors are a new field integrating chemical thin film technology with solid-state fabrication techniques to make devices capable of detecting chemicals in the environment. This thesis evaluated commercially available fabrication processes and numerous sensor designs for working chemical sensors. The commercial processes used were MUMPS for surface micromachined devices and MOSIS for bulk micromachined devices. Overall, eight fabrication runs and 29 different designs were made. Of these designs, two were shown to work effectively. Other designs failed due to fabrication problems and design errors that caused release problems. One design that worked was a surface micromachined chemoresistor with interdigitated gold sensing fingers and a polysilicon heater. The other design was a bulk micromachined suspended bridge structure with bimorphic action drivers at each end.

Thin films were also investigated to determine which would have the most affinity to specific chemicals and therefore provide measurable responses. Once selected, a technique was developed to apply the thin film in such a way as not to damage the devices. Several thin films were identified for application, but only two polymers, poly(isobutylene) and poly(vinyl tetrachloride), were successfully applied and tested.

Because the sensing devices were released micro-electro-mechanical structures, they were extremely susceptible to forces and could be damaged easily. This thesis showed that released MEMS devices could be subjected to a complete photolithographic process including spin-coating, baking, exposure, and development without damage. A hybrid mask process was developed that used photoresist to expose sensing areas for thin film deposition, bond pads for packaging, and a physical mask to cover regions and bond pads during the actual film application. The photoresist acts as a passivation layer and is non-conductive so it can be left on the chip after thin film deposition without interfering with device operation.

Coated devices were tested by exposing them to saturated gas vapor using a nitrogen carrier. Chemicals tested were toluene, trichloroethylene, and 1,1,1-trichloroethane. For the bridge device,

readings were taken at different drive frequencies. For the chemoresistor, readings were made after purges at different applied voltages of the heater. Frequency sweeps of the devices (100 Hz - 4 MHz for the bridge and 10 - 20 MHz for the chemoresistor) provided impedance and phase information that was used to compare device responses after exposure to a chemical and after purging the chemical. Results of the devices showed that distinct features occurred as a function of the polymer, the chemical it was exposed to, and how it was purged (either by increased voltage to the chemoresistor or drive frequency on the bridge). Possible factors influencing the behavior of the chemoresistor are chemical reactions occurring due to applied heat and various diffusion mechanisms that are affected by heat such as electrostatic and physical barriers to desorption. Since heat was not applied to the bridge, all desorption changes accounted for in the response data are most likely due to diffusion mechanisms. These mechanisms were affected by the frequency at which the device was driven, raising the possibility that frequency desorption is occurring.

As a side element to this thesis, a process was developed to make bulk micormachined sensors using available AFIT resources. A three-mask, eight-step fabrication process was developed, simulated and executed to make interdigitated trampoline sensors with boron-doped heaters. The sensors were successfully fabricated and released; however, due to time constraints, they were not fully tested nor was a thin film coating applied. This process opens the way for in-house MEMS fabrication for simple devices instead of relying on commercial processes. This also demonstrated how easily and cheaply a MEMS device could be fabricated.

Design, Fabrication, Processing and Testing of Micro-Electro-Mechanical Chemical Sensors

I. Introduction

In the beginning the Universe was created.
This has made a lot of people very angry and been widely regarded as a bad move.

- *The Restaurant at the End of the Universe*, Douglas Adams

1.1 Background

New environmental legislation requires periodic monitoring of industrial emissions to ensure that allowable pollution levels are not exceeded [1, 2]. Under this legislation, known polluters may be required to obtain permits which specify the types and quantities of pollutants that can be released to the environment. Failure to meet these specified permit levels could result in heavy fines for the polluter as well as damaging health effects to exposed individuals and the environment.

One area of practical concern is storm water outfalls. Unlike waste water collected in a sewage system, most storm water systems discharge directly into streams and other public waters without any form of active treatment. Typically, a storm water outfall will have an oil-water separator prior to the discharge point as shown in Fig. 1. However, oil-water separators are only capable of capturing free-phase petroleum products (or anything else lighter than water) and must be periodically inspected and maintained to ensure operability. Aromatic compounds within petroleum and other solvents will dissolve in the water and be carried past the separation chambers and into the environment.

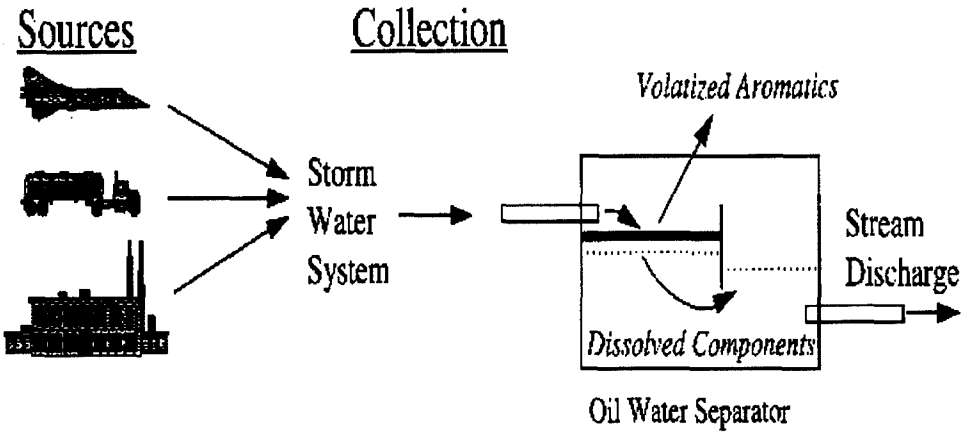

Figure 1. Storm water system.

Storm water systems are particularly at risk of contamination because of the nature of the wide surface areas that drain into them. In addition to accidental releases (spills), storm water systems will carry petroleum residue created by motor vehicles parked on hard surfaces as well as fertilizers and pesticides from landscape run-off. Depending upon the permit requirements of each individual discharge point, laboratory analysis may only be required once a week or once a year [1]. However, the lag time associated with sampling, analyzing, and reporting results may take weeks using conventional lab methods, during which time an unobserved toxic spill could be passed into the environment.

Continuous environmental monitoring of storm water discharges could alert hazardous material response teams to undetected releases and be used to build credibility with regulators that the permit levels are being met. Continuous monitoring could also be used to establish base-line emission data that can in turn justify pollution-prevention investments.

1.1.1 Legislative Requirements. Basic requirements for water testing are set forth in the National Pollution Discharge Elimination System (NPDES), a program that originated in the 1990 Clean Water Act (Title IV, Sec 402). While managed by the individual states, the NPDES establishes permit requirements, testing frequency of discharge points and chemicals to be tested for [1]. The frequency of testing can be annually, monthly, or weekly depending upon the issuing agency, the

permitted facility, and the required laboratory analysis for results. Some tests, such as Biological Oxygen Demand (BOD) and pH, can be performed on-site as part of a regular monitoring program.

Currently available field monitoring equipment that can be placed at outflows and discharge points measures the water's physical properties, such as changes in the water's conductivity or dielectric constant, in order to sense a spill or possible release [3]. These devices are useful in remote oil-water separators in which the lighter petroleum-based products float on the surface, making a pronounced dielectric constant gradient. The devices cannot, however, identify dissolved chemicals in the water that may pose an even greater risk than the readily biodegradable constituents in oils.

1.1.2 Possible Contaminants. A typical petroleum product, such as diesel fuel, is made up of over 200 different (mostly organic) chemicals which can be broken down roughly as 64% aliphatic alkanes (paraffins), 35% aromatics (benzene, toluene, xylene), and 1-2% olefins (styrene). In water, the groups begin to break up, forming individual compounds [4]. The aliphatics and olefins will readily break down as a result of biodegradation. The aromatics contain the most hazardous compounds and include known carcinogens such as benzene, toluene, ethyl-benzene, and xylene (BTEX). These compounds will either volatize into the air or dissolve into the water. Since these four volatile organic compounds are considered to be the most dangerous chemicals in petroleum, they are often the target species of monitoring systems. Other pollutants found in storm water include phospho-organics from pesticides, and nitrogen compounds such as ammonia (NH_3) from fertilizers.

1.2 Silicon Sensors

Because of widespread applications and environmental conditions, Continuous Environmental Monitors (CEMs) must be sensitive to a large range of chemicals and concentration levels, resilient enough to be placed in a field environment, and inexpensive to manufacture and use. Silicon-based microsensors using chemical-selective (chemiphilic) polymer coatings have the potential of meeting these requirements. Using arrays of individually polymer-treated sensor cells and pattern recognition

algorithms [5, 6, 7, 8], sensors no larger than 1 cm^2 could conceivably detect and classify hundreds of chemicals at a fraction of the costs associated with traditional analytic techniques.

This thesis is limited to silicon-based chemical microsensors manufactured through micro-electro-mechanical systems (MEMS) technology. Micro-electro-mechanical systems is a spin-off from integrated circuit technology that exploits the mechanical and semiconducting properties of silicon in conjunction with chemical etchants that selectively etch a MEMS structure out of a silicon substrate. Because the technology used to make MEMS devices is also that used by industry to manufacture integrated circuits, the possibility exists to incorporate full data processing circuitry into the sensor, creating a monolithic package that is very light, inexpensive, and energy-efficient. This area of processing integration, as integral as it is to new sensor design, is beyond the realm of this thesis.

Micromachined devices often incorporate an embedded polysilicon resistor that acts as a heating element. By isolating the device from the substrate, high temperatures (300 - 1000° C) can be obtained within a precise area [5]. Using this heating source, chemicals can be sorbed onto the sensor for measurements and then desorbed by increasing the sensor's temperature. Micro-electro-mechanical systems sensors can therefore be reversible.

By varying the temperature of the sensor, it may be possible to create a thermal spectrum of chemicals that react with a specific polymer coating based on the chemical's heat of reaction (enthalpy) values. The resulting sorption could then be measured as either an electrical operating parameter change or a change in mass for a frequency sensitive device.

Most MEMS microsensor research has focused on pollutants in a gaseous state due to sensor packaging considerations. In a water environment, especially an ion-enriched environment, care must be taken to ensure that a device does not short out.

1.3 Problem Statement

Continuous environmental monitors (CEMs) on storm water outfalls would reduce the chances of undetected toxic releases to the environment while providing regulators with credible proof that permit levels are being met. Continuous environmental monitors must be inexpensive to purchase, resistant to harsh operating conditions, and sensitive to target chemicals and their concentrations. In addition, the sensor must be reversible in order to account for varying environmental conditions. Micro-electro-mechanical systems sensors using chemically sensitive thin film coatings and embedded heaters will be designed, fabricated, analyzed, theoretically and empirically modeled, and evaluated with these goals in mind.

1.4 Research Questions

Specific questions this thesis will explore are:

Device Operations-

Can a MOSIS-fabricated CMOS or MUMPS-fabricated device detect chemicals?

This is the fundamental question of this thesis: whether or not commercially available fabrication processes can produce usable chemical microsensors and if a MEMS approach to chemical sensing is a practical option. From this, other questions arise:

Can enough chemicals be sorbed to create a detectable resonance change?

If a mass loading approach is used, will the weight of sorbed chemicals be sufficient to produce a measurable effect?

Can graduated heating provide a thermal spectrum of chemicals?

What effect, if any, will varying heat have on an operating device other than to purge chemicals at high temperatures? Can a device become chemically selective based on thermal variations?

Will the device be sensitive to different concentrations and mixtures of chemicals?

Will the device be selective among chemicals or individual chemicals at various concentrations? What is the lowest concentration the device will register?

Will the device be reversible?

At the end of a sensing cycle, will the device return to pre-operating conditions or will it be permanently affected by exposure to a chemical?

Can enough chemicals be sorbed to create a detectable current change?

Will sorbed chemicals create enough impedance variation to measure?

Thin Film Selection-

Can a thin film be selected to successfully attract and sorb chemicals?

Of all the thin films to choose from, which detect chemicals when used with specific devices?

Application-

Can masks be made and fitted on released chips without damaging devices, including devices that may be pre-stressed due to fabrication procedures (i.e. curve out of the plane after being released)?

Due to their fragile nature, applying photresist, patterning, developing, and then applying a film may destroy a released device prior to operation. How rugged MEMS devices are to post-processing will be a key concern.

Can thin films be applied without binding actuators or bonding heat sources to the sub-strate?

Even if the devices stand up to the masking processes, can thin films be applied without interfering with the device operation to such an extent that the device is unusable? Such an example may be weighing down a suspended electrostatic structure so that it shorts out with its ground pad.

1.5 Approach

1.5.1 Micromachining. Silicon has excellent mechanical properties and would be an ideal building material for lightweight structures if it were not so brittle. Table 1 shows the differences of properties of silicon to other structural materials such as iron and steel.

Table 1. Comparison of Mechanical Properties of Materials [9].

	Yield Strength $10^9 N/m^2$	Knoop Hardness kg/mm^2	Young's Modulus $10^{11} N/m^2$	Density g/cm^3	Thermal Conductivity W/cm-°C	Thermal Expansion $10^6/°C$
Diamond	53	700	10.35	3.5	20	1
Iron	12.6	400	1.96	7.8	0.803	12
Silicon	7	850	1.9	2.3	1.57	2.33
Stainless Steel	2.1	660	2	7.9	0.329	17.3
Aluminum	.17	130	0.7	2.7	2.36	25

The crystalline nature of silicon is readily exploited by anisotropic water-based etchants such as ethylenediamine-pyrocatechol (EDP) or potassium hydroxide (KOH) that selectively etch in some silicon crystal planes faster than others [10]. Ethylenediamine-pyrocatechol is often used because it does not attack metal pads as readily as KOH and has a higher selectivity of etch rates for different materials (silicon dioxide to silicon is 1:5000 as compared to 1:400 for KOH) [11].

The process of preferential directional etching is shown in Fig. 2. Other etchants such as water-diluted hydrofluoric acid (HF) are isotropic in that they etch at the same rate in all crystal directions.

1.5.1.1 Bulk Micromachining. Bulk micromachining can be combined with the complimentary metal dioxide semiconductor (CMOS) device fabrication process in which devices are formed as a result of deposited or grown layers of various materials on the silicon substrate. Structures can be designed into the fabrication process using standard photoresist/masks methods of layer growth, depositing masks of etch-resistant materials such as silicon nitride (SiN_3) or silicon dioxide (SiO_2),

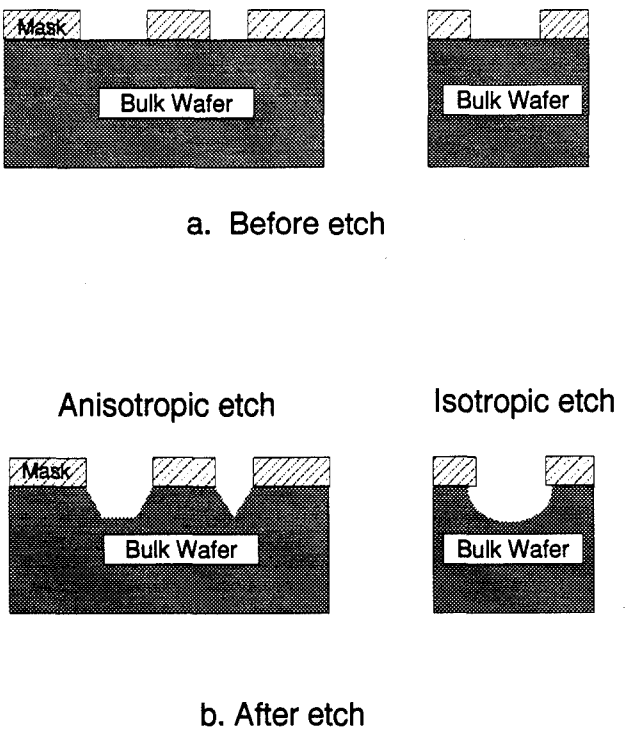

Figure 2. Examples of anisotropic and isotropic etching in wafer substrate. The mask on the wafer surface may be silicon dioxide or a chemical thin film such as photoresist. If the wafers were assumed to be bulk silicon in (100) orientation with a silicon dioxide mask, anisotropic etchants would be EDP or KOH. If the bulk wafer were silicon dioxide and the mask was a photoresist, an isotropic etchant would be hydrofluoric acid buffered with ammonium fluoride.

and heavily doping a region of silicon with boron. The overall effect of the last two processes is a reduction or cessation of the etching rate at the boundaries. Structures that can be formed in bulk micromachining using anisotropic etchants are categorized in Table 2.

Table 2. Bulk Micromachining Etch Results. [10]

Window Opening	Surface Orientation	Structure
Square	(100)	Pyramidal pit
Rectangle	(100)	Rectangular pit
Circle	(100)	Pyramidal pit
Polygon	(100)	Rectangular pit
Square or rectangle	(110)	Hole with vertical side walls

By exploiting the etched structures, devices can be formed by undercutting into the substrate. The extent of undercutting is determined by the time the device spends in the etchant. Care must be taken to ensure that the device does not spend too much time in the etchant; otherwise, the intended structure may be etched away or irrevocably damaged.

1.5.1.2 Surface Micromachining. Similarly to bulk micromachining, surface micromachining also relies on grown or deposited layers to form MEMS devices. However, instead of etching away the substrate, surface micromachining utilizes sacrificial layers (typically phosphosilicate glass (PSG)) to create microstructures. Fig. 3 shows how layers are deposited on the substrate and how an etchant selectively etches only the sacrificial layers, leaving behind a micromechanical structure on the substrate. Also unlike bulk micromachining, surface micromachining was developed specifically for MEMS applications because highly complex, very small devices can be fabricated using it. When the PSG is etched away by an isotropic etchant, conductive layers such as metal contacts and polysilicon are left exposed. As a result, some care must be given to ensure proper packaging of surface micromachined devices prior to immersion in water.

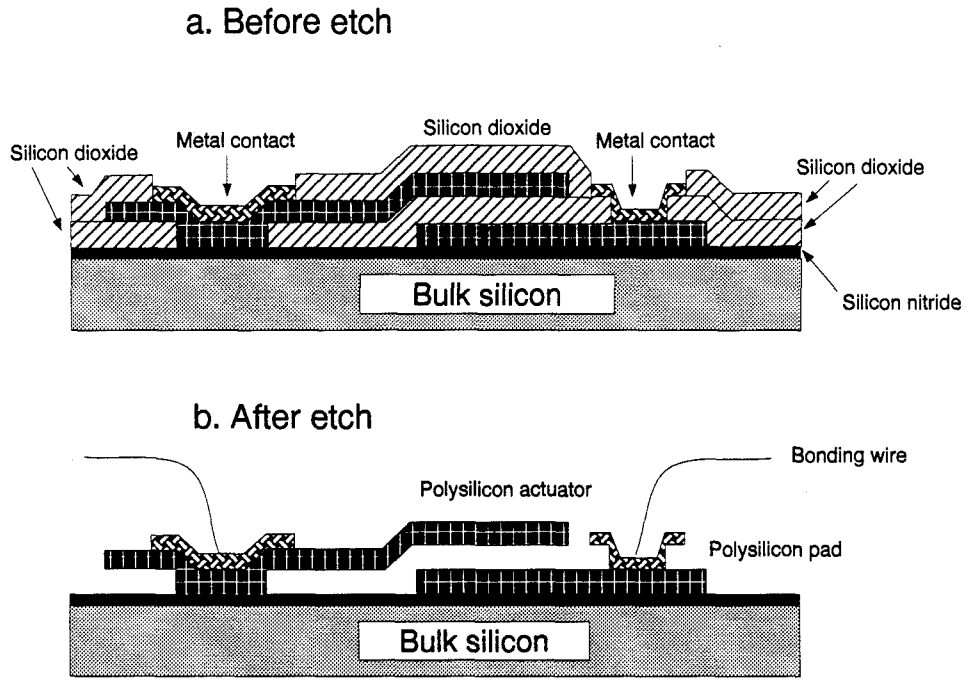

Figure 3. Example release of a surface micromachined actuator. The silicon dioxide sacrifical layers are etched away, leaving the embedded polysilicon and metal surface contacts.

Although not a consideration in this thesis, one element of surface micromachining that should be noted is that at this time, the process is incompatible with monolithic integrated circuit fabrication methods since the PSG is etched away from the chip to release it. These dioxide layers are necessary for electronic devices because they act as insulators between devices and doped regions.

1.5.2 Fabrication Processes. Micromachined devices can be fabricated at the Air Force Institute of Technology (AFIT) by designing the devices using layout Computer Aided Design (CAD) software such as MAGIC [12] and CADENCE [13] available in the Very Large Scale Integration (VLSI) lab, and sending the design file to an external foundry for fabrication. Bulk micromachined devices are manufactured through MOSIS using standard CMOS processes, while surface micromachined devices are manufactured through the Multi-User MEMS Process (MUMPS), an ARPA-financed foundry at MCNC in North Carolina. Descriptions and typical thicknesses of layers for the CMOS and MUMPS

processes are given in Tables 3 and 4 respectively. Epitaxially deposited layers available to the designer for both the CMOS and MUMPS processes are shown in Fig. 4.

Table 3. CMOS layers available through MOSIS [14].

Layer	Fabrication Name	Thickness	Purpose
1	Gate dioxide	10000 Å	Isolate initial polysilicon layer from substrate
2	Polysilicon 1 (P1)	4000 Å	First current-carrying layer
3	P1/P2 dioxide		Isolate P1 and P2 layers
4	Polysilicon 2 (P2)	10000 Å	Second current-carrying layer
5	P2/M1 dioxide	10000 Å	Isolate P1 and M1 layer
6	Metal 1 (M1)	6000 Å	First aluminum conductor layer
7	M1/M2 dioxide	10000 Å	Isolate M1 and M2 layers
8	Metal 2 (M2)	11500 Å	Second aluminum conductor layer
9	Overglass dioxide	6000 Å	Final isolating dioxide layer

Table 4. Working layers available through MUMPS (Thicknesses from MUMPS 6 run).

Layer	Fabrication Name	Thickness	Purpose
1	Silicon nitride	6213 Å	Isolate initial polysilicon layer from substrate
2	Polysilicon 0 (P0)	5200 Å	First current-carrying layer
3	First dioxide	20151 Å	Isolate P0 and P1 layers
4	Polysilicon 1 (P1)	20220 Å	Second current-carrying layer
5	Second dioxide	5230 Å	Isolate P1 and P2 layer
6	Polysilicon 2 (P2)	15650 Å	Third current-carrying layer
7	Metal	5540 Å	Gold conductor layer

In both processes, the designer has no control over the fabrication processes and must therefore adhere to specialized design rules when laying out the device.

Once received from the manufacturer, devices can be chemically etched and tested at the AFIT Cooperative Microelectronic Research Laboratory. In addition to testing and post-processing the devices, this laboratory also has the capability of making bulk-micromachined devices.

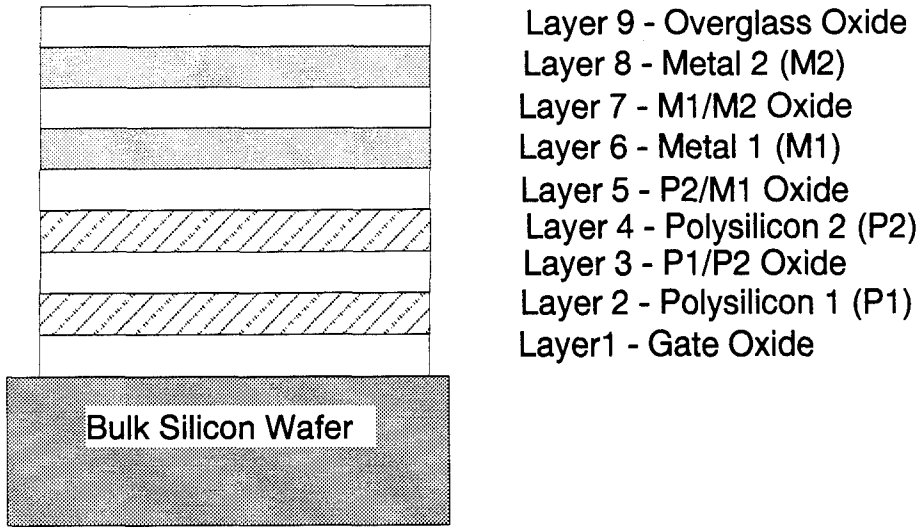

a. Layers in CMOS process

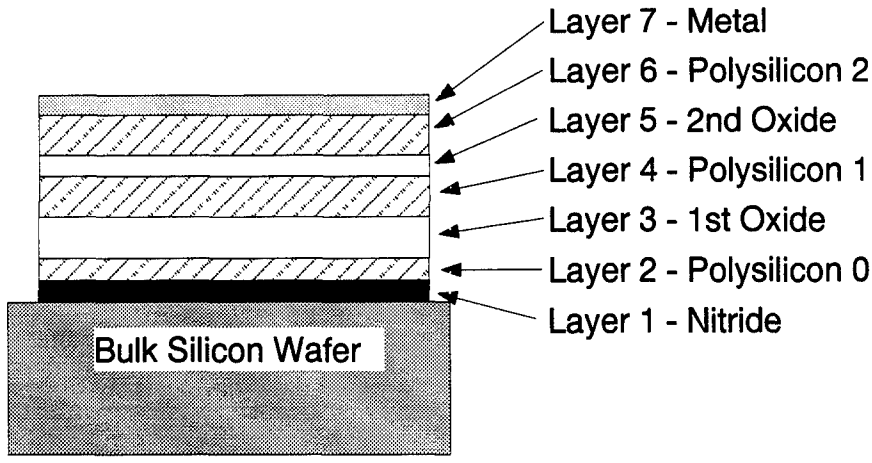

b. Layers in MUMPS process

Figure 4. CMOS and MUMPS process layers.

1.5.3 Sensing Methods. Two classes of sensing are investigated as part of this research: frequency shifting via mass loading on a vibrating surface, and conductivity change caused by impurities in a thin film coating.

1.5.3.1 Thin Film Coatings. Coatings used in this research include tin dioxide (SnO_2) and iron II trioxide (Fe_2O_3), metal phthalocyanines (MPcs where M = copper, lead, and/or magnesium), and the polymers poly(isobutylene) and poly(vinyl tetradecanal). Tin and iron II dioxide were applied via radio frequency sputtering, while the MPcs and the polymers were applied via a regulated air brush.

1.5.3.2 Bimorphic Sensors. This device uses two heaters on a bimorphic bridge actuator. The first heater drives the device by heating up two dissimilar structural materials (aluminum and silicon dioxide). As the materials are heated, they expand at different rates, creating a deflection of the bridge. When the heat is turned off, the device cools, returning to its original shape. By cycling the heater ON and OFF, a mechanical oscillation can be created with ranges from 0 - 300 Hz indefinitely without noticeable fatigue to the device [15].

A second heater is placed along the span of the bridge and coated with a chemically sensitive thin film. This heater is controlled independently from the driver heater and is used to induce heat of reaction transformations based on chemicals under measurement and to purge the device at set time intervals. The heaters are isolated from each other by silicon dioxide.

As chemicals sorb onto the actuator, the effective mass of the actuator changes along with its resonant frequency. By comparing this frequency change to another uncoated device, the concentration of a species of chemical can be detected. The basic design of this sensor is shown in Fig. 5.

This device is fabricated using the bulk micromachining method, creating a layer of silicon dioxide around all current-carrying elements. It is assumed that this field dioxide layer is sufficient to protect the device when exposed to water.

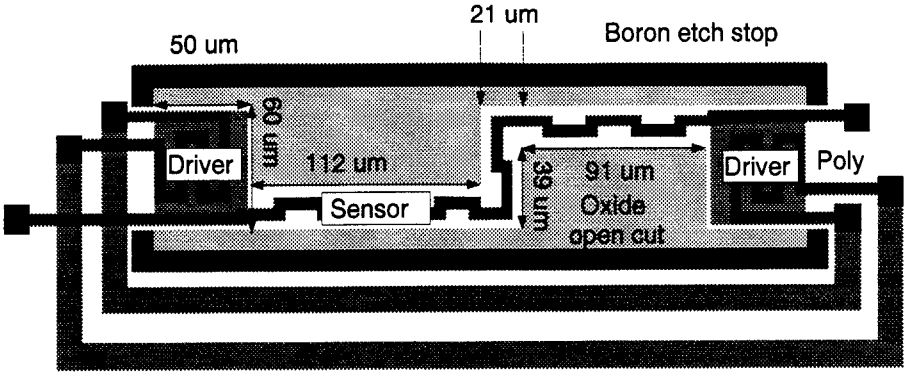

Figure 5. Bimorphic bridge device with embedded heater. Thin film coatings are deposited on the span of the bridge. The white area is the silicon substrate. The dimensions of the device are 440 microns by 140 microns.

1.5.3.3 Electrostatic Sensors. Another approach using frequency shift to measure mass changes is shown in Fig. 6. This device is constructed via the MUMPS process and vibrates through electrostatic force. Charged polysilicon pads are suspended over an immobile polysilicon pad, similar to Howe's resonating bridge structure [16]. With a thin layer of chemophilic coating applied, the vibrating layer should attract chemical species, changing its weight and vibration characteristics. A constant DC bias voltage can also be applied across the suspended element providing resistance heating in order to purge the device after a set time period.

The vibrating layer operates at several kilohertz while the heater operates at DC levels. This difference of operating frequencies should have no impact on either element. The drawback in using this device is that it cannot be immersed directly in water and can only sense gaseous chemicals. However, because it operates at a much higher frequency range than the bimorphic actuator, it is more sensitive to mass changes.

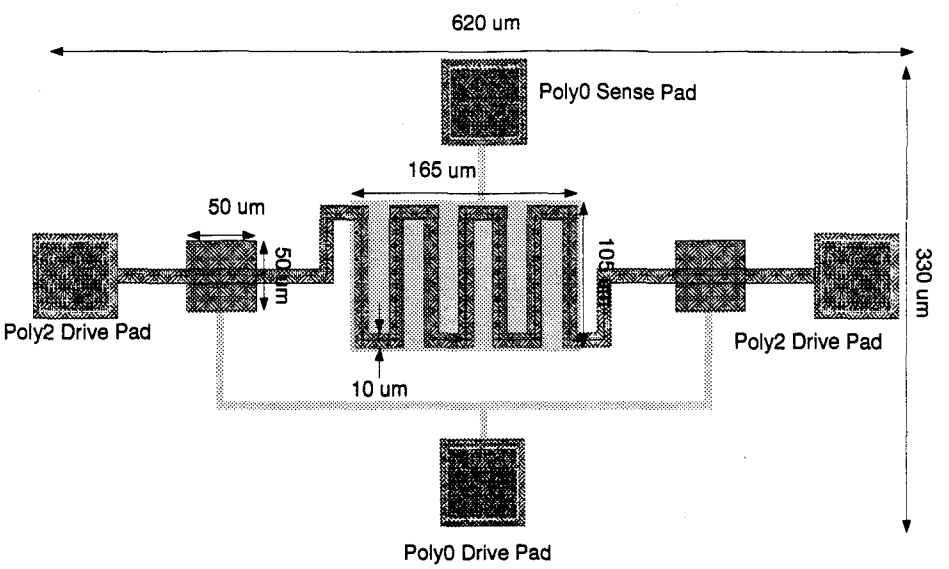

Figure 6. An electrostatic bridge device showing driver pads and sense pad.

1.5.3.4 Hotplate Sensor. Hotplate sensors were originally described by Cavicchi *et al.* in which a suspended trampoline heater heats an aluminum surface coated with tin dioxide [5]. This device was successfully used to detect methanol and ethanol in the atmosphere. A device similar to this was designed using a second polysilicon sensing layer above the first polysilicon heater. A thin film coating will be applied and the conductivity change measured in the secondary polysilicon as chemicals sorb to the surface, affecting the rate at which heat dissipates from the device's surface. The basic device is shown in Fig. 7.

1.5.3.5 Thermal Sensors. This device is similar to a chemoresistor (see Chapter 2), with some modifications. An embedded heater is available to heat the thin film coating, effecting both an intrinsic conductivity change due to the semiconducting material and an extrinsic change due to chemical sorbtion. This feature is shown in Fig. 8.

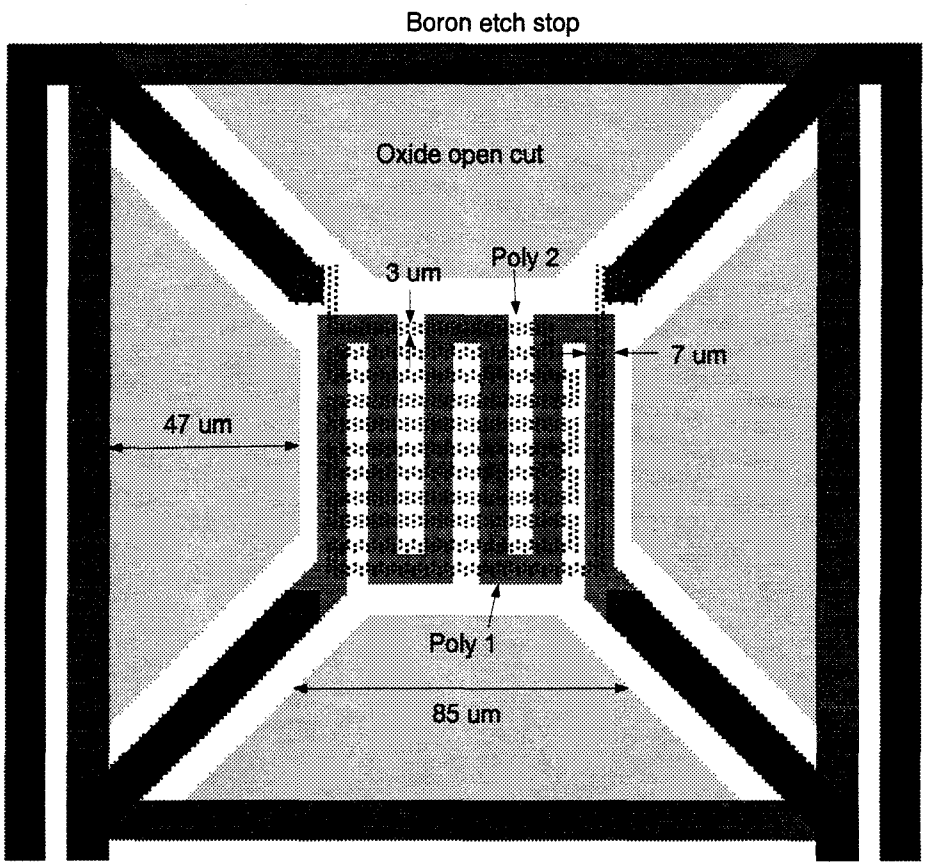

Figure 7. Trampoline-style hotplate device. The dark polysilicon line is the heater while the dotted line is the sensing element.

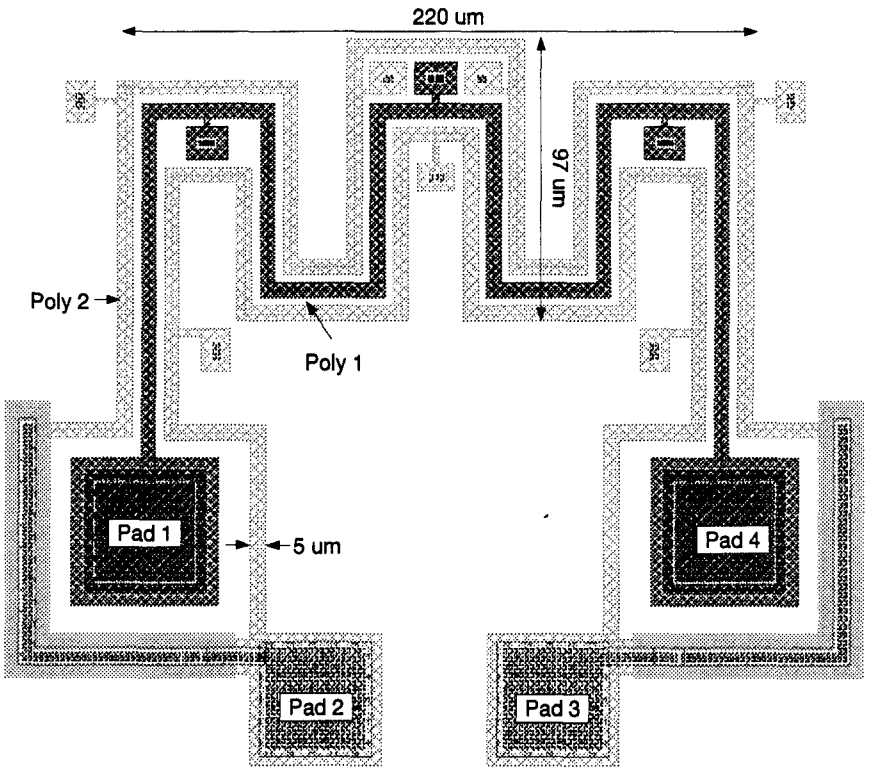

Figure 8. Thermal conductivity device. Outside polysilicon runs have equal length.

1.6 Thesis Overview

In this chapter, an introduction to solid-state sensors was presented along with micromachining techniques, environmental monitoring requirements, sensor designs and overall goals of this thesis. In Chapter 2, a review of current sensing technology is given along with other solid-state sensor research including chemically-sensitive thin films. Chapter 3 provides a discussion of the theory of operation behind the working devices, the surface chemistry involved in coated solid-state sensors, device fabrication, and principles surrounding chemical film selection. Chapter 4 describes the many device designs and fabrication runs made during the course of this research. Chapter 5 describes various thin films used and the various application methods developed. Instrumentation and experimental design are included in Chapter 6. Chapter 7 describes the fabrication process of an in-house AFIT microsensor using bulk-micromachining technology. Results, conclusions and recommendations are provided in Chapter 8.

II. Literature Review

They sought it with thimbles, they sought it with care
They pursued it with forks and hope;
They threatened its life with a railway share;
They charmed it with smiles and soap.

The Hunting of the Snark, Lewis Carroll

2.1 Overview

The use of semiconductor fabrication technology to construct microsensors for chemical analysis is still a relatively new field. Combining the disciplines of Very Large Scale Integration (VLSI) technology with environmental chemistry, chemical microsensors (CMSs) have employed a number of measurement techniques that exploit the physical properties of the analytes they are measuring. Successful devices have used frequency shifts, conductivity changes, and current and voltage gains to measure organics and inorganics in gases and solutions. To accomplish this, CMSs use thin film coatings that are sensitive, or chemiphilic, to particular chemicals or groups of chemicals. This chapter surveys existing devices, construction techniques, and chemiphilic coatings used in previous works.

2.2 Historical Perspective

Dissolved hydrocarbons in surface water are a significant source of water pollution throughout the world. Because of the extensive use of hydrocarbon-based chemicals in industry, transportation, and agriculture, no single source for any one compound can be easily identified. Instead, hydrocarbon contamination occurs predominantly via non-point sources, as when rains wash pesticides off fields

and petroleum products off roads, or as a result of spills. Surface run-off collection systems such as storm-water and drainage systems concentrate non-point source pollution by becoming point sources when they discharge into a larger body of water without prior treatment as shown in Fig. 9.

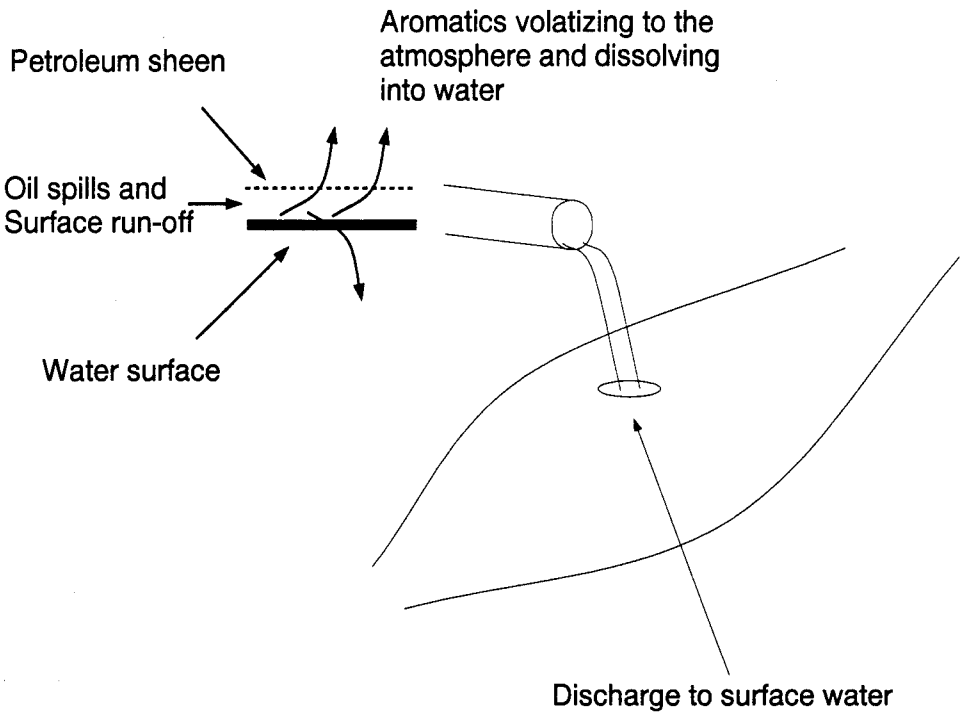

Figure 9. Fate of hydrocarbons in water. Petroleum from spills and surface water run-off form a sheen on the water surface. Aromatic elements in the oils will volatize into the atmosphere, but other components will dissolve into the water and be released to into navigable waterways.

Point sources are subject to regulation under the Clean Water Act (CWA) of 1972 and all its successive amendments, and the NPDES [1]. The basis for permits to discharge into surface water is usually conditional to the concentration of pollution in the discharge water. In order to ensure that compliance to the permitted levels is met, some form of monitoring program must be in place for each point of discharge. Typically, samples are taken from the discharge point and sent to an Environmental Protection Agency (EPA)-certified laboratory for analysis on a regular schedule as indicated on the discharge permit.

The first widely used continuous environmental monitors were strips of rubber that measured ozone (O_3) in Los Angeles during the 1950s [2]. Ozone was known to attack rubber and by watching the rubber deteriorate, concentrations of ozone could be quantified. As sensing technology developed, more accurate methods were established to identify and quantify individual chemicals and their concentrations using gas chromatography and mass spectrometry. These systems require careful collection of samples and analysis under laboratory conditions, since the measuring equipment is large and expensive. In this section of the thesis, various detection techniques currently used by laboratories are discussed. While not continuous environmental monitors, these methods are the most reliable measurement techniques currently available.

2.2.1 Gas Chromatography. Gas chromatography (GC) analyzes the captured product by heating the trap and backflushing with an inert gas to a gas chromatographic column. In the column, the compounds in the analyzed gas are separated through thermal drift until they reach a detector. Lichtenthaler reported that up to 30 different compounds were identifiable in the parts per trillion (ppt) range using this method [17]. For most organic analyses, a flame ionization detector (FID) is used [18]. The FID works by injecting the organic compounds into a hydrogen burning flame, forming electrically charged intermediates as shown in Fig. 10.

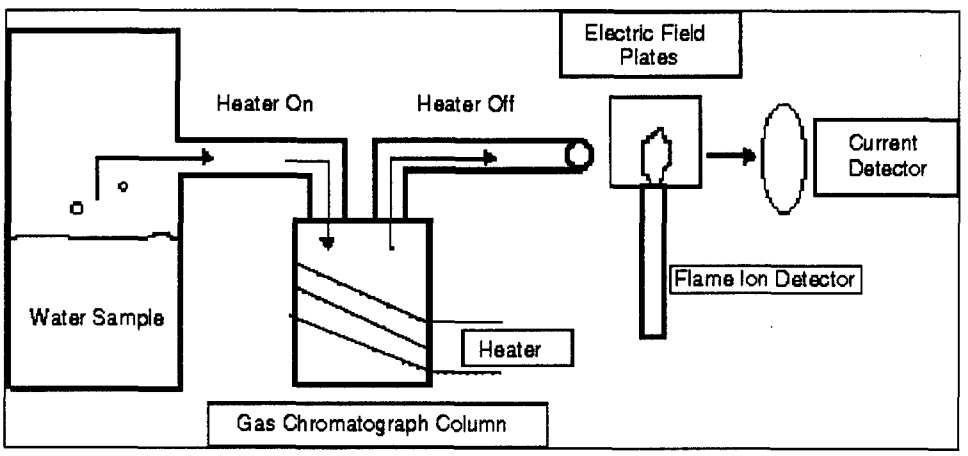

Figure 10. Gas chromatograph with Flame Ion Detector.

A voltage applied across the flame directs the resulting current to an amplifier for measurement. The FID response is proportional to the total mass entering the detector but independent of the mass of the carrier gas. The FID has many desirable qualities, such as high sensitivity and a large linear operating region. However, because it effectively "burns" the substance under examination, the test for any particular sample can only be done once.

2.2.2 Mass Spectrometry. The mass spectrometer (MS) also relies on vapor stripped samples and can be used as a detector for a GC system. The MS ionizes injected molecules with an electron beam (typically 70 eV) and accelerates the charged molecules through a series of electric fields [18]. The accelerated molecules separate out due to their mass-to-charge ratios and can be sorted via detectors placed along the acceleration length. By cycling the electric fields, ionic separation of molecules will arise. These scatterings produce patterns distinctive to each compound and are called mass spectra. By comparing the spectra of sampled substances to known substances, carrier gases can be filtered out. Mass spectrometery is typically used to identify single aliphatic or aromatic components in a sample [17].

2.2.3 Other Methods. Other methods are available to extract dissolved oil and grease from water that do not quantify individual constituents as the GC and MS do, but instead measure the total mass per sample. The most common method of oil measurement is the solvent-extraction method that uses a solvent such as hydrochloric acid (HCl) or trichlorotrifluoroethane (TCFE) to literally pull the oil chains out of the water. The extracted oils can then be measured through a variety of techniques such as the Partition-Gravimetric Method (which measures the mass of the oil via distillation from the sample), the Partition-Infrared Method (which measures the heat absorbed by the carbon-hydrogen bonds which can be compared to measurements taken from known samples) and silica gel [18]. Silica gel can adsorb polar molecules such as fatty acids leaving only hydrocarbons behind. The residuals can then be measured via distillation or infrared techniques.

Other techniques include: ultraviolet (UV) and fluorescence spectroscopy, in which solvent-extracted aliquots are subjected to UV light and wavelength absorbance is measured, and liquid chromatography (LC), in which a mobile liquid is introduced to a stationary liquid column that allows individual compounds to separate and be detected with absorbance detectors [17]. Giger *et al.* suggest using an LC technique to identify the chemical structure of complex organics [19].

2.2.4 Fiber Optic Chemical Sensors. Fiber optic chemical sensors (FOCSs) have been successfully used in the field of environmental monitoring [20]. By applying a chemically sensitive coating to the tip of a fiber optic cable, placing it in a liquid or gaseous sample, and illuminating it with a light source, molecules attracted to the tip will create interference patterns that can in turn be analyzed. A basic system is shown in Fig. 11 [21].

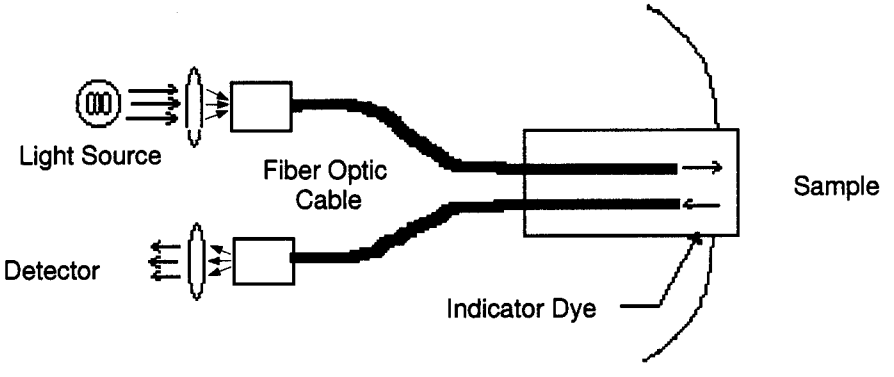

Figure 11. Fiber optic chemical sensor system showing light source, light-wave guides, chemical coating and detector.

Light sources for FOCS devices can be either monochromatic (lasers) or polychromatic (tungsten halide). Chudyk effectively used a Nd:YAG laser to measure dissolved hydrocarbons in ground water [22] while Dandge used tungsten halide to identify jet fuel components in soil [20]. Because of the research and proven use of these devices, coating types are not often published due to their commercial sensitivity. Only Angel *et al.* identified their coating as a solvatochrome dye (nile red) when it was used to measure various hydrocarbon-based solvents [23].

2.2.5 Current Limitations. While all the methods described above provide accurate measurements, they are each (except for the FOCS) limited because the analyses must take place away from the location where the sample was taken. Some of these limitations are:

- Sampling control. Because a sample of the population must be taken, a sampling quality control program must be in place to ensure that the samples accurately represent the system. This may include elaborate sampling kits, chain-of-custody documentation, and environmentally controlled storage and transportation.

- Time Sensitivity. Results from analyses may take several days to complete during which time the pollution that may have been present would have long since been discharged into the surface water body. While the results may prove useful for future preventative programs or regulatory action, they cannot detect the release of a pollutant between samples.

- Cost. Laboratory analysis is labor- and resource-intensive, requiring expensive analytic tools such as GCs and MSs and conditioning equipment such as autoclaves and incubators. Laboratories also produce hazardous waste as a result of their work. This all adds up to significant expense for each sample analyzed.

2.3 Solid-State Sensors

Most CMSs use silicon as their basic construction block. In addition to being inexpensive to manufacture and having excellent semiconducting properties, silicon is also 100 times stronger than steel, one third as dense, and much more flexible [10]. Indeed, silicon would be an ideal structural material were it not so brittle. Nonetheless, silicon is an excellent medium for micromechanical devices requiring structural support.

Solid-state sensors are constructed using traditional fabrication techniques to make hybrid transistors, solid-state resistors, and oscillators. By utilizing the etchant capabilities of certain compounds

on sacrificial layers, entire micro-electro-mechanical systems (MEMS) can be "carved" out of silicon or its oxides.

All CMSs rely on a chemiphilic coating in direct contact with the medium (gas or liquid) being analyzed that is sensitive to a particular chemical or group of chemicals. The chemical under investigation affects the operating condition of the device in such a manner that the device's output is proportional to the concentration of the chemical. Ideally, the coating should only be sensitive to a single chemical and not be affected by the presence of other chemicals. Since this is not the case, recognition of chemicals in a mixed environment can be achieved using arrays of similar devices with different coatings. This has been done successfully by a number of researchers [24, 25, 26, 27] to identify and group a wide range of chemicals. Using an array of sensors is economically practical due to their small size, as most sensor chip packages are less than 1 cm^2 and the packages can contain hundreds of sensors. As a result, power consumption is very low and could theoretically be easily supplied by a 9V battery for one year.

The current direction of solid-state CMSs is the concept of an intelligent sensor that combines sensor and signal processing hardware in one monolithic chip. Besides requiring lower power consumption, a sensor could be cheaply manufactured using the same bulk processes already in place for the more traditional semiconducting industry. More research is needed in this area to fully integrate the micromechanical, electronic, and packaging elements into one assembly that is robust enough to withstand MEMS post-processing and direct environmental contact.

The vast majority of CMSs measure organics in a gaseous state using Surface Acoustic Wave (SAW) devices. Chemical Field Effect Transistors (CHEMFETS) are also popular. Several other devices exist that use micro-machined heaters to activate gases beyond ambient room temperatures. A number of coatings is also used. Few researchers looked at measuring liquids or chemicals in solutions; those who did concentrated mainly on inorganic ions instead of dissolved organics [28, 29].

Metal oxides such as tin oxide (SnO_2) and zinc oxide (ZnO) were widely used as chemical coatings [5, 6, 30, 31] along with sputtered platinum and palladium [7, 32, 33].

2.4 Devices

The majority of CMS devices can be grouped into either a frequency- or conductivity-sensitive category based on their measurement method. In the frequency-sensitive category are surface acoustic wave devices, thickness shear mode resonators (TSMRs), capillary electrophoresis (CE) systems and CHEMFETS. On the conductivity side are metal oxide semiconductors, chemoresistors, micro-electro-mechanical systems (MEMS), and CHEMFETS. CHEMFETS can straddle both groups depending on their operating mode set-up.

The few devices that do not fit these categories are micro gas chromatographs which use micromachining techniques to construct miniaturized gas chromatographs [34, 35]. In these devices, the same principles used by conventional gas chromatographs are exploited to analyze gas samples at the micro level.

2.4.1 Frequency Devices.

2.4.1.1 Surface Acoustic Wave Devices. The most common frequency device in the literature is the Surface Acoustic Wave (SAW) device. Surface acoustic wave devices are manufactured on a piezoelectric substrate such as quartz or lithium niobate. Pairs of interdigital transducers (IDTs), typically 25 mm long and 25 mm wide, are deposited onto a piezoelectric substrate (such as quartz) that acts as a delay line transmitter/receiver of a high frequency (30 - 1000 MHz) Rayleigh wave (surface acoustic waves with elliptical polarization normal to the surface). A typical SAW device is shown in Fig. 12.

When used as a CMS, the surface of the SAW device is coated with a thin-film (50 - 200 nm) chemiphilic coating [26, 36]. Gas molecules of the chemical under observation sorb into the coating,

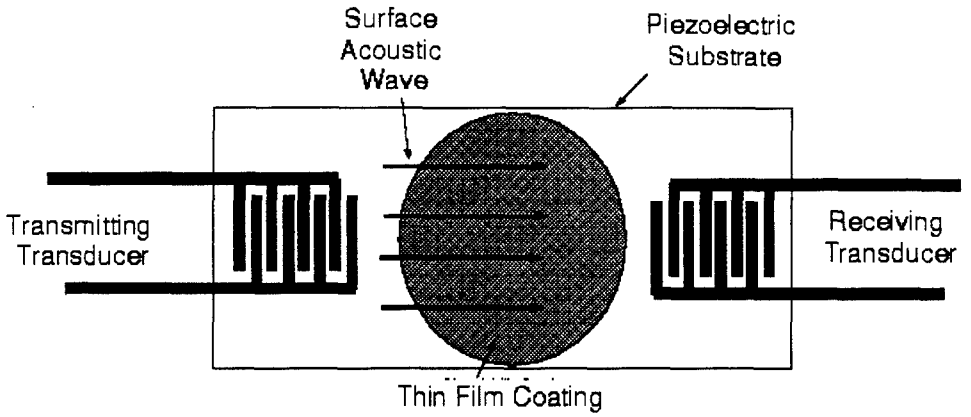

Figure 12. Surface acoustic wave device.

changing the phase velocity of the transmitted acoustic wave by changing the parametric characteristics of the medium being transversed. This change of velocity can be measured as a frequency shift when compared to the device's oscillation frequency. The change in frequency occurs as a result of the change in mass of the coating in the wave path as molecules cling to or detach from the surface. The sensitivity of SAW devices varies with frequency, with detection of mass changes ranging from $3x10^{-9}$g at 30 MHz to $3x10^{-15}$g at 1 GHz [37]. This basic concept of mass change due to molecular level sorption is fundamental to CMSs. Surface acoustic wave gas sensors have been very successful in identifying various chemical species and concentrations (mass resolution of $<$ 1 picogram [38]), especially when fitted in arrays with different polymer coatings [3, 26, 25], despite long-term instability and sensitivity to temperature and humidity.

Coatings can be applied to SAW devices in a number of ways. Reichert dissolved polymers in 0.2 mg/ml acetone and toluene and then spin-coated the whole device at 8000 rpm [26]. Wu also used a spin-coating technique to coat devices with tin oxide dissolved in xylene [7]. Ricco used self-assembled monolayers (SAMs) and plasma grafted films (PGFs). SAMs were soaked in solutions of a coating dissolved in ethanol for times ranging from a few minutes to overnight. PGFs used a plasma polymerization method, cross-linking thin layers of coating together and then "grafting" them in an unsaturated monomer coating while in the gaseous phase [27].

Thin films used on SAWs and chemicals detected are shown in Table 5.

Table 5. Summary of SAW chemical sensors in literature. All tests were done in gas unless otherwise noted. The "Chemicals Sensed" field indicates chemicals used in the overall study as target chemicals and not specifically with the individual "Thin Film Coating" field.

	Thin Film Coating	Chemicals Sensed	Sensitivity	Reference
1.	$HS(CH_2)_{15}CH_3$ $HS(CH_2)_{10}COO^-/Cu^{2+}/COOH$ Eugonol-30 poly(isobutylene) w/ acrylic acid plasma-polymerized acrylic acid	trichloroethylene, toluene, benzene, carbon tetrachloride, cyclohexane, octane, acetone, DIMP, DMMP	100 pg/cm^2	[27]
2.	mercaptoundecanoic acid	DIMP, DMMP, n-heptanethiol, alkanethiol	100 ppb	[36]
3.	lead phthalocyanine	NO_2	3 ppm	[39]
4.	$HS(CH_2)_{15}CH_3$ $HS(CH_2)_{10}COO^-/Cu^{2+}/COOH$ Eugonol-30 poly(isobutylene) w/ acrylic acid ethyl cellulose poly(isobutylene) nafion	trichloroethylene, toluene, benzene, carbon tetrachloride, cyclohexane, octane, acetone, DIMP, DMMP, methanol, water, chloroform, isopropanol	100 pg/cm^2	[25]
5.	poly(acrylic) acid nafion poly(dimethylsiloxane) paraffin	methanol, water, octane	20 ppm	[26]
6.	fluorpolyol	DMMP, water, isooctane, halothane, butanol	N/G	[40]

2.4.1.2 Thickness Shear Mode Resonators. Like SAWs, thickness shear mode resonators (TSMRs) are cut from piezoelectric material; however, instead of using oscillating IDTs to generate a wave on the crystal surface, the TSMR relies on oscillation of the crystal itself via electrodes. Thickness shear mode resonators are also referred to in literature as Quartz Crystal Microbalances. The crystal achieves several resonant modes, each corresponding to an eigenmode standing wave pattern. Mass loading at the face of the crystal changes the eigenmodes which can then be measured. Only one

TSM device was used as a CMS in the literature and was the only device that did not use a chemiphilic coating [41].

2.4.1.3 Capillary Electrophoresis Systems. Capillary electrophoresis systems (CEs) are commercially available devices that have been, in one application, integrated into a micro-machined system [32]. In CEs, an unknown liquid sample is introduced into a channel filled with a buffer solution similar in nature to chemiphilic coatings. A high DC potential (1 - 30kV) is applied across the channel and different constituents migrate to the pole based on molecular weight and subsequent mobility. By knowing the mobility factor of constituents, a window of time can be allocated to measure each compound. Reay *et al.* constructed a micro-CE using a plasma-etched silicon wafer. Trenches were etched to the depth of 150 μm using photoresist masks with platinum electrodes deposited in the trenches as sensing elements [32].

2.4.2 Conductivity Devices. As mentioned previously, CHEMFETs can take advantage of molecular mass changes by measuring frequency or electrical current shifts. CHEMFETs include a group of hybrid solid-state active devices that use modified gates to affect their drain current. Such devices include Ion Sensitive Field Effect Transistors (ISFETs), Charge-Flow Transistors (CFTs), and Interdigitated Gate Electrode FETs (IGEFETs). The basic construction of a CHEMFET follows standard FET methods using p-type silicon substrates with diffused n-type sources and drains. It is the gate construction which is the distinction among the different CHEMFET types. The gate of an ISFET is similar to any other surface-fabricated MOSFET device, except that the metal gate is replaced by an external reference electrode and is coated with a chemically sensitive compound. An encapsulant may also be present to protect the non-sensing elements of the device (such as the source and drain). Coatings can be polarized, adding a capacitive effect, or non-polarized, adding a pure resistance. An uncoated reference electrode is placed in the solution to form the bias that attracts charged particles to the coating (Fig. 13).

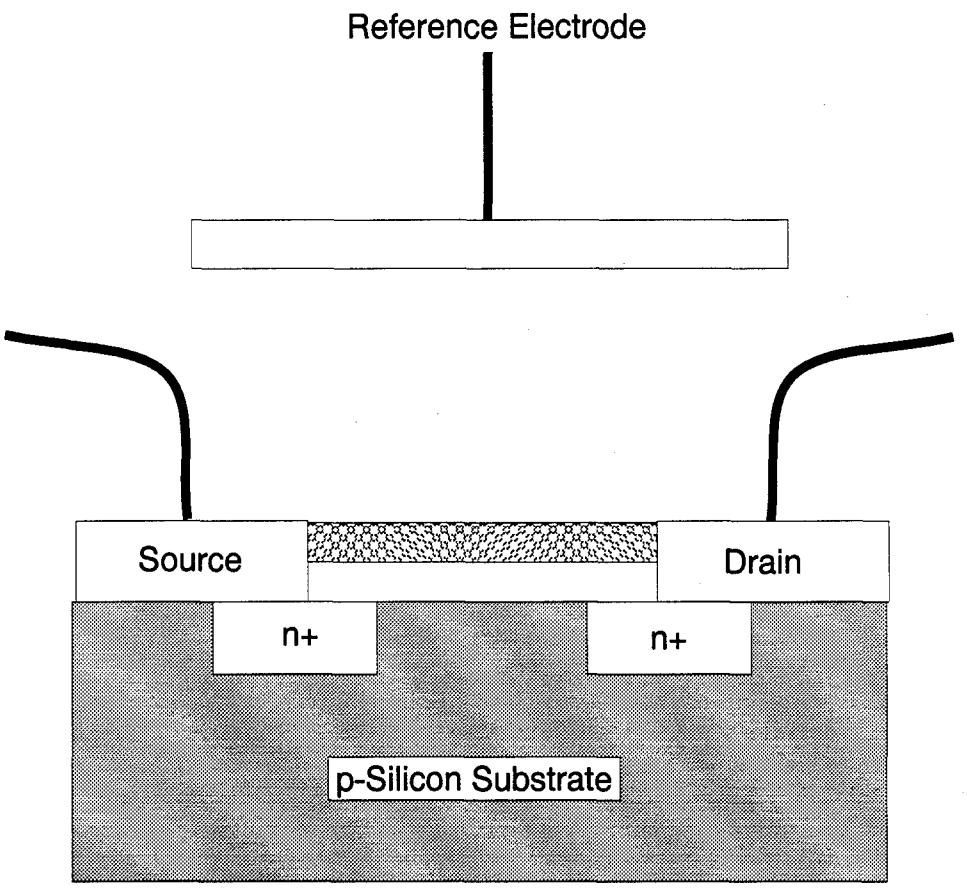

Figure 13. Chemotransistor.

Ion Sensitive Field Effect Transistors (ISFETs) are typically operated either in constant gate charge (maintaining a constant drain current and measuring voltage flux required for equilibrium) or constant applied gate voltage and measurement of the change in drain current.

Ion sensitive field effect transistors usually use sputtered tin and zinc oxides to detect gases [42]. Other researchers have used palladium [43] and poly(isobutylene) [27]. Hunag used poly(4-vinylpyridine) to detect inorganic ions in solution [29].

Interdigitated Gate Electrode FETs (IGEFETs) are an extension of ISFETs in that the external reference electrode is replaced by a floating interdigitated metal gate on the device substrate coated with a chemiphilic layer and exposed to a medium to be measured. The IGEFET uses voltage pulses to a driven IDT gate physically isolated from the floating gate to drive a characteristic response change that is sensed by the floating gate. Hauschild used such a device coated in metal-doped (Cu and Pb) phthalocyanine to measure inorganic and organic gases [24]. While widely studied, CHEMFETS suffer from temperature and pressure instability [38].

Thin films used on CHEMFETs and chemicals detected are shown in Table 6.

Table 6. Summary of CHEMFET sensors in literature. All tests were done in gas unless otherwise noted. The "Chemicals Sensed" field indicates chemicals used in the overall study as target chemicals and not specifically with the individual "Thin Film Coating" field.

	Thin Film Coating	Chemicals Sensed	Sensitivity	Reference
1.	palladium	hydrogen	2 ppm	[33]
2.	poly(isobutylene)	trichloroethylene, acetate, cyclohexane, acetone	1000 ppm	[44]
3.	lead phthalocyanine copper phthalocyanine	hexane, methanol, DIMP, DMMP, isopropyl alcohol, NO_2	10-50 ppm	[24]
4.	poly(4-vinylpyridine)	methane, cycropentanone, butanone	10^{-7} moles/cm^2	[29]

2.4.2.1 Chemoresistors. Chemoresistors, such as the one shown in Fig. 14, are simple devices with a semiconducting chemical coating spanning two electrodes [38]. The resistance between the electrodes varies with the concentration of ambient chemicals in the coating. Potential problems with these devices are a lack of reversibility, and their inherent instability with temperature and pressure changes.

2.4.3 Micro-Electro-Mechanical Systems. Micro-Electro-Mechanical Systems (MEMS) represent a new technology emerging from existing semiconductor technology. Instead of using silicon and its compounds (silicon oxide, polysilicon, and silicon nitrite) to form active devices, MEMS use selective etchants to "carve" out electrically driven mechanical devices on the micron scale. Originally proposed in 1956 by Dr. Richard Feynman [45], it was not until the late 1980s with the industry advances of silicon fabrication that MEMS became feasible. Actual devices include motors, cantilevers, pumps, nozzles, actuators and heaters. While applications have not been found for each individual device, combinations can be used to make MEMS-based sensors or to be incorporated into other devices to enhance sensor response.

One application of MEMS is found in a hotplate design in which a polysilicon resistor is suspended in a substrate over a void. Free from thermal contact with the substrate, the hotplate resistor was heated to high temperatures ($> 500^{o}$ C) with a small power input (milliwatts) [5]. This high temperature ability can be used to "activate" analytes in gases to react with the applied chemiphilic coating. The device can then be purged by simply superheating the pad in an inert environment. Cavicchi used such a hotplate with a tin oxide coating to measure the change of conductance as sorbed chemicals increased the thermal resistance of the device. Using a pulsed temperature cycle, the device only used 470 mW [5]. Heiland and Kohl embedded a microheater in a ceramic device with a metal-doped phthalocyanine coating [31]. Both devices were designed to measure gases.

Thin films used on MEMS sensors and chemicals detected are shown in Table 7.

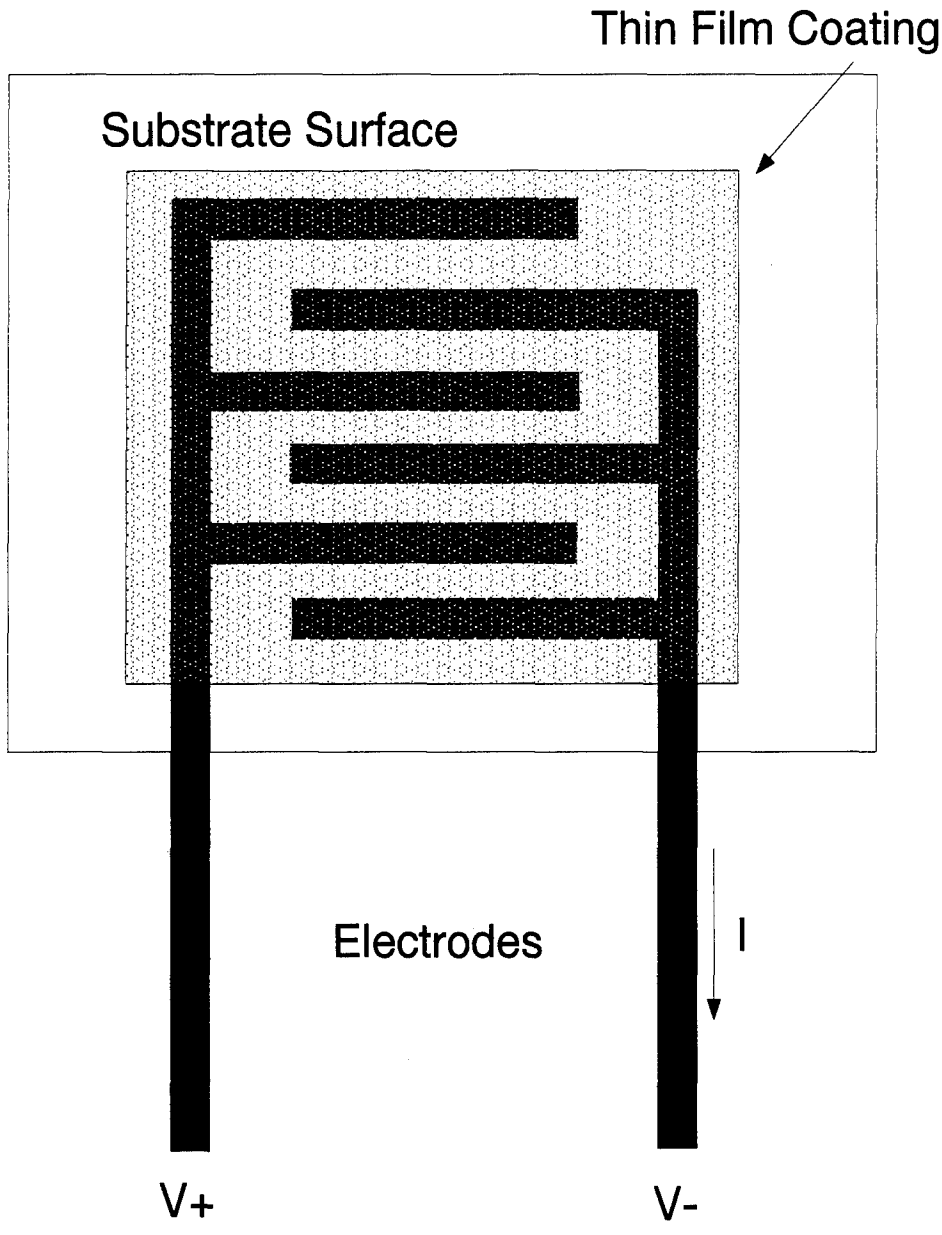

Figure 14. Chemoresistor.

Table 7. Summary of MEMS sensors in literature. All tests were done in gas unless otherwise noted. The "Chemicals Sensed" field indicates chemicals used in the overall study as target chemicals and not specifically with the individual "Thin Film Coating" field.

	Thin Film Coating	Chemicals Sensed	Sensitivity	Reference
1.	tin oxide	ethanol, propanol, hydrogen, water	Not Given	[5]
2.	tin oxide	methanol, glycol, octane, ethyl ether	Not Given	[30]
3.	tin oxide zinc oxide copper phthalocyanine	carbon tetrachloride	Not Given	[31]
4.	platinum	hydrogen, carbon dioxide, propane, propylene	2 ppm	[33]
5.	aluminum	glycol	100 ppm	[28]
6.	cyclized poly(isoprene)	xylene	.3 Hz/ppm	[46]

2.5 Thin Films

Any substance that can be applied uniformly on a semiconducting substrate can be used as a chemical sensing thin film. Whether the film provides a useful response to the chemicals being sensed based on the characteristics mentioned earlier may be another issue. Selecting chemiphilic thin film coatings seems to be an art more than a science in the literature. No justification is typically given as to why one particular coating was chosen over another. Wohltjen suggested choosing coatings that allowed "rapid diffusion" [37] while Howe stated that the difference in solubility parameters [δ] of a coating and a chemical to be analyzed determined the rate at which the chemical will be sorbed. The solubility parameter is given as

$$\delta = \sqrt{\frac{\Delta H_{vap} - RT}{V}} \tag{1}$$

where ΔH_{vap} is the heat of vaporization, R is Rayleigh's gas constant, T is temperature in degrees Kelvin and V is gas volume. $\frac{\Delta H_{vap}-RT}{V}$ is defined as the cohesive energy density of material [47, 48].

Comparing δ's for each film, Howe suggests that if $\mid \delta_1 - \delta_2 \mid > 3$, then there is low solubility between the two products [16].

To further increase diffusion, the coating should be soft or "rubbery" at the sensing temperature. Rubbery coatings display less hysteresis due to their heightened internal energy that can accommodate the reversibility of the sorbed molecules. For his thin film coating, Howe used a commercially available negative photoresist to sense xylene vapor [16]. Other thin films more commonly used in the literature fell into one of three categories: metal oxides [30, 5, 49], self-assembling monolayers [36] or phthalocyanines [24, 50, 51] and polymers [40].

Since the overall function of the film is to adsorb chemicals to its surface, a film must be chosen that can bond appropriately with the chemical that the designer wants to sense. Like a doped semiconductor, thin films also display n- or p-type characteristics. If the coating donates electrons during a bonding reaction, it is considered n-type; if it accepts electrons, it is p-type. Chemically speaking, these properties may be designated as Lewis acids and bases. If a substance donates electrons, it is considered a Lewis base, while it is a Lewis acid if it accepts electrons [52]. Lewis acid-bases are very powerful in estimating the selectivity of the sensor in response to various chemicals.

2.5.1 Metal Oxides. Metal oxides were the first films used specifically for chemical sensors. Oxides that have been used include transition metals such as tin, copper, zinc, and palladium, as well as noble metals such as gold, platinum and silver [53]. Chemoresistors and CHEMFETS have been made with these types of films, relying on a conductivity change based on a change of surface defect density within the film due to adsorbing compounds. The principle driver behind the use of oxides is the high reactivity of oxygen. Making compounds with various metals affects the binding energy necessary to form bonds. The resulting change of conductivity can be quantified as ratio

$$\Delta G/G_b = \Delta n_s/n_b d \tag{2}$$

where $\Delta G/G_b$ is the change in the conductance over the original bulk conductance while $\Delta n_s/n_b$ is the change of density in the space-charge region over the change in density of the bulk film, and d is the film thickness [54].

2.5.2 Polymers. Polymers are simple chemicals that chain together to form long, complex molecules. Successful chemical sensors have been made using polymer thin films on surface acoustic wave, thickness shear mode, and fiber optics chemical sensors [55, 56]. Many polymers, such as poly(isobutylene) in Fig. 15 and poly(vinyl tetrachloride) in Fig. 16, are highly permeable, have low density, and are rubbery, making them ideal adsorbents.

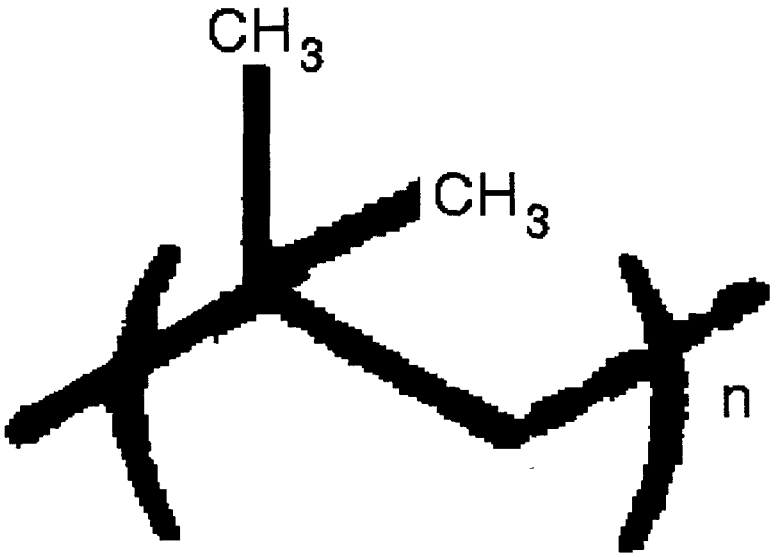

Figure 15. Poly(isobutylene) or (PIB) structure [55].

To apply, polymers are dissolved in a solvent such as toluene or chloroform and sprayed on with an air brush or spun on with a spin-coater. The solvent evaporates, leaving the polymer coating. The coating then sorbs other chemicals that act as solvents by creating cavities that bind the chemical on contact. As the chemical becomes attached to the polymer, different interactions take place, including polarization, hydrogen-bonding, and van der Waals forces. The overall transformation changes the mass and resistivity of the polymer and can be reversed with the addition of heat [56]. Since each

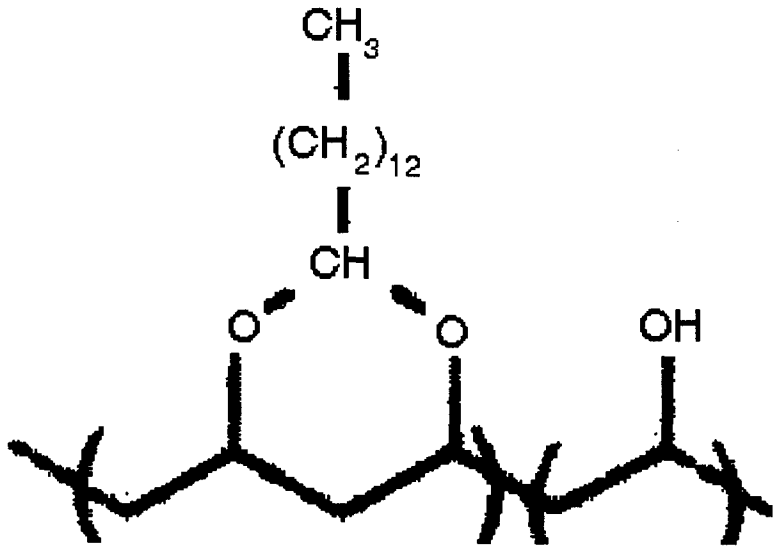

Figure 16. Poly(vinyl tetrachloride) or (PVTD) structure [55].

polymer is different in structure and parameters, each polymer will have particular chemicals with which it will react well. The selectivity of polymers to one chemical over another chemical has been defined as a selectivity factor S and

$$S_B^A = \frac{K_p^A * C_A}{K_p^B * C_B} \tag{3}$$

where A is chemical A, B is chemical B, K_p is the air-polymer partition coefficient and a measure of the solute-solvent interaction strength, and C is the saturated vapor concentration. While K_p can be found experimentally by

$$K_p = C_p/C_v \tag{4}$$

where C_p is the chemical concentration in the polymer phase and C_v is the chemical concentration in the vapor phase, it can also be calculated using the linear solvation energy relationship (LSER) for each polymer

$$LogK_p = c + r * R_2 + s * \pi_2^H + a * \alpha_2^H + b * \beta_2^H + I * LogL^{16} \tag{5}$$

where c is a constant, r is polarizability, s is the dipolarity coefficient, a is the hydrogen-bond basicity coefficient, b is the hydrogen-bond acidity coefficient, I is a dispersion and cavity constant, R_2 is a constant based on n and π electrons, π_2^H is dipolarity, α_2^H is hydrogen-bond basicity, β_2^H is hydrogen-bond acidity, and L^{16} is the gas-liquid coefficient on n-hexadecane [56]. Based on this equation and values given by McGill, poly(isobutylene) would have a general LSER of

$$LogK_p^{PIB} = -0.77 - 0.08 * R_2 + 0.37 * \pi_2^H + 0.18 * \alpha_2^H + 1.02 * LogL^{16} \quad (6)$$

and poly(vinyl tetrachloride) would have an LSER of

$$LogK_p^{PVTD} = -0.59 - 0.02 * R_2 + 0.74 * \pi_2^H + 2.44 * \alpha_2^H + 0.22 * \beta_2^H + 0.92 * LogL^{16} \quad (7)$$

Other variables would be included depending upon which chemical was being sensed [56].

2.5.3 Self-Assembling Monolayers. Self-assembling monolayers (SAMs) are a family of polymers that form one molecule-thick layers spontaneously on a substrate when dipped in a solvent bath [57]. The basic structure of a SAM is shown in Fig. 17.

The basic molecule is amphiphilic in that it has a hydrophobic end that binds with the substrate surface and a hydrophilic end that reacts with chemicals in solution. As shown in the figure, the molecules align themselves via electrostatic van der Waals forces.

2.5.4 Phthalocyanines. Phthalocyanines (Pcs) were developed as industrial dyes and have since been used for a number of applications including fuel cells, LCD displays, and electronic devices [58, 59]. Phthalocyanines also make very good chemical sensor films because of their stable benzene ring structure and their ability to physically adsorb a variety of chemicals that can desorb easily when the device is reset. The basic structure of Pc is shown in Fig. 18 along with a chain of Pcs as would be expected on a thin film.

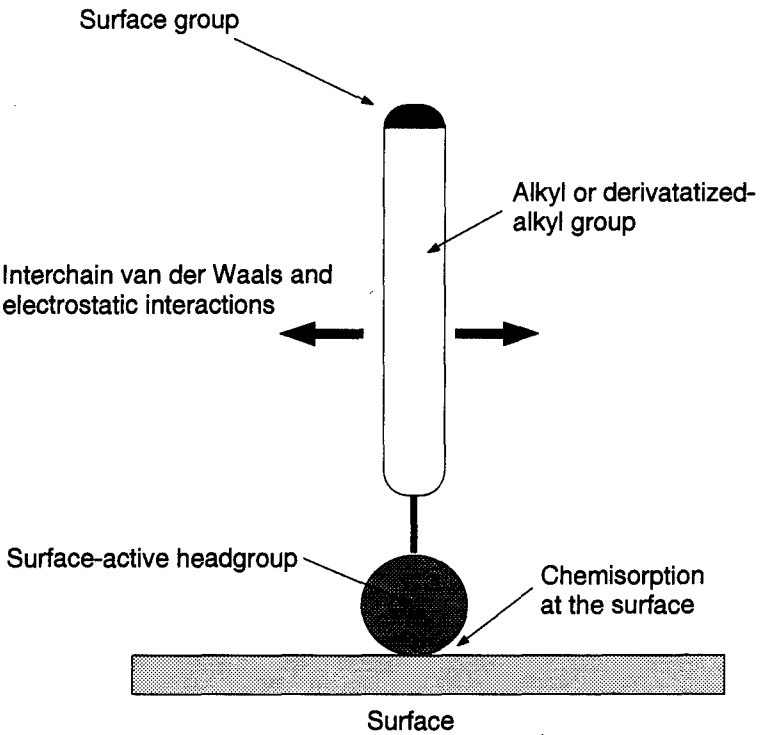

Figure 17. Self-assembling monolayer [57].

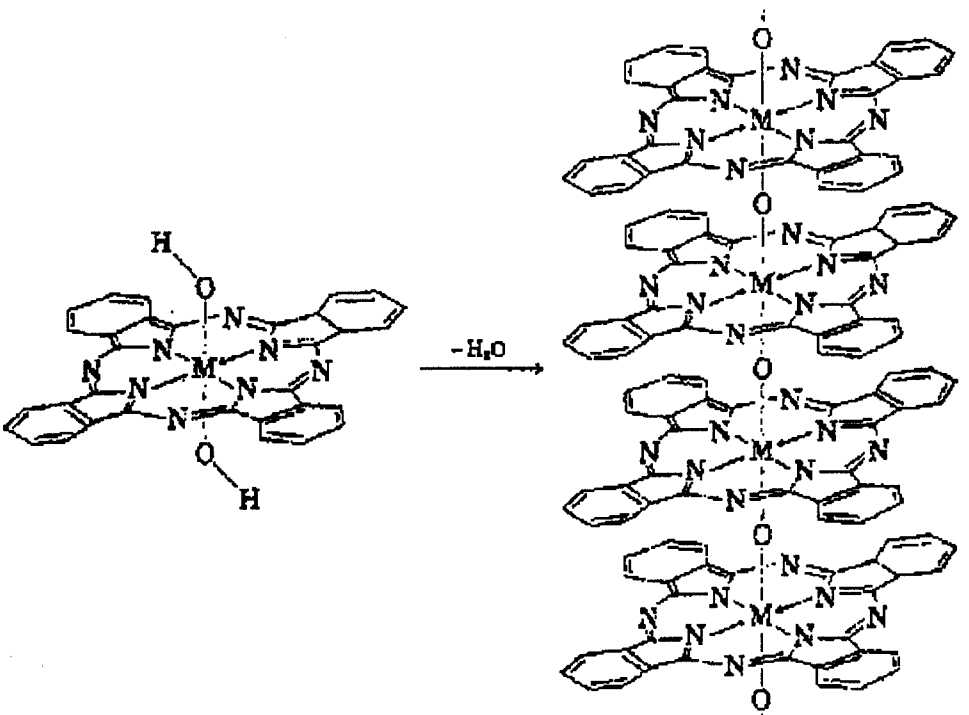

Figure 18. Phthalocyanine structure and chain along interfacial bonds [59].

Phthalocyanines chemisorb to the silicon substrate at one of its outer benzene rings. The chelated metal ion in the middle affects electron movement in the outer rings, determining bonding sites and required energy for attracted molecules. Among the metals and semiconductor ions that form the center are lead, copper, zinc, and silicon [59].

A particularly useful property of phthalocyanines is their solid phase transitions. Normally resting at room temperature in an α crystal structure, Pc will undergo a phase transition to a β structure when heated to temperatures greater than 180^o C or in the presence of particular solvents. The process is reversible and the Pc can be reset to its original α state by reducing the heat and removing the solvent [58, 59].

2.6 Film Application Methods

This section is concerned with the practical aspect of actually applying uniform thin films to a semiconducting substrate. While there are many processes used in actual electronic device fabrication, such as chemical vapor deposition and molecular beam epitaxy, this discussion will focus on the four processes available in the AFIT laboratories: thermal evaporation, spin coating, pressure-regulated air brushing and Langmuir-Blodgett film application. Except for thermal evaporation, these methods are performed at room temperature and pressure, ensuring that the thin film is not affected during application through heat or pressure stresses.

2.6.1 Thermal Evaporation. In thermal evaporation, a crucible filled with material that will become the thin film is heated in an evacuated chamber until the material evaporates. The substrate is placed nearby and given an electrostatic charge to attract the evaporated molecules. Buildup of the film is monitored by a quartz resonance mass balance whose resonance frequency changes as more mass is deposited upon it. This process is typically used to apply metal oxides, although Pcs can also be applied this way. The problem that arises with this application process is the lack of reproducibility. Changes in material purity, vacuum pressure, and evaporation timing all create trial-unique coatings.

2.6.2 Radio-Frequency Sputtering. Sputtering is a process whereby an atom receives enough kinetic energy via collisions with other atoms to escape from its surface [60]. An inert gas such as argon is used to provide the necessary ions. As the target is hit, the surface molecules detach and sputter away, reattaching themselves to another substrate. Radio-frequency sputtering uses high-energy ions to bombard a target surface in a plasma under vacuum by changing the potential of the target and the substrate at high frequencies (in the megahertz range). The basic radio-frequency sputtering system is shown in Fig. 19. In addition to the elements shown in Fig. 19, an operating system may also insulate thickness monitors and power meters. Power meters will typically read forward power, or power being delivered to the system, and reflected power, or power being returned by the target. A low reflected to forward power ratio is always desired.

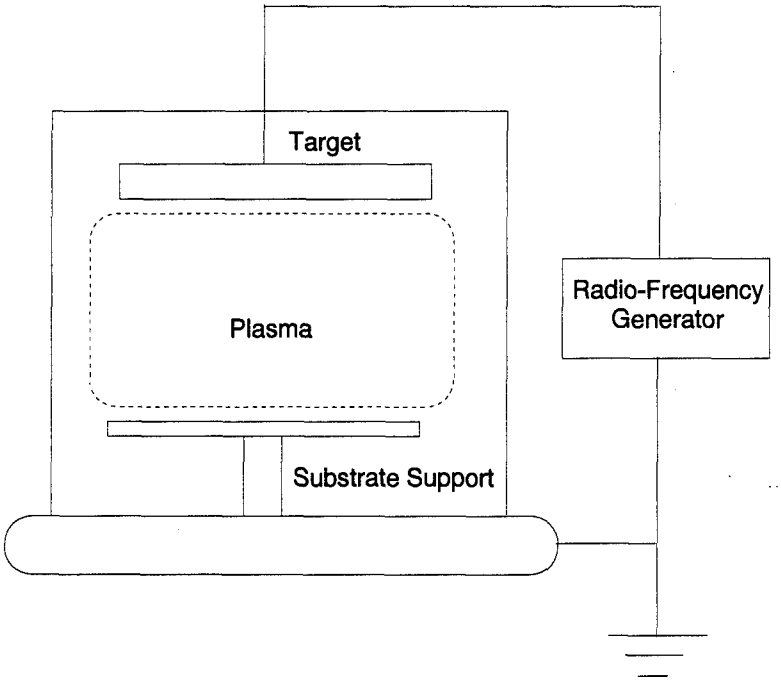

Figure 19. Radio-frequency sputtering system. [60]

2.6.3 Spin Coating. Spin coating uses the forces of angular acceleration at high revolutions per minute (rpms) to uniformly spread a liquid over a surface. The resulting layer thickness is a

function of the liquid's viscosity, the speed at which the substrate is spinning, and the percentage of solids in the applied coating [61]. Typically used to apply photoresist for lithographic purposes, this technique has been useful in applying SAMs and Pcs that have been diluted in a solvent such as toluene or chloroform.

2.6.4 Langmuir-Blodgett Films. Langmuir-Blodgett (L-B) films exploit a phenomenon first written about by Benjamin Franklin [57]. He observed that a small drop of oil spread out over the water of a small pond far beyond his expectations. While not actually able to see the oil, he could see that the wind did not ruffle the part of the water near where he had dropped oil. Without realizing it, Franklin was watching the oil spread out to a molecule-thick monolayer held together by van der Waals forces, the same way a SAM is constructed [62]. Langmuir-Blodgett films take dissolved polymers capable of dipole charges and drop them into a trough filled with a subphase (usually distilled water). As the solvent evaporates, a polymer film forms on the surface of the subphase. Surface tension is increased until the polymers align as shown in Fig. 20.

A substrate is then dipped into the solution and removed as shown in Fig. 21. Successive dips form multilayers of known quantities in discrete levels [57, 63]. Typical values range from 3-5 mm/minute and are found empirically.

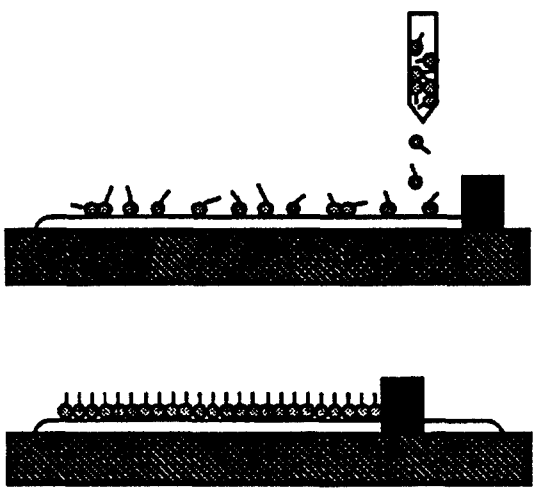

Figure 20. Alignment of polymers in a Langmuir-Blodgett Film. Molecules are deposited on a solvent surface (top), and compressed to form a monolayer (bottom). [63].

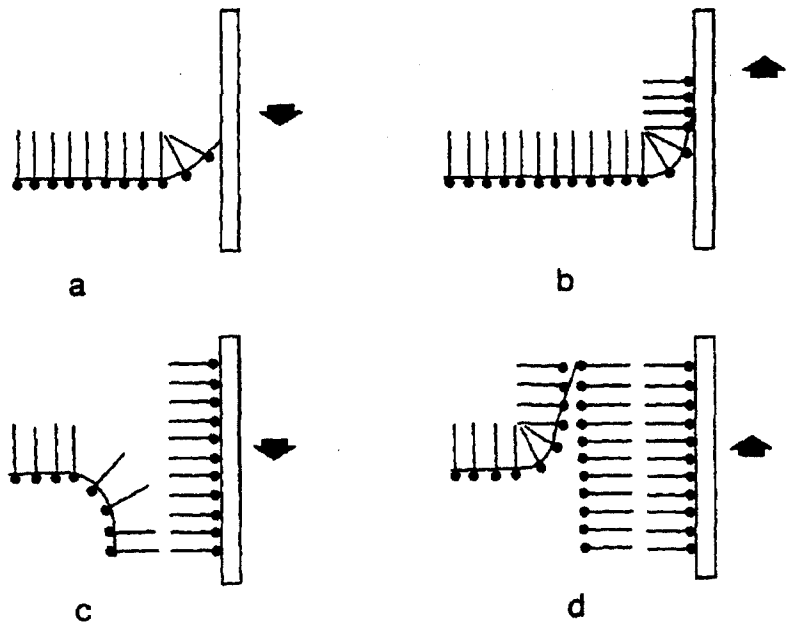

Figure 21. Dipping substrates into a Langmuir-Blodgett Film: (a) first immersion, (b) first withdrawal, (c) second immersion, and (d) second withdrawal. [63].

III. Theory and Design

"If there's no meaning in it," said the King,
"that saves a world of trouble, you know, as we
needn't try to find any. And yet, I don't know,"
he went on, spreading out the verses on his knee
and looking at them with one eye; "I seem to see
some meaning in them after all..."

- The King of Hearts
Alice's Adventures in Wonderland, Lewis Carroll

3.1 Introduction

Chemical microsensors utilize multiple disciplines and theories to explain and model the various processes required to fabricate, post-process, and sense chemical agents. The first part of this chapter discusses the various forms of mechanisms that can be used to drive a MEMS structure. By driving the structure into some form of mass-dependent action, measurements can be made as the mass changes. The next part of the chapter describes the transport mechanisms chemical species use to sorb in and out of thin films. The understanding of this process is necessary to appreciate the complexity of mass loading effects on the sensor. The last part of the chapter is devoted to solid-state fabrication theory and the processes used to make the AFIT Microsensor.

3.2 *Device Theory*

This section covers the two basic drive forces that make a MEMS structure oscillate: bimorphic action and electrostatic forces. In addition, variable dielectric capacitance is covered as a sensing medium.

3.2.1 Bimorph Theory. The basis of bimorph theory is that as two different materials are heated, they will expand at different rates. The difference in expansion will manifest as stress in the structure. If the structure is flexible enough, it will deform to the shape of lowest energy until the heat is removed and it cools back to its original shape. By changing the mass of a structure, the rate at which heat is applied and released can be affected, thereby changing the rate of expansion and bimorphic action.

A suspended bridge is shown in Fig. 22. If oscillated, the structure could be driven to resonance based on the internal properties of the device materials. This frequency is given as [64]

$$f_o = 0.615\frac{d}{l^2}\sqrt{\frac{E}{\rho\left[1-\nu\right]^2}} \tag{8}$$

where f_o is the fundamental resonance frequency, d and l are the depth and length of the device respectively, E is Young's modulus, ρ is the device density and ν is the Poisson's ratio. For multi-layered devices, values for E, ρ and ν are weighted and averaged over the depth of the device.

For a MEMS device in the micron-scale, resonance frequency is many kilohertz. A bimorphic device cannot expect to drive itself into this region because the heating and cooling cycles are too slow. Frequencies of 100-300 Hz are usually the extreme [15].

Bimorphic devices can still be used to register mass changes due to chemical sorbing by measuring the lag of response as the device's mass changes. This may best be done optically using a laser interferometer to compare a loaded and unloaded device.

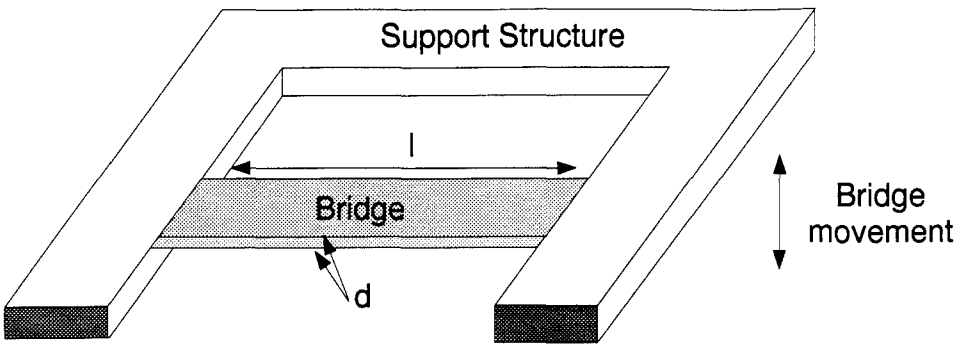

Figure 22. Bridge structure.

3.2.2 Electrostatic Theory. When two separated planar surfaces are charged by a potential difference, they will behave like a parallel plate capacitor with an electric field between them:

$$\varepsilon_{pp} = \frac{V}{\epsilon z_m} \tag{9}$$

where $\varepsilon_p p$ is the electric field, V is the applied voltage, ϵ is the material dielectric constant and z_m is the separation distance. If one plate is movable, it will feel an attractive force

$$F_{pp} = \frac{\epsilon_o}{2}\left[\frac{V}{z_o - d_f}\right]^2 A \tag{10}$$

where F_{pp} is the parallel plate, ϵ_o is the dielectric constant for free space, z_o is the separation between plates at rest, d_f is the displacement of the plates when energized, and A is the surface area of the plates [65].

Since the plates must be attached to some support structure, there is a resisting force that must be overcome for the plates to move. The support structure acts as a spring, deforming if enough voltage is applied to overcome the spring resistance minus the weight of the device, and returning to its rest state when the voltage is removed. The spring force F_s is given by Hooke's Law:

$$F_s = kd_f \tag{11}$$

where k is the spring constant.

A device driven by electrostatic force will have a deflection oscillation based on the spring resistance and the plate attraction [66]. The resulting motion is given as

$$z(t) = \frac{F_o cos\omega t}{m\left(\omega_o^2 - \omega^2\right)} \tag{12}$$

where $z(t)$ is oscillation motion over time, F_o is the displacement amplitude, m is the total mass of the moving plate, ω is the drive frequency, and ω_o is the natural resonance frequency given by

$$\omega_o = \sqrt{\frac{k}{m}} \tag{13}$$

Equations 12 and 13 show that changing the mass of the device changes the resonance frequency. As chemicals sorb onto an electrostatic device, a measurable resonance shift should occur. The forces acting on an electrostatic device are shown in Fig. 23.

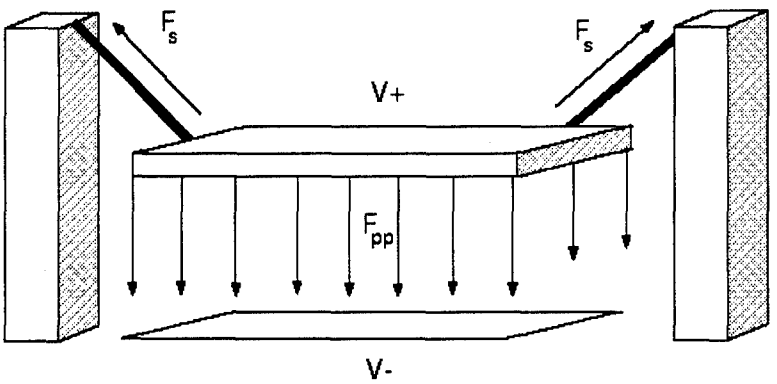

Figure 23. Forces on an electrostatic device where F_{pp} is the electrostatic force, F_s is the spring force, and $V+$ and $V-$ are the applied voltage. Gravitational forces are not shown but are assumed to be present.

3.2.3 Capacitance. Chemoresistors are essentially interdigitated parallel-plate capacitors whose thin films act as dielectrics that change during mass sorbing. The capacitance of two parallel plates is defined as

$$C = \frac{Q}{V} = \frac{\epsilon S}{d} \tag{14}$$

where Q is electric charge, V is the potential difference between the two plates, ϵ is the dielectric constant of the material between the two plates, S is the surface area of shared by both plates and d is the plate separation [67]. This is shown in Fig. 24.

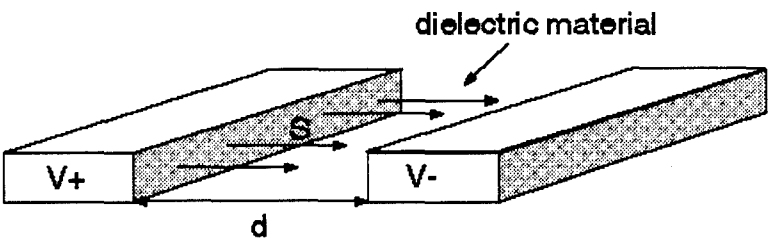

Figure 24. Capacitance in parallel plates as experienced by interdigitated chemoresistors. Capacitance is dependent on the surface area (S), plate separation (d) and the dielectric constant of the material the electric field has to cross. In chemoresistors, the dielectric is the thin film that changes as chemicals sorb in and out.

When an alternating current source is applied to a capacitor, an impedance is created

$$Z_c = \frac{C}{j\omega} \tag{15}$$

where Z_c is the capacitive impedance, $j\omega$ is the applied frequency in radians per second, and C is the device capacitance [67].

It is obvious from Equations 14 and 15 that any parametric change in a chemoresistor is due to dielectric changes in the thin film since the other variables are fixed based on the device design.

3.3 Chemical Transport Theory

This section describes the complex mechanisms used by chemical molecules to move between different concentration gradients and surfaces.

3.3.1 Surface Chemistry. Surface chemistry deals with the arrangement and reactions of matter that occur when two compounds in different states meet. A surface is thus defined as that area of contact between two different states or phases of matter [68]. A surface interface can be defined as the area of contact between two unmixable surfaces [68]. The two surface interfaces of importance in this thesis are the solid-gas and solid-liquid interfaces.

In order to form a surface, bonds must be broken in the solid substrate, as illustrated in Fig. 25. The dangling bonds will recombine with neighboring bonds or ambient chemicals. Surface energy (E_s) is defined as the extra energy required to make a surface [69]. Comparing the surface energies of materials determines which material will "wet" another material. A classic example of this effect is wax on a car. The lipids in wax bond with the highly energetic metal surface, lowering the overall surface energy and causing water to bead [69].

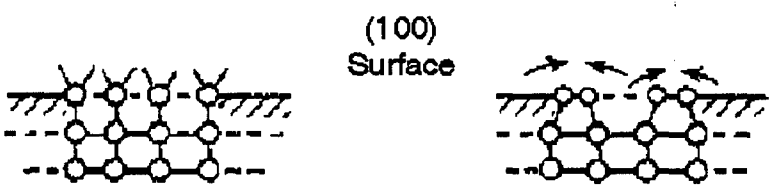

Figure 25. Surface reconstruction bonding in (100) silicon as a result of a new surface [69].

At the interface, intermolecular forces create an inward pull from the surface of highest energy state to that of the lowest. This surface pull is called surface tension (γ) in liquids and adsorption in solids. Surface tension is defined as the surface energy divided by the surface area [69]. Adsorption will be discussed below.

3.3.1.1 Energy Surfaces. Atomic bonds are broken at solid surfaces resulting in incomplete electron pairs. As electrons migrate to find stable states, the Fermi level shifts at the semiconducting substrate's surface such that $E_f \neq E_{fss}$, where E_f is the materials intrinsic Fermi level and E_{fss} is the surface Fermi level [53]. This shift affects the internal properties of the semiconductor and can be exploited by chemical sensors as conductivity changes. Such a shift is shown in Fig. 26.

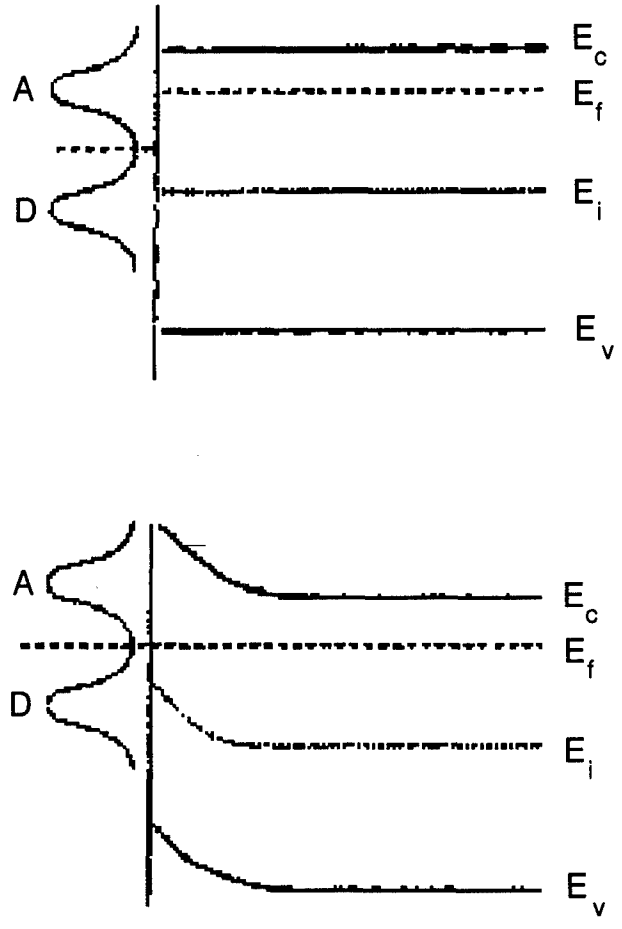

Figure 26. Surface bandgap shift showing energy levels before (a) and after (b) an impurity has attached itself. Areas of donors and acceptors are marked D and A respectively [70].

3.3.2 Adsorption. Adsorption plays a significant role in chemical sensors by bringing a chemical species to the sensor and attaching it to the sensor film for measurements to be made. Unlike absorption in which a substance is taken into another substance and inherently changed, adsorption brings substances to a surface and leaves the substance bonded, but unchanged [68].

Depending on the bond energy between the surface and the substance bound to it, adsorption can be broken into two distinct phenomena: physical adsorption and chemisorption. Physical adsorption is described by weak bonds ($\leq$ 6 kcal/mole) such as those formed via van der Waals or hydrogen bonds and tend to be easily reversible [54]. Chemisorption bonds are much stronger ($\geq$ 15 kcal/mole) and are usually not reversible [54]. Figure 27 shows a typical relationship between physical adsorption and chemisorption. Temperature can be considered as heat added to the system, thus providing more energy for bonding.

3.3.2.1 Physical adsorption. Physical adsorption is heavily influenced by the number of binding sites available on the solid surface. If the surface area is pocked with valleys or crevices that enhance the overall area versus a strict planar area, more adsorption will take place. Physical size of the adsorbing molecule is also a factor. Smaller molecules can adsorb in greater numbers than large molecules. These two parameters can greatly affect adsorption results and can be classified into five distinct ranges of response as shown in Fig. 28.

3.3.2.2 Chemisorption. Chemisorption is also affected by the number of binding sites on a surface; however, due to the strength of bonding associated with chemisorbed substances, multilayers can be more readily formed than during physical adsorption. A common description of chemisorption is the Freundich Isotherm as shown in Fig. 29. The basic equation of this measure is

$$C_s = KC_w^n \tag{16}$$

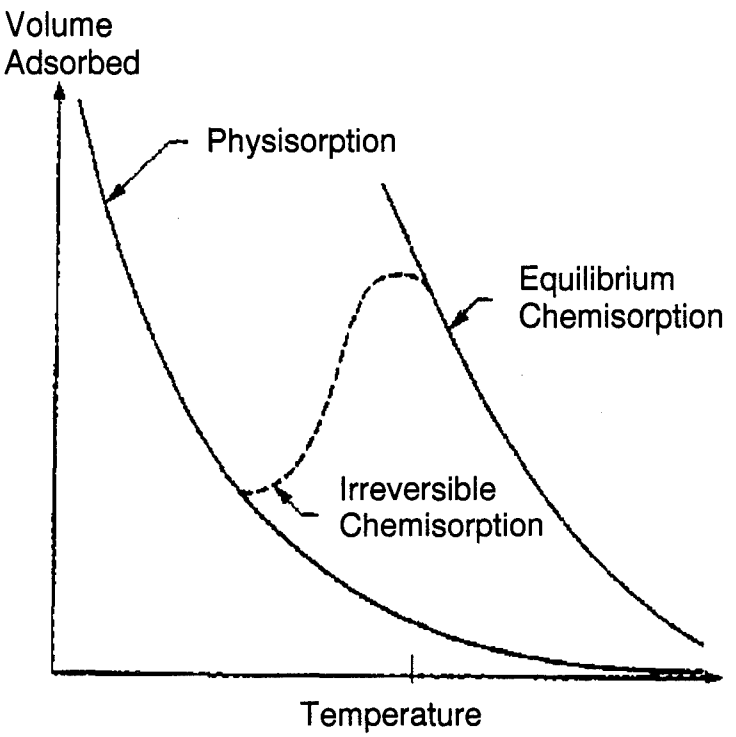

Figure 27. Physical adsorption and chemisorption relationship [54].

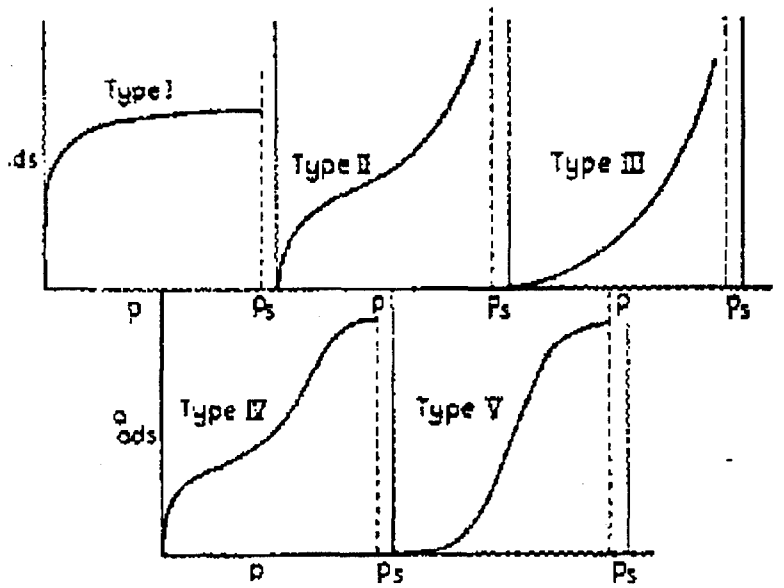

Figure 28. The five types of physical adsorption: I. Vapors on solids with small pores (no multilayers can be built); II. Multilayers built at high pressures in porous solids; III. Heat of adsorption is less than heat of liquidification; IV. Medium sized pores (20-500 Å) V. Small heat of adsorption on small porous surface [71].

where C_s = the concentration of substance chemisorbed, C_w = the concentration of the substance in bulk solution, and n = a rate constant [52].

3.3.2.3 Adsorption Barriers. Prior to being adsorbed to a surface, molecules must overcome a number of energy barriers just to get in contact with the surface. The three different barriers, diffusion, electrical, and interfacial, are shown in Fig. 30.

The first barrier of diffusion (a), is the process of moving a molecule from the bulk solution or gas to the sublayer region where adsorption can take place. A general diffusion rate is given as

$$dN/dt = C_o T^{-\frac{1}{2}} \sqrt{D/\pi} \tag{17}$$

where N = number of moles, C_o = bulk solution concentration, D = diffusion coefficient, and T = temperature [70].

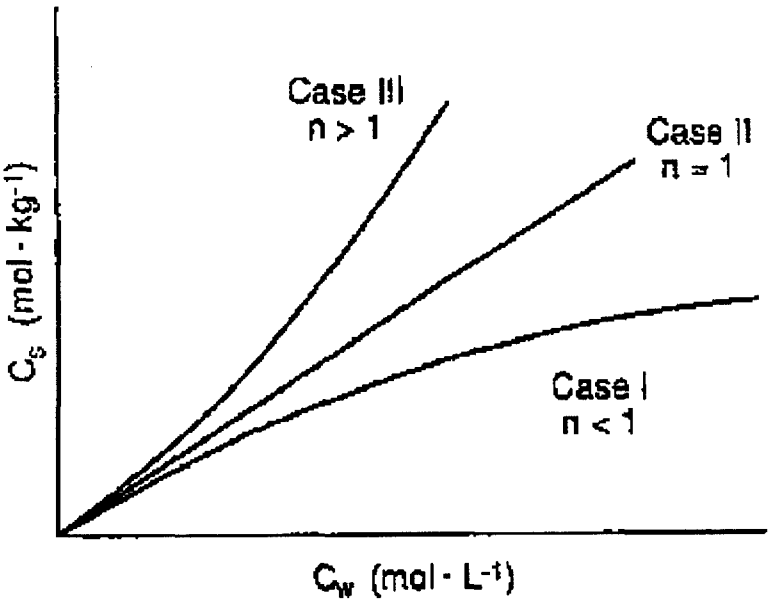

Figure 29. Freundich isotherm of chemisorption. For n < 1, sites are filled and new molecules must wait for a vacant site before they can sorb (weak chemisorption). For n = 1, a linear isotherm, sites are filled as they become available. For n > 1, previously adsorbed sites are sorbing additional molecules, forming multilayers (strong chemisorption) [52].

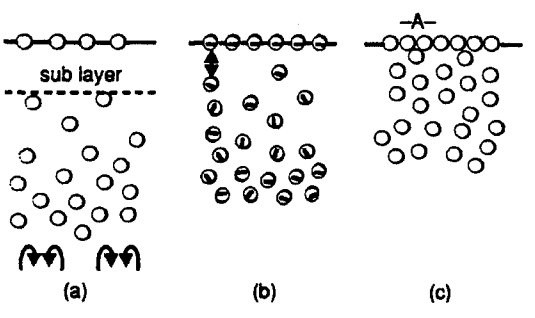

Figure 30. Barriers to adsorption: (a) diffusion, (b) electrical repulsion and (c) physical incompatability [70].

At the next barrier, (b), charges in molecules must overcome possible repulsion by like charges at the surface to be adsorbed. This rate is given by

$$dN/dt = k_1 C_o e^{-q\tau/kT} \tag{18}$$

where k_1 = rate constant, q = electronic charge, τ = electrical potential, and k = Boltzman's constant [70].

Once a molecule overcomes (a) and (b), it may still be too big to bind to an open site as shown in (c) [70]. In order for the molecule to bind, additional energy must be added to the system to force higher energy bonds.

3.3.3 Diffusion. Once a molecule has been bonded to the surface, it may do one of three things: 1) it may desorb from the site if it has enough energy to break the bond, 2) it may diffuse into the substrate, moving into an interstatial position, or 3) it may move laterally to another surface site. If a molecule diffuses into the substrate, it may assume a binding site in one of five ways as illustrated in Fig. 31.

A molecule may move into an open site (a), move into a neighboring interstatial site (b), push an existing atom out of its interstatial site (c), swap sites with a neighbor (d), or (e) swap sites with a number of neighbors [69]. These mechanisms can all be described via Fick's laws of diffusion.

3.3.3.1 Fick's Laws. Fick's Laws describe the rate of diffusion through matter based on the principle that a substance in a high concentration will seek a low concentration. The first law,

$$J = -D\partial N/\partial x \tag{19}$$

where D is a diffusion coefficient for the substance being diffused through and $\partial N/\partial x$ is the concentration gradient between an area of high concentration and low concentration, describes the molar flux of material through the substrate [61, 72]. The second law,

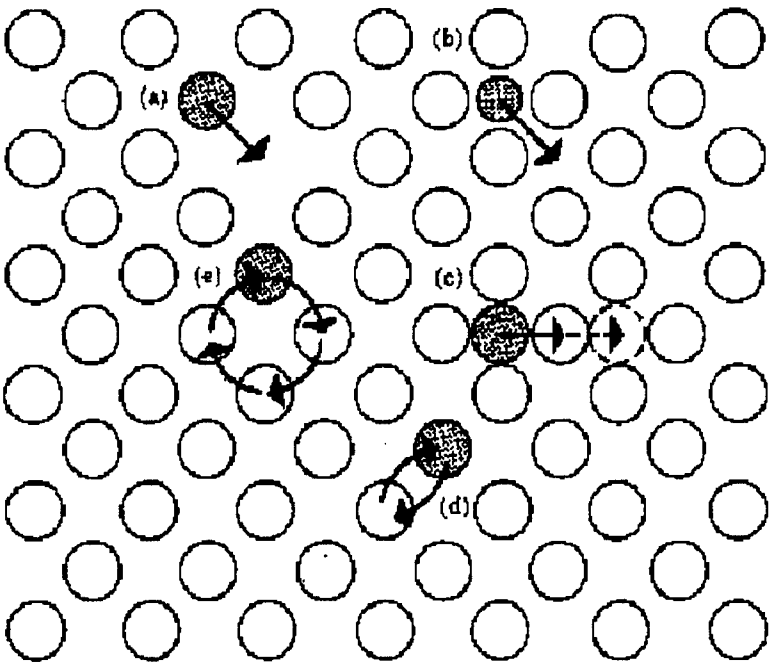

Figure 31. Diffusion mechanisms: (a) move to an open site, (b) move into a neighboring interstatial site, (c) push an existing atom out of its interstatial path, (d) swap sites with a neighbor or (e) swap sites with a number of neighbors [69].

$$\partial N/\partial t = -\partial J/\partial x = D\partial^2 N/\partial x^2 \tag{20}$$

is the general form of Eq. (17). Solutions for this equation that describe the concentration movement over distance from the surface can be taken from impurity doping models in solid-state manufacturing processes. The two models for this process are the Gaussian distribution for limited source doping and the complementary error function (Erfc) for constant source doping [72]. A concentration distribution based on the Erfc is given as

$$N(x) = N_o erfc\left(\frac{x}{2\sqrt{Dt}}\right) \tag{21}$$

where $N(x)$ is the impurity concentration, N_o is the surface impurity concentration, x is the distance from the surface, D is the impurity diffusion coefficient, and t is time. The Dt product is affected by impurity type, temperature and diffusion time. Since the solution or gas can be assumed to be a constant source, the Erfc is selected and shown in Fig. 32.

3.3.3.2 Surface Diffusion. As mentioned previously, one of the options an adsorbed molecule has is to diffuse laterally across the surface to another binding site. Whereas bonds must be broken to move from site to site, the free energy involved is still significantly less than that of desorbing completely ($\Delta G_{sur} \ll \Delta G_{des}$) [69]. While Fick's Laws still apply to this mechanism, a new diffusivity constant must be defined as

$$D_{sur} = \lambda^2 \nu_{dif} \tag{22}$$

where λ = the distance to the new site and ν_{dif} is defined as

$$\nu_{dif} = \nu_s e^{\frac{-\Delta G_{sur}}{kT}} \tag{23}$$

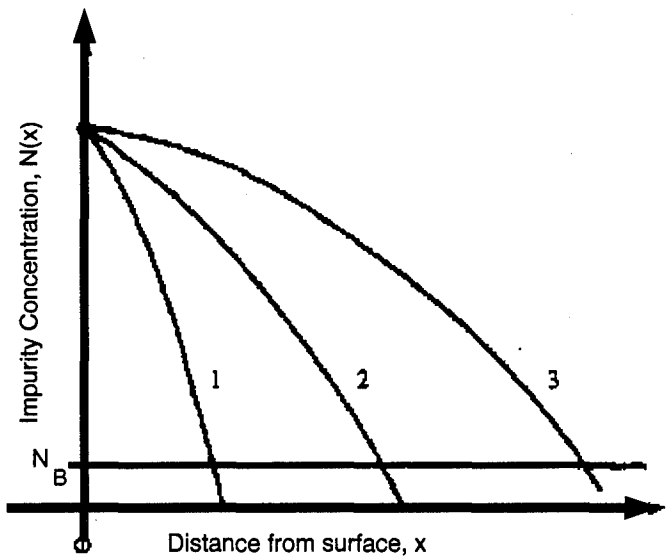

Figure 32. The complimentary error function distribution for constant source diffusion [72]. The Dt product is affected by impurity type, temperature and diffusion time. Three different Dt products are shown in the figure. N_B is the background impurity concentration. Junctions occur where the Erfc distributions cross the background level.

where ν_s = surface vibration frequency ($\simeq 10^{13} sec^{-1}$) [69].

3.4 Device Fabrication

Integrated circuit fabrication relies on a number of distinct processes to prepare, pattern, deposit, grow, or etch individual layers. This section describes the basic models used in these processes as well as the models used by TSUPREM-4 during fabrication simulation. The main topics to be covered include oxide growth, photolithography, diffusion, and metallization. In all cases, the substrate under consideration will be assumed to be (100) silicon initially doped with 10^{15} atoms/cm^3 of boron (p-type).

3.4.1 Oxide Growth. Silicon dioxide is used as an insulator on integrated circuits and is therefore critically important for device fabrication. By growing and masking oxides, active layers can be created and isolated from each other.

Oxides form on a silicon substrate upon exposure to atmospheric oxygen but are typically no more than 27 Å thick [61]. Thicker oxide layers can be deposited by chemical vapor deposition (CVD) or sputtering; however, the most common way is to grow oxide by forcing oxygen over the substrate at high temperatures (900-1200°C) [72]. Oxygen can be supplied in two ways: as a gas (dry oxide growth)

$$Si + O_2 \longrightarrow SiO_2 \tag{24}$$

or as water vapor (wet oxide growth)

$$Si + 2H_2O \longrightarrow SiO_2 + 2H_2 \tag{25}$$

Oxides grown in these ways grow both out and into the original substrate surface. Fractional values for this growth are given in Jaeger as 54% above the surface and 46% below [72].

The oxide growth on silicon is a function of temperature, pressure, and time and governed by Fick's First Law of Diffusion:

$$J = -D\partial N(x,t)/\partial x \tag{26}$$

where J is the particle flux, D is a diffusion coefficient for the process and N is the particle concentration. Oxygen must diffuse through the existing silicon dioxide interface till it reaches the substrate interface. As more oxide builds up, it takes more time for the oxygen to diffuse. As a result, oxide growth slows considerably after a period of time. A generalized model describing the thickness of oxide over time is given as

$$X_o(t) = 0.5A\left[\left[1 + \frac{4B}{A^2}(t+\tau\right]^{0.5} - 1\right] \tag{27}$$

where τ is an equivalent time to account for previous oxide growth, B = the parabolic growth rate constant and B/A = the linear growth rate constant [72]. Charts are available for values of B and B/A. Alternatively, the values can be calculated as

$$A = \frac{2D}{k_s} \tag{28}$$

where k_s is a rate constant at the substrate-oxide interface,

$$B = \frac{2DN_o}{M} \tag{29}$$

where N_o = concentration of the oxidizing species (O_2 or H_2O) at the substrate interface and M = number of oxidizing species used in a unit volume of oxide, and

$$\tau = \frac{X_i^2}{B} + \frac{X_i}{B/A} \tag{30}$$

where X_i = initial oxide thickness prior to the new oxide growth. For short times, $(t+\tau) \ll A^2/4B$, Equation 27 can be reduced to

$$X_o(t) = (B/A)(t+\tau) \tag{31}$$

and for long times, $(t+\tau) \gg A^2/4B$,

$$X_o(t) = \sqrt{Bt} \tag{32}$$

Besides being affected by temperature, pressure and time, oxide growth is also affected by impurities in the substrate and the oxidizing species. Oxide grows faster in doped silicon and in the presence of hydrochloric acid (HCl) at small concentrations (< 5%) [61]. The dopants act to weaken the silicon dioxide bonds, thereby making it easier for oxygen to diffuse to the substrate interface. Chlorine from the HCl removes impurities from the substrate interface, increasing the surface efficiency.

3.4.2 TSUPREM-4 Diffusion Model. TSUPREM-4 uses an oxidation model based on the Deal and Grove theory [73] in which the vector flux of the oxidant (J) is

$$\vec{J} = h(C^* - C_o)\vec{n_s} \tag{33}$$

where C_o is the oxidant concentration at the oxide surface, $C^* = HP_{ox}$ where H = Henry's law coefficient for the oxidant, P_{ox} is the partial pressure of the oxidant at the ambient temperature, and $\vec{n_s}$ is a unit vector in the direction of the wafer surface [74]. The oxide growth rate can be described as

$$\frac{d\vec{Y}}{dt} = \frac{\vec{J}}{N_1} + r_{thin} \tag{34}$$

where $d\vec{Y}/dt$ is the interface velocity of oxidants striking the surface, N_1 is the number of oxidant molecules per cubic unit of oxide growth and r_{thin} is a term to account for rapid initial growth [74]. Deal and Grove build their model from Fick's Law (Eq. 26). In one dimension, Eq. 34 becomes

$$\frac{dy}{dt} = \frac{B}{A + 2y} \tag{35}$$

where A is given by Eq. 28 and B by Eq. 29.

3.4.3 Dopant Diffusion. Doping is used primarily to form p-n junctions for electronic devices. The process of doping is accomplished in two steps: an initial deposition in which a known dose, or number of dopant atoms per unit area, is deposited on the substrate surface from a constant source; and a drive-in step to force the dopant into the substrate. In the process used to fabricate sensors in this thesis, the dopant is used to increase the concentration of boron atoms to provide an effective etch stop and no drive-in step was used.

There is a limit to the amount of dopant that can be adsorbed into the silicon substrate at a given temperature. This limit is called the solid-solubility limit and can be found in tables and charts. For a diffusion of boron at 1150^oC, the solid-solubility limit is given as 4 x 10^{20} atoms/cm^3 [72].

3.4.4 Spin Coating. Spin coating uses the forces of angular acceleration at high rpm's to uniformly spread a liquid over a surface. In this application, spin coating was used to apply photoresist to the silicon wafers in preparation for a photolithographic masking. The thickness of the spun layer (l_R) is a function of the liquid's viscosity, the speed at which the substrate is spinning, and the percentage of solids in the applied coating [61]:

$$l_R = \frac{(viscosity)(\%solids)}{\sqrt{spinspeed}} \tag{36}$$

This value does not account for evaporation that may occur.

3.4.5 Lithography. After the photoresist has been applied, the wafer is lithographically processed. A mask is placed in proximity to the surface and exposed to ultraviolet radiation. For a negative resist, the UV light strengthens the area of the photoresist not masked, leaving the unexposed areas open when developed. For a positive resist, exposed areas are weakened, leaving the masked areas intact after development with the exposed areas open.

As successive masks are placed over the same wafer, alignment error must be accounted for and typically limits the resolution of features. Other limits include the cleanliness of the room (presence of impurities that may land on a device surface) and the exposure response of the photoresist. The photoresist exposure response is a function of the required threshold energy to become completely soluble.

3.4.6 Photoresist Removal. The final step of lithography is the removal or lift-off of the applied photoresist. This step can be accomplished through dry or wet processing. In the dry process, the photoresist is stripped away in an oxidizing plasma called plasma ashing. More typically, the photoresist is removed by a wet chemical such as acetone, or a proprietary removal substance. Lift-off is critical as a final step when depositing a layer over the photoresist and onto an exposed area of the device. To ensure proper lift-off, the photoresist must make contact with the removal agent. This means that the deposited layer cannot completely cover the sidewalls of the photoresist as shown in Fig. 33. A general rule adopted in this thesis was to have a minimum 2:1 ratio of photoresist thickness to deposited layer thickness.

3.4.7 Chemical Etching. Chemical etching follows three steps: 1) chemicals are brought to the wafer surface via diffusion, 2) a chemical reaction takes place, and 3) reaction products are carried away by diffusion [61]. Two basic etchant solutions will be briefly discussed. The first etch of 3:2, sulphuric acid (H_2SO_4): hydrogen peroxide (H_2O_2) removes all organic material from the wafer

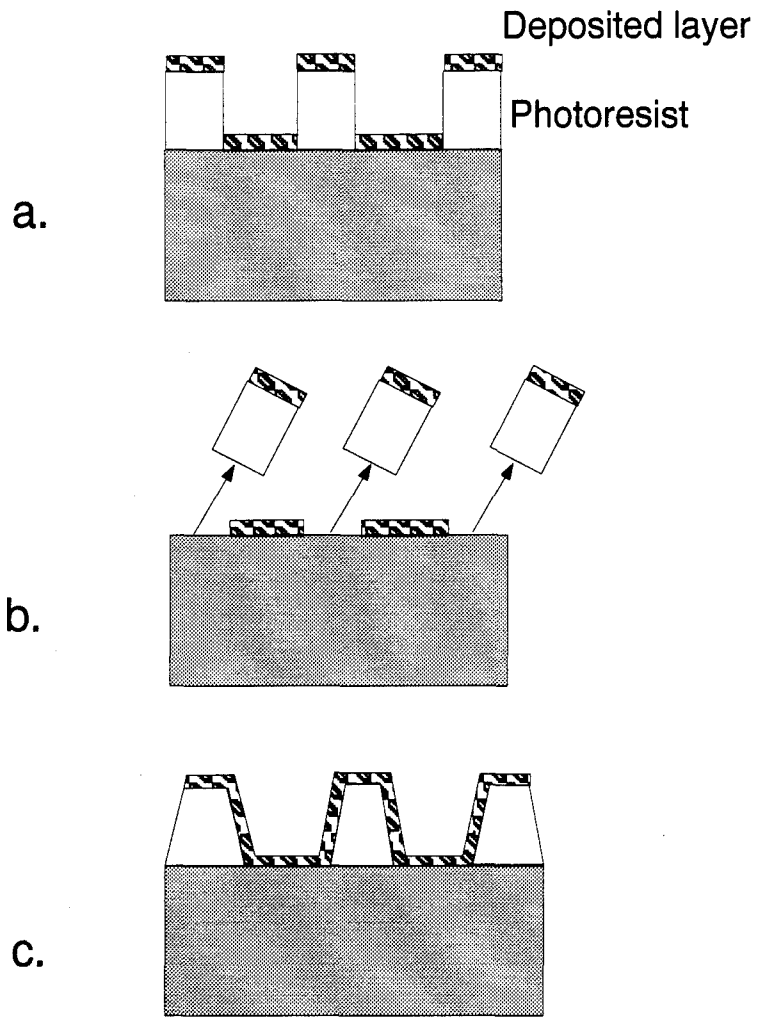

Figure 33. Photoresist liftoff process. If the photoresist patterning forms good straight walls as in (a), photoresist remover (such as acetone) can attack the exposed photoresist and remove the deposited layer on top as in (b). If the walls are slanted as in (c), the deposited layer forms a barrier that the photoresist remover cannot readily penetrate.

surface without etching the substrate silicon or silicon dioxide [61]. This is a cleaning "piranha" etch used before a process such as oxide growth or photoresist application is performed.

The second etch isotropically etches silicon dioxide after a photolithographic mask has been applied. The solution uses a buffered mixture of 4:1, ammonium fluoride (NH_4F): hydrofluoric acid (HF). This etch is used to expose the silicon substrate after an oxide growth in order to deposit thin films or allow a diffusion of dopants. The basic reaction is given as [61]

$$SiO_2 + 6HF \longrightarrow H_2SiF_6 + H_2O \tag{37}$$

While isoetch curves are available for this solution, actual rates are found empirically.

3.4.8 Etch Stops. The final release of a MEMS device using an anisotropic etchant such as EDP or KOH relies upon selective etch rates along crystalline orientations. Etches can also be controlled by heavily doping ($>2.5x10^{19}$ atoms/cm^3) a region with boron [10]. The relative etch rate of EDP in a high boron concentration is shown in Fig. 34. Boron can be diffused into a region or implanted to create etch stops or regions of silicon that will not be eaten away as readily as undoped regions.

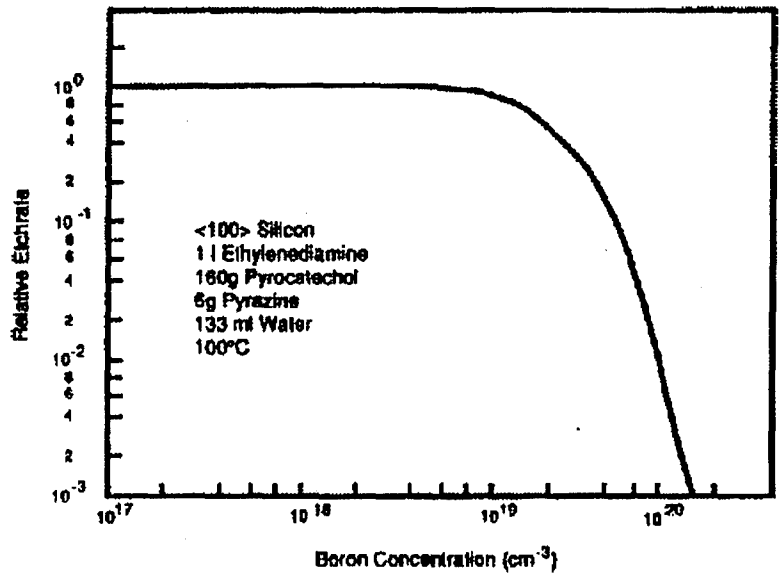

Figure 34. The effects of boron concentration on EDP etch rates [10].

IV. Device Designs

You get what you want, then you never want it again.

Violet, Hole

4.1 Introduction

Several sensor designs were completed and sent out to commercial foundries for fabrication. Bulk micromachinined devices were fabricated through MOSIS and surface micromachined devices were fabricated through MUMPS. This section describes the different device designs that were sent to be fabricated over eight different fabrication runs including device dimensions. Also included are the results of the runs and the actual devices that were returned.

4.2 Fabrication Schedule

Most of the devices used in this thesis were manufactured outside AFIT. Bulk micromachined devices using CMOS p-well technology were designed using MAGIC version 6.0 and fabricated through MOSIS. Surface micromachined devices were designed using Cadence version 4.3.3 and fabricated through MUMPS at MCNC. A schedule of fabrication runs for both processes is shown in Table 8.

4.3 Fabrication Results

Results from each fabrication run varied in terms of parameters (i.e. resistivity of materials and layer thickness) and manufacturing quality. Other fabrication problems were specific to each run and are described below.

Table 8. Micromachining Fabrication Schedule.

Run Name	Type of Fabrication	Design Complete	Devices Received
MUMPS 6	Surface	14 Nov 94	26 Feb 95
CMOS 3	Bulk	28 Dec 94	1 May 95
MUMPS 7	Surface	27 Feb 95	14 May 95
CMOS 4	Bulk	5 Apr 95	14 Jun 95
CMOS 5	Bulk	3 May 95	1 Jul 95
MUMPS 8	Surface	15 May 95	13 Aug 95
MUMPS 9	Surface	14 Aug 95	23 Oct 95
CMOS 6	Bulk	14 Sep 95	27 Nov 95

4.3.1 MUMPS 6. This was primarily a trial run to gain familiarity with the Cadence design software and the MUMPS surface micromachining process. Only three designs were incorporated into this run and each relied on changes in conductivity in a thin film. The first two devices were chemoresistors with interdigitated elements to measure the changes as shown in Figs. 35 and 36. The middle element could be used as a heater to reset the device after a sensing cycle was completed.

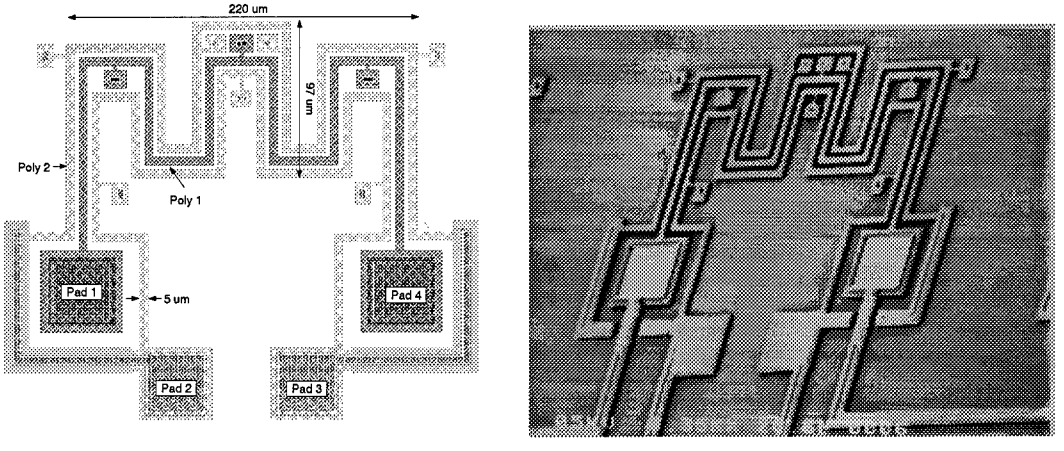

(a) (b)

Figure 35. Device 1: Heated chemoresistor 1. A thin film is applied over the entire surface area contacting the polysilicon fingers. The resistance between the two elements (poly 1 and poly 2) is measured. The poly 1 element can be heated to reset the sensor at the end of the sensing period. An SEM micrograph of the device is shown in (b).

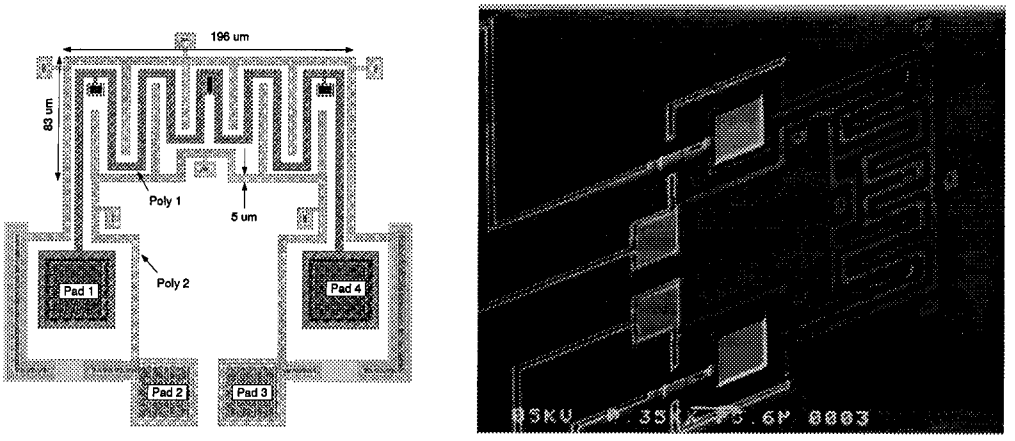

(a) (b)

Figure 36. Device 2: Heated chemoresistor 2. This device is similar to Device 1 with a larger interdigitated area. An SEM micrograph of the device is shown in (b).

The third device on this run utilized a polysilicon table supported over a heating element. A thin film would be applied to the table and heated. The rate at which heat escaped would be controlled by the mass of the film. This design was not successful due to fabrication problems in MUMPS 6, 7, and 8 in which the poly 1 heating layer did not have enough separation from the poly 2 sensing layer and thus shorted. The device is shown in Fig. 37.

Statistics for the MUMPS 6 run were provided in Table 4 in Chapter 1.

4.3.2 CMOS 3. This run was also a preliminary run to gain experience with MAGIC and bulk micromachining. A transfer error in the CalTech Intermediate File (CIF) to the fabrication plant caused a production error in which necessary field oxide cuts were not made. Once identified, the design was re-CIFed and sent back to the plant. One problem this caused besides the time lag was that problems in devices were perpetuated into the CMOS 4 and CMOS 5 runs as their design dates were due before the second CMOS 3 run was returned. One problem noted that would have been corrected was that the large devices such as those shown in Figs. 38 and 39 on this run did not release easily. Release times of three to four hours were necessary to fully underetch the larger cantilever sensors, by

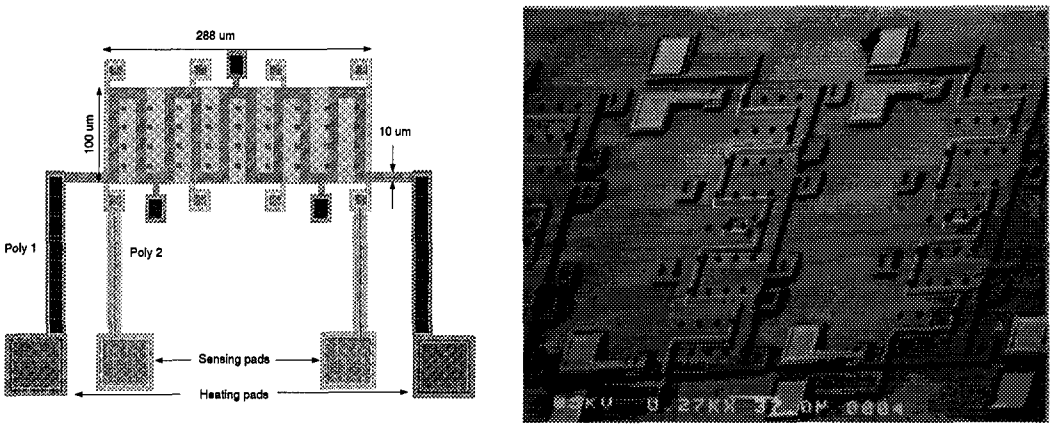

(a) (b)

Figure 37. Device 3: Heated conductivity sensor. A thin film would be applied to the suspended poly 2 table and heated. The rate at which heat escapes would be controlled by the mass of the film. The perforations on the top poly layer are release holes to allow the etchant access to subsurface oxide layers. An SEM micrograph of the device is shown in (b).

which time the exposed aluminum pads were also eaten away. Only small devices such as the heat activated bridge in Fig. 40 released after only an hour with enough aluminum on the pads to allow adequate bonding and measurements to take place. A variant of Device 7 in Fig. 40 was the only design that provided measurable responses to challenge chemicals. Device 8 differs from Device 7 in that Device 8 has a larger surface area. It is shown in Fig. 41.

4.3.3 MUMPS 7. A number of different sensing strategies were incorporated into this run such as electrostatically-driven and heat-driven pads. However, this run had significant fabrication problems and none of the devices were able to be properly released. The problem on this run was bad fabrication of the oxide between the poly 1 and poly 2 layers in which insufficient oxide was deposited to properly isolate these two active layers. As a result, the two polysilicon layers bonded together forming mechanically immobile and electrically shorted structures. Design of new devices on this run stemmed from movable mirror work done in other research [65]. Instead of applying metal to the poly 2 surface, a thin film was to be applied. A poly 1 heating element was included below the moving structure to provide reset capability; however, as mentioned above, the process did not properly release.

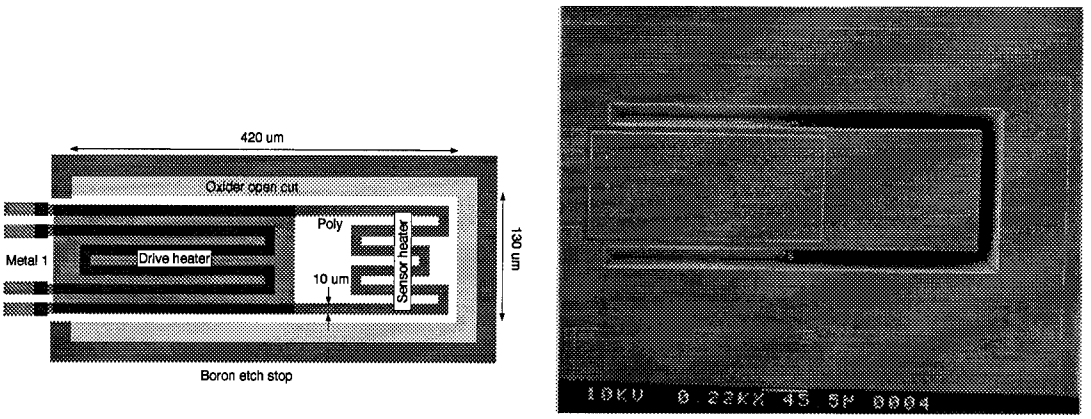

(a) (b)

Figure 38. Device 4: Heated Actuator Sensor. Bimorphic action drives the actuator at the base while a thin film is applied to the end. As the mass increases due to chemical loading, the actuation motion will be affected and measured. A polysilicon heater is embedded at the end to regulate temperature and provide a reset capability at the end of a sensing cycle. An SEM micrograph of the device is shown in (b). Note that the device is not completely released.

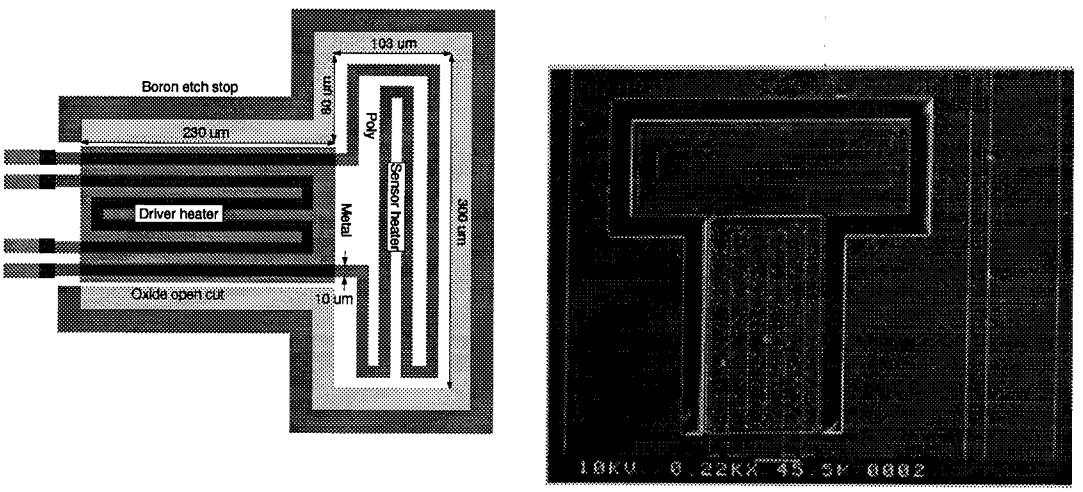

(a) (b)

Figure 39. Device 5: Hammerhead heated actuator sensor. This device is a variation of Device 5 taking advantage of a larger thin film surface area. An SEM micrograph of the device is shown in (b).

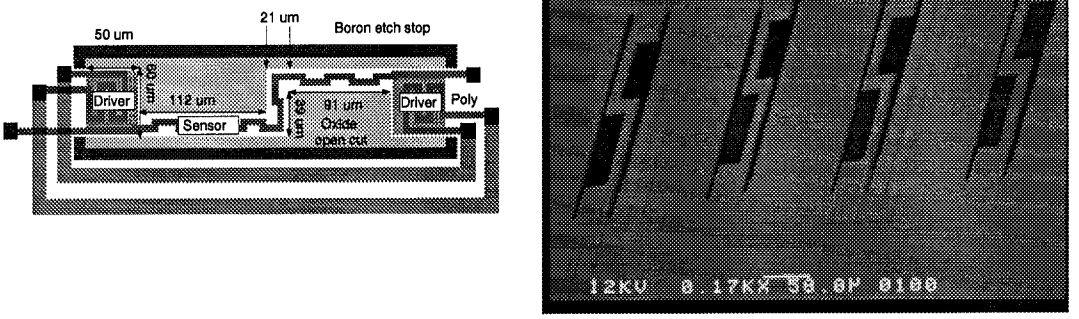

(a) (b)

Figure 40. Device 6: Heat actuated resonating bridge. This device also uses the mass loading concept of Devices 4 and 5; however, instead of a single drive heater, two drivers are used at both ends of the suspended structure. A thin film is applied to the suspended surface. A frequency sweep of the center silicon sensor element is conducted while the entire bridge is driven at low frequencies (>100 Hz). The changing mass of the device affects its motion and the sensor impedance. An SEM micrograph of the device is shown in (b).

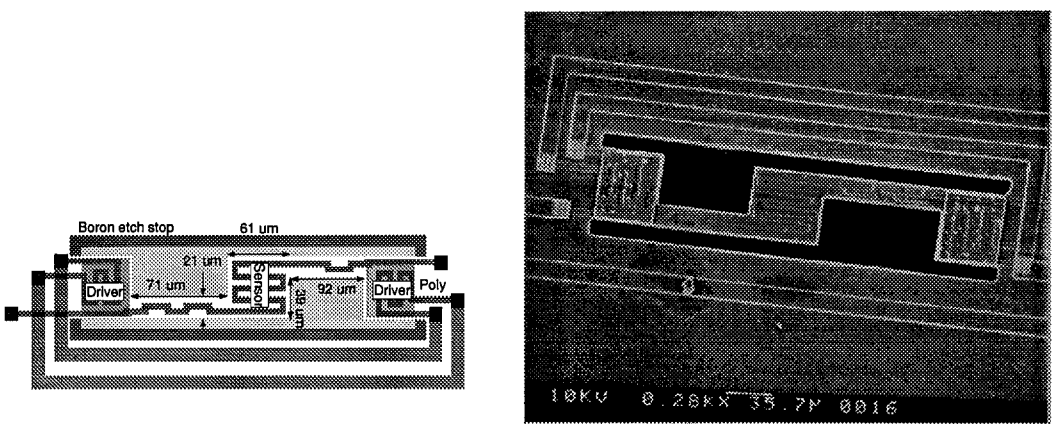

(a) (b)

Figure 41. Device 7: Heat actuated resonating bridge 2. This device is similar to Device 6 and was the only CMOS design that worked. An SEM micrograph of the device is shown in (b).

The basic device design is shown in Figure 42. While several different surface designs were tried such as circles and squares, none worked effectively, even in later runs. Statistics for this run are given in Table 9.

Table 9. Statistics for the MUMPS 7 Fabrication run. (C) = compressive stress, (T) = tensile stress.

Layer	Thickness (Å)	Stress (MPa)	Resistivity (ohm-cm)
poly 0	4880	–	2E-3
poly 1	20100	8.0 (C)	1.65E-3
poly 2	14706	11.1 (C)	1.54E-3
metal (Cr/Au)	5318	21 (T)	3.30E-6
nitride	6049	41.0 (T)	–
oxide 1	20400	–	–
oxide 2	5281	–	–

4.3.4 CMOS 4. This bulk micromachining run incorporated many of the devices originally designed for CMOS 3 but also incorporated a trampoline style sensor with a polysilicon heating element under a polysilicon conductivity sensor element. As with CMOS 3, many of the larger devices did not release due to their size. Since CMOS 3 returned after CMOS 4 and CMOS 5 designs were due, the lessons learned could not be incorporated into later runs until CMOS 6. The heated trampoline sensor is shown in Fig. 43.

4.3.5 CMOS 5. This bulk micromachining run was similar to CMOS 4 but with additional test structures not directly related to this research. As with CMOS 3 and CMOS 4, many of the larger devices did not release due to their size. Another difference from the other CMOS runs was a thinner

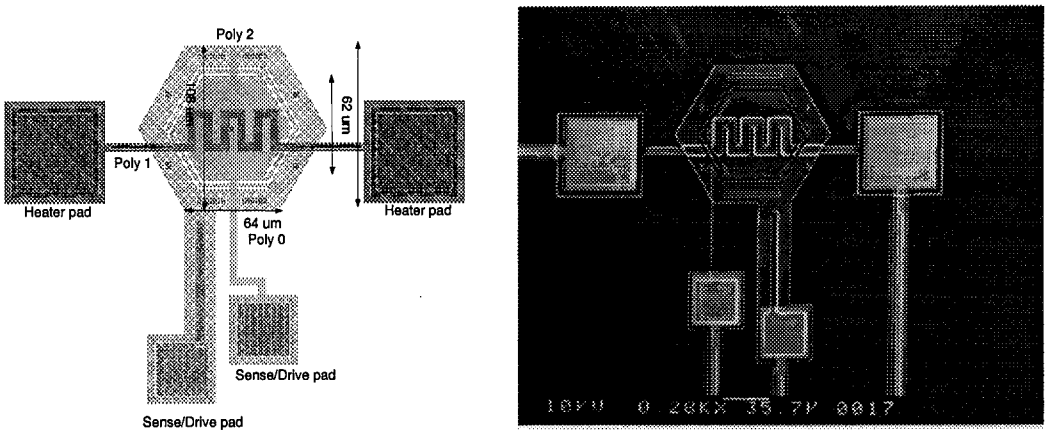

Figure 42. Device 8: Electrostatic Heated Sensor (MUMPS 7). This device uses electrostatic attraction between the suspended poly 2 and the surface layered poly 0. The design was intended to have higher operating frequencies than the heat actuated devices. A problem with this design and associated designs was a lack of measuring capabilities. Experience gained from these designs led to better designs in later fabrication runs. An SEM micrograph of the device is shown in (b).

layer of aluminum on the bonding and probe pads. This defect meant that release times could not exceed 60 minutes before severe deterioration of the pads occurred. As a result, none of the larger devices released completely and only small devices like Devices 6, 7 and 9 were used.

4.3.6 MUMPS 8. This run was a repeat of MUMPS 7 in order to validate the operation of the devices caused by fabrication errors. While this run was successful, inherent design problems of the devices and the overall fabrication process were reasons devices on this run failed. Devices on this design included electrostatic devices such as Device 4 and the heated conductivity sensor of Device 3.

4.3.7 MUMPS 9. The final MUMPS run in this research incorporated many new designs gained from the experience working with the earlier fabrication results. A total of six new designs were included that improved upon original designs. These designs are shown in Figs. 44, 45, 46, 47, 48, and 49. The fabrication statistics for this run are given in Table 10.

Table 10. Statistics for the MUMPS 9 Fabrication run. (C) = compressive stress, (T) = tensile stress.

Layer	Thickness ($\mathring{A}$)	Stress (MPa)	Resistivity (ohm-cm)
poly 0	5122	3 (C)	1.5E-3
poly 1	19948	3 (C)	2.2E-3
poly 2	15048	6 (C)	3.0E-3
metal (Cr/Au)	4923	5 (T)	3.0E-6
nitride	6243	67 (T)	–
oxide 1	20008	–	–
oxide 2	7598	–	–

4.3.8 CMOS 6. A design package was submitted for this run on 14 Sep 95; however, it returned too late to be included in this thesis. New designs incorporated for this run included new trampoline sensor designs with aluminum contacts on the device surface (Fig. 50), a resonating bridge structure driven in the middle instead of the ends (Fig. 51), and a heated actuator with angled geometry to facilitate the release process (Fig.52).

4.4 Summary of Designs

4.4.1 Terminology. In order to compare the physical characteristics of the designs, the following terms are defined:

Total Sensor Area (TSA). This refers to the total surface area of the sensor including active sensing surface, drive structures, and support. It does not include bond and probe pad areas. This measure describes the overall size of the sensor.

Heater Area (HA). This measures the total amount of space occupied by a heating element. In some devices with multiple heaters, a distinction is made between drive heaters (DHA) and sensor heaters (SHA).

Sensor Area (SA). This measures only the active sensing surface area of the device; i.e., the area over which the thin film is applied.

4.4.2 Device Comparison. The following tables show the physical differences between the different device designs. Table 11 shows devices included in the MUMPS 6, 7 and 8 runs. Table 12 shows devices included in the CMOS 3, 4 and 5 runs. Table 13 shows devices included in the MUMPS 9 run.

Table 11. MUMPS 6, 7, and 8 device summary. TSA is total sensor area , HA is heater area, and SA is sensor area/length.

Device Number	Device Name	MUMPS Run	TSA	HA	SA
1.	Heated chemoresistor 1	6	13503 μm^2	3215 μm^2	13503 μm^2
2.	Heated chemoresistor 2	6	17678 μm^2	—	17678 μm^2
3.	Heated conductivity sensor	6, 7, 8	28080 μm^2	12000 μm^2	28080 μm
8.	Electrostatic heated platform	7, 8	3286 μm^2	985 μm^2	3286 μm^2

Table 12. CMOS 4 and 5 device summary. TSA is total sensor area , DHA is driver heater area, SHA is sensor heater area and SA is sensor area.

Device Number	Device Name	TSA	DHA	SHA	SA
4.	Heat actuated sensor	54600 μm^2	9000 μm^2	12400 μm^2	14300 μm^2
5.	Hammerhead heat actuated sensor	59770 μm^2	9000 μm^2	16210 μm^2	30900 μm^2
6.	Heat actuated resonating bridge 1	10704 μm^2	2420 μm^2 total	2615 μm^2	4704 μm^2
7.	Heat actuated resonating bridge 2	13083 μm^2	2420 μm^2	3365 μm^2	7083 μm^2
9.	Heated trampoline sensor	8836 μm^2	3234 μm^2	2421 μm^2	7225 μm^2

Table 13. MUMPS 9 device summary. TSA is total sensor area, HA is heater area, and SA is sensor area/length.

Device Number	Device Name	TSA	HA	SA
10.	Comb-driven electrostatic mass balance sensor	6105 μm^2 per pad	3375 μm^2 per pad	3375 μm^2 per pad
11.	Comb-driven (large)	11550 μm^2 per pad	6810 μm^2 per pad	6810 μm^2 per pad
12.	Heated interdigitated chemoresistor	44010 μm^2	10870 μm^2	1458 μm
13.	Heated-pad chemoresistor	102025 μm^2	94000 μm^2	67190 μm^2
14.	Electrostatic bridge	17325 μm^2	7960 μm^2	7960 μm^2
15.	Electrostatic bridge	17325 μm^2	7960 μm^2	7960 μm^2
16.	Dual-element electrostatic bridge	9450 μm^2 per pad	3550 μm^2 per pad	3550 μm^2per pad

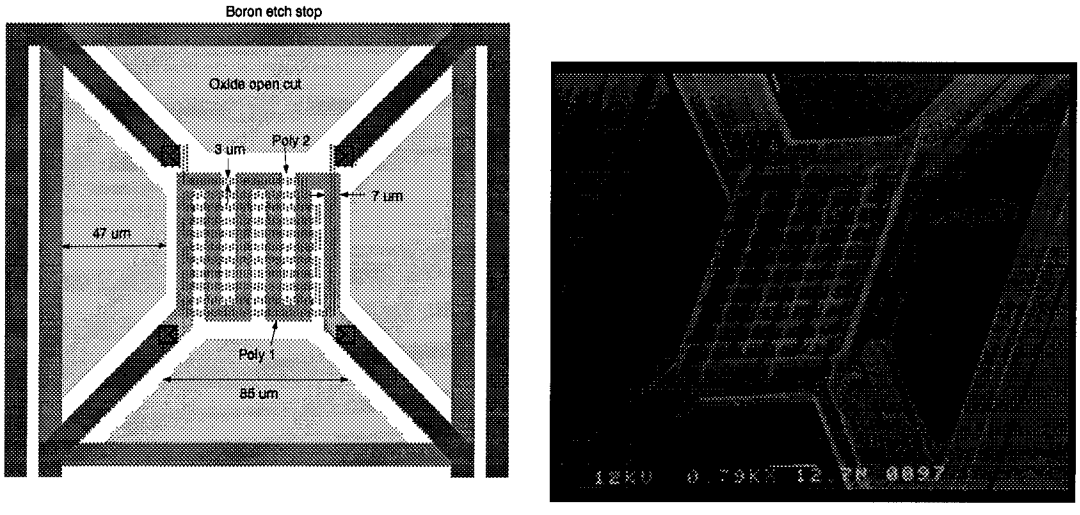

(a) (b)

Figure 43. Device 9: Trampoline heater sensor. This device is similar to Device 3, the heated conductivity sensor in which an embedded heater heats a resistive element that has an applied thin film. Heat conduction from the device is affected by the mass loading of the thin film which in turn affects the resistance of the top element. Unlike Device 3, this process uses silicon dioxide to isolate the two polysilicon layers. The poly 1 layer is used to heat the device while the poly 2 layer acts as the sensing element. This device did not provide any measurable response. An SEM picture of the device is shown in (b).

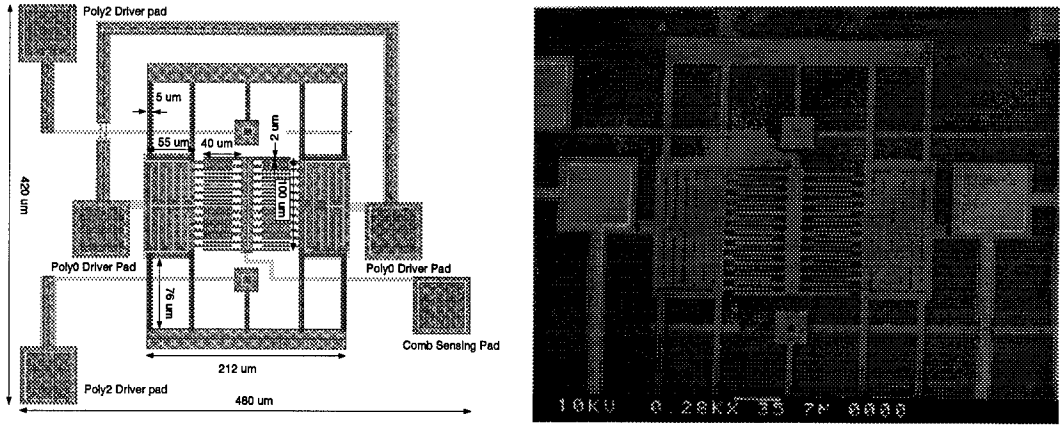

(a) (b)

Figure 44. Device 10: Comb-driven electrostatic mass balance sensor design (a) and SEM micrograph (b).

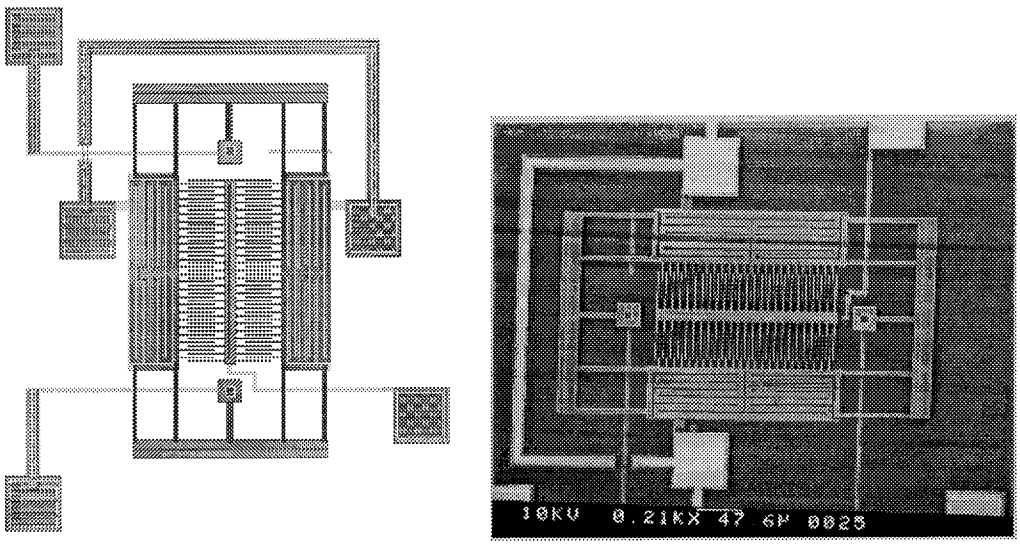

(a) (b)

Figure 45. Device 11: Comb-driven (large) electrostatic mass balance sensor design (a) and SEM micrograph (b).

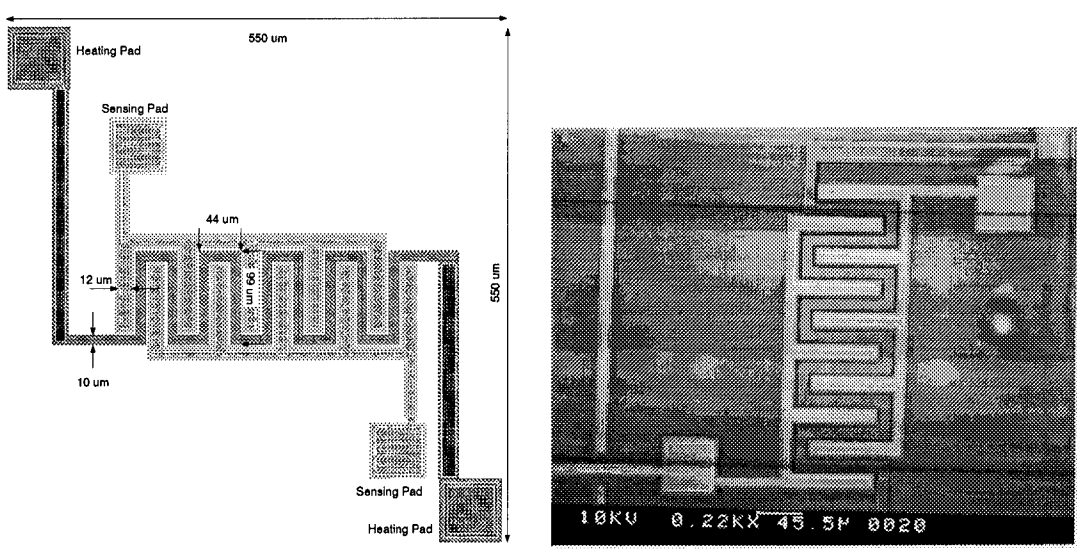

(a) (b)

Figure 46. Device 12: Heated interdigitated chemoresistor design (a) and fabricated scan (b).

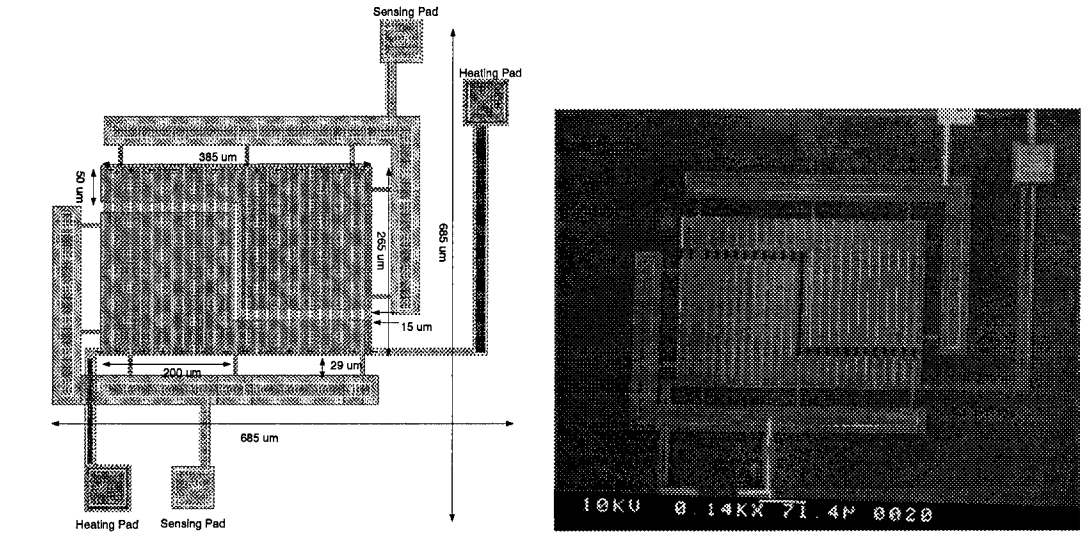

(a) (b)

Figure 47. Device 13: Heated-pad chemoresistor design (a) and fabricated scan (b).

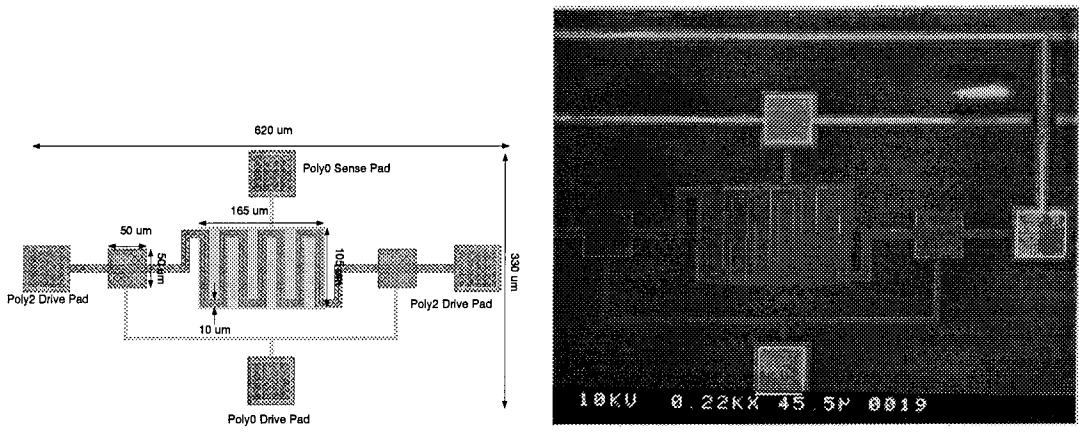

(a) (b)

Figure 48. Device 14: Electrostatic bridge sensor design (a) and fabricated scan (b).

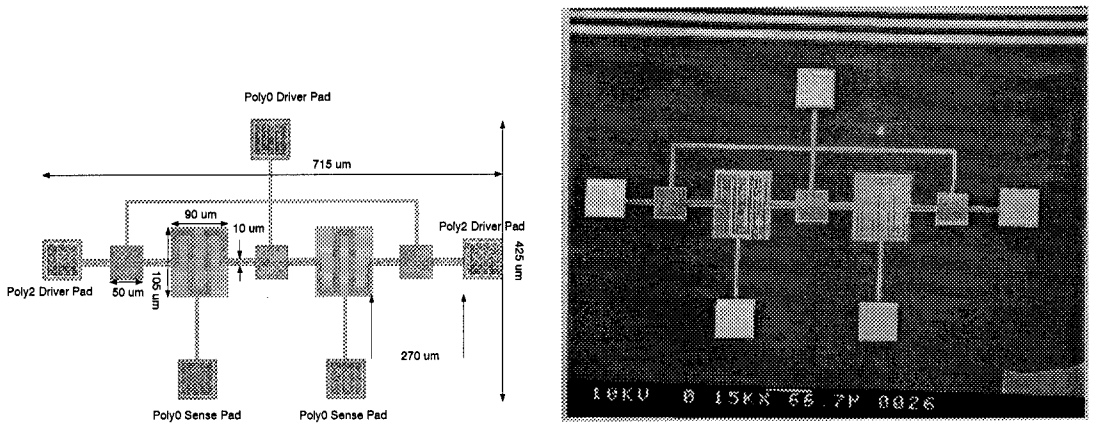

(a) (b)

Figure 49. Device 15: Dual-element electrostatic bridge sensor design (a) and fabricated scan (b).

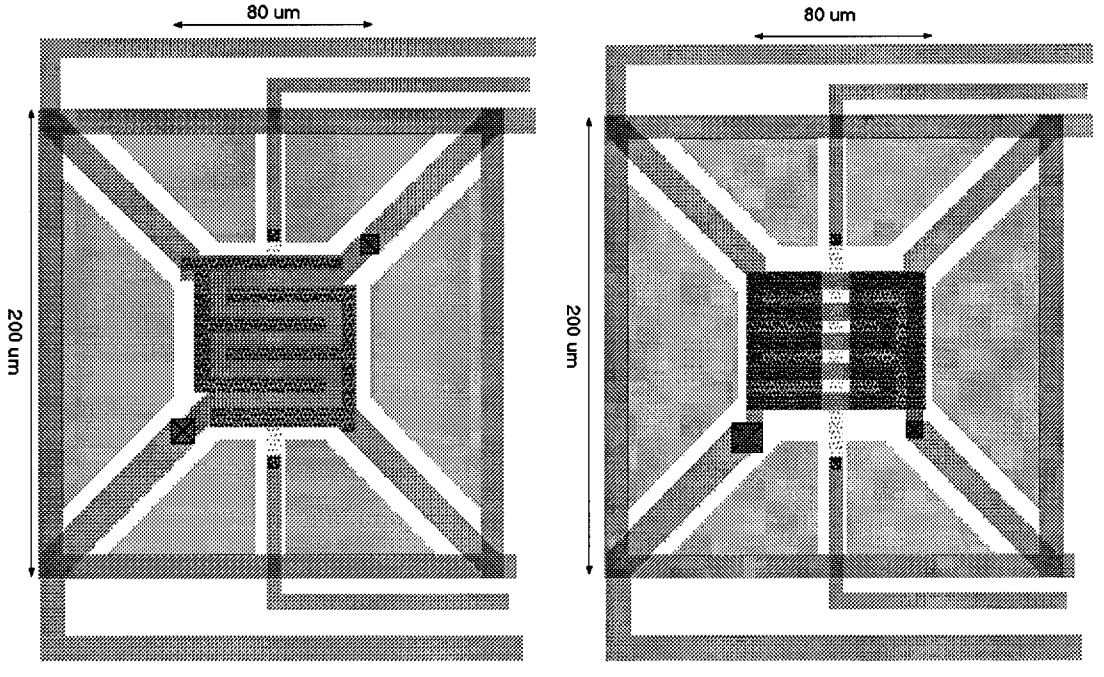

(a) (b)

Figure 50. Devices 16 and 17: Metal padded trampoline sensors. These redesigns of Device 9 use the aluminum pad layer as the sensing electrodes and incorporate a poly 2 temperature sensing element. Device 16 in (a) uses interdigitated electrodes while Device 17 in (b) uses pads.

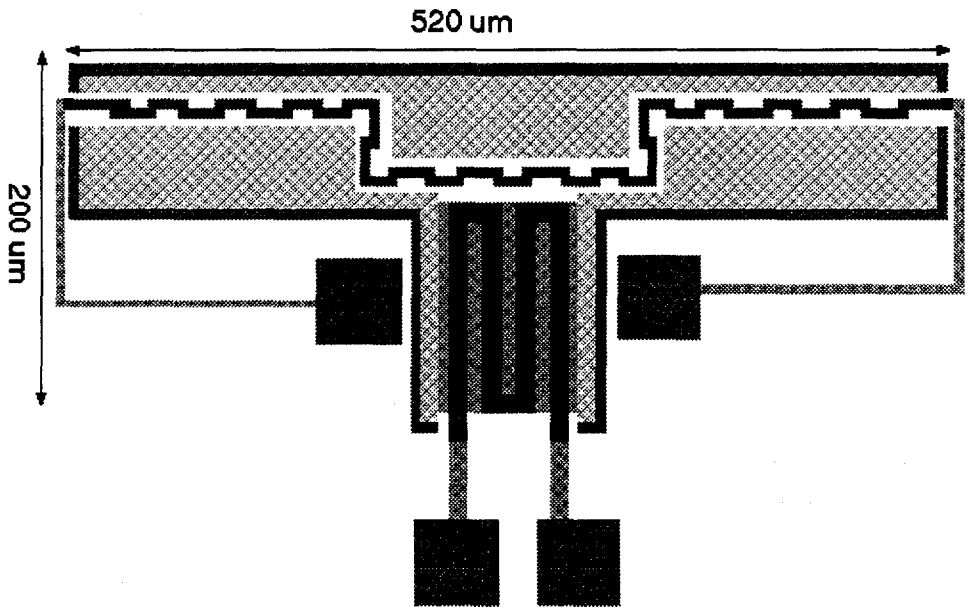

Figure 51. Device 18: Resonating bridge sensor 3. Unlike Devices 7 and 8, the bridge structure is driven by flexing the middle of the device.

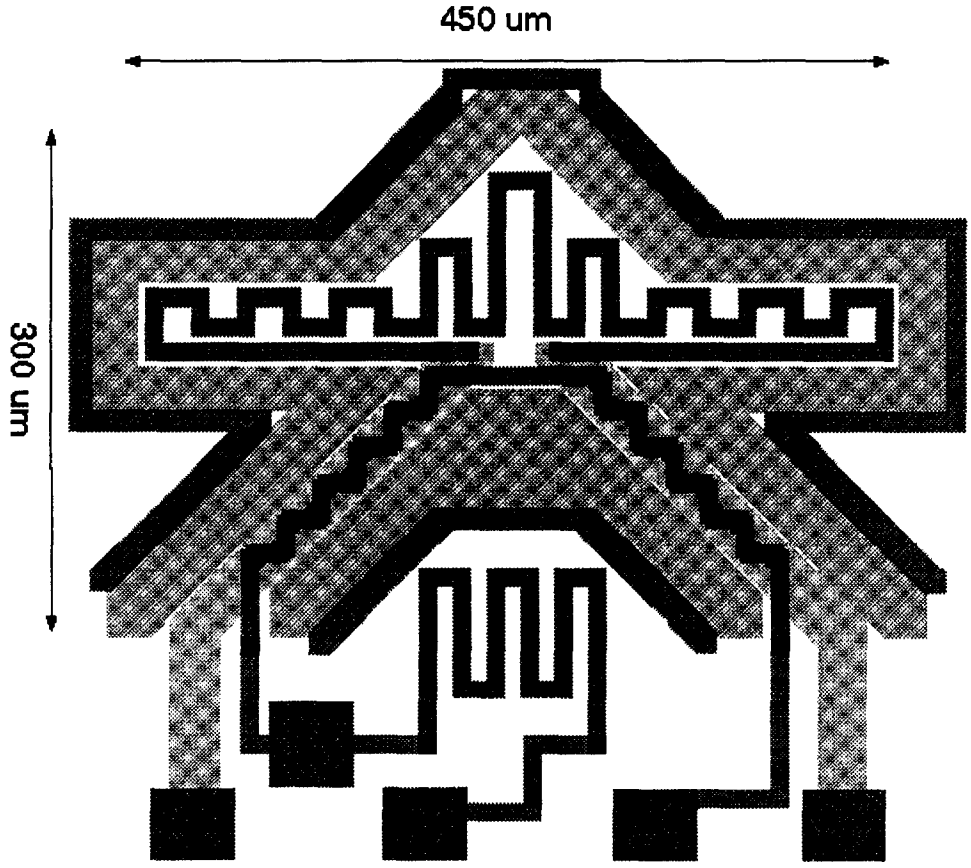

Figure 52. Device 19: Angled hammerhead actuator sensor. Because of the device release problems associated with rectangular actuators, an angled device was designed with 45^{o} sides to exploit the etchant's crystalline orientation selectivity.

V. Thin Film Application

Things worked out better than we had planned.

Everything's Ruined, Faith No More

5.1 Introduction

In order to make a chemical microsensor, a thin film must applied to the sensing area (SA). This section describes the various processes used to deposit thin films on a specific area of a die. A straight deposition over the entire chip could not be done. Bond pads must be exposed for wire bonding and packing while depositing only one thin film eliminates the opportunity of depositing many films on a single chip for array sensing. A photolithographic process was used on all sensing devices to deposit the chemically sensitive thin film only on the SA of both CMOS and MUMPS fabricated dies. The SA is the active area on the device in which adsorption takes place. The basic steps to apply a thin film to a device using a photolithographic process are:

1. Make a photolithographic mask.
2. Spincoat photoresist onto the die.
3. Align the mask to the devices, expose, develop, and postbake the die.
4. Apply the thin film.
5. Remove the resist mask via lift-off.

5.2 *Laboratory Procedure*

A number of toxic and carcinogenic chemicals were used in this research and special care was taken to prevent and minimize exposure. All work was done in hooded workbenches that were annually certified by Bioenvironmental Engineering. Personal protection measures (PPM) included latex gloves (Ansell Industrial Products) and respirators with organic vapor filters (Freedom 2000 Series, Wilson Safety Products, Reading, PA). Generated waste was placed in individually labeled containers and disposed of through the 88 EM Hazardous Waste Program.

5.3 *Mask Making*

Masks were made for each individual fabrication run design, as each layout was different. The complete mask making process using Cadence and MAGIC, as well as masks used, is given in the Appendix. A 50:1 reduction standard was used for all masks once a transparency of the desired mask was hung in the center of a backlit wall (Model TM-8, Lektra Laboratories, New York, NY). Rubylithe was used to shade the wall area which was not part of the mask in order to reduce bleedthrough in the final print.

A mounted 35mm camera (Dekacon Camera System) reduced the image onto 4-inch glass photolithography plates (Kodak High Resolution Plate, Type 1A) in 1 minute exposures. Once developed, these plates would be the masks.

The plates were developed in three stages of developer (Kodak HRP Developer), Stop of 50 ml acetic acid ($C_2H_4O_2$, Sigma Chemical Co., St Louis, MO): 1 gal of deionized water, and fixer (Kodak HRP Fixer) with two-minute immersions in each bath.

5.4 *Photolithographic Process*

5.4.1 Preparation. Prior to photoresist application and exposure, all devices were cleaned in acetone for five minutes to remove organics and rinsed for two minutes each in deionized water and

2-propanol. The dies were dried by placing them on a heated glass slide and allowing the 2-propanol to evaporate. A 3:2 sulphuric acid (H_2SO_4):30% hydrogen peroxide (H_2O_2) piranha etch was not used for devices because it reacted with the aluminum pads on the CMOS chips.

5.4.2 Negative Photoresist Application and Development. For masks requiring a negative photoresist, Waycoat HR 200 (Olin Hunt, West Patterson, NJ) was liberally applied to a die mounted on a vacuum spincoater (Photo-Resist Spinner, Headway Research, Inc., Garland, TX) and allowed to spin at 5000 rpms for 30 seconds. The photoresist was allowed to soft-bake at 65° Celsius for 15 minutes before being exposed in the mask aligner. Once exposed, the dies were developed by applying xylene (Mallinckrodt, Paris, KY) and butyl acetate ($C_6H_{12}O_2$, EM Chemicals, Darmstadt, Germany) while spinning at 500 rpms for 30 seconds each. The die was then hard-baked at 135° Celsius for fifteen minutes. The resulting resist thickness was 8500 Å.

5.4.3 Positive Photoresist Application and Development. Most of the masks used in this research required positive photoresist in order to open sharp holes for thin film application and to have overhangs to enhance the final lift-off. Microposit 1350J (Shipley, Newton, MA) positive resist was used along with a hexamethyl disilazane (HMDS, Mallinckrodt, Paris, KY) sticking promoter. Dies were mounted on the spincoater and HMDS was initially applied and spun at 4000 rpms for 30 seconds. The positive resist was then applied and spun at 5000 rpms for 30 seconds. The die was soft-baked at 90° Celsius for 20 minutes before it was exposed. After exposure, the die was immersed in a chlorobenzene (C_6H_6Cl, Mallinckrodt, Paris, KY) bath for five minutes in the dark or in subdued light and baked again at 90° Celsius for fifteen minutes. Chlorobenzene causes the photoresist to swell at the edges of the non-exposed area, thereby creating an overhang of exposed photoresist even after a thin film has been applied. Some photoresist along the walls must be exposed in order for the lift-off agent (acetone or plasma-etching) to be effective. The amount of time the dies were left in the chlorobenzene

was found empirically. Five minutes provided the greatest swelling in the most reasonable amount of time. Table 14 shows results of various soaks.

Table 14. Results of Chlorobenzene Baths to Developed Photoresist Walls.

Time	Wall Height
2 minutes	7000 $\mathring{A}$
5 minutes	12,000 $\mathring{A}$
10 minutes	15,000 $\mathring{A}$

The die is developed using a 3:1 deionized water:developer (KTI Chemical Inc, Sunnydale, CA) by spinning for one minute at 500 rpms. After the developed die is hard baked at 135^o Celsius for 15 minutes it is ready for further post processing.

5.5 Mask Alignment and Exposure

After the soft bake, the die with photoresist is placed in a holder consisting of a standard 3-inch silicon wafer cut in half by a diamond scribe and attached by the glue side of standard 3M Post-It notes as shown in Fig. 53. The holder acts as a support to keep the die from moving and ensure even mask contact over the entire surface when the die and mask are brought in contact with each other on the mask aligner.

A mask aligner (Karl Suss MJB3) is used to orient the mask with the die and bring both into direct contact. Once aligned, the die is exposed by a 243 watt ultraviolet lightsource. The exposure time for negative resist was 36 seconds (0.6 minutes) while the exposure time used for positive resist was 42 seconds (0.7 minutes). Both times were found empirically.

5.6 Masking Techniques

5.6.1 Masking Procedures. The most crucial element of this thesis was to develop and use practical methods to apply a variety of thin films onto a released MEMS device. From there, it was

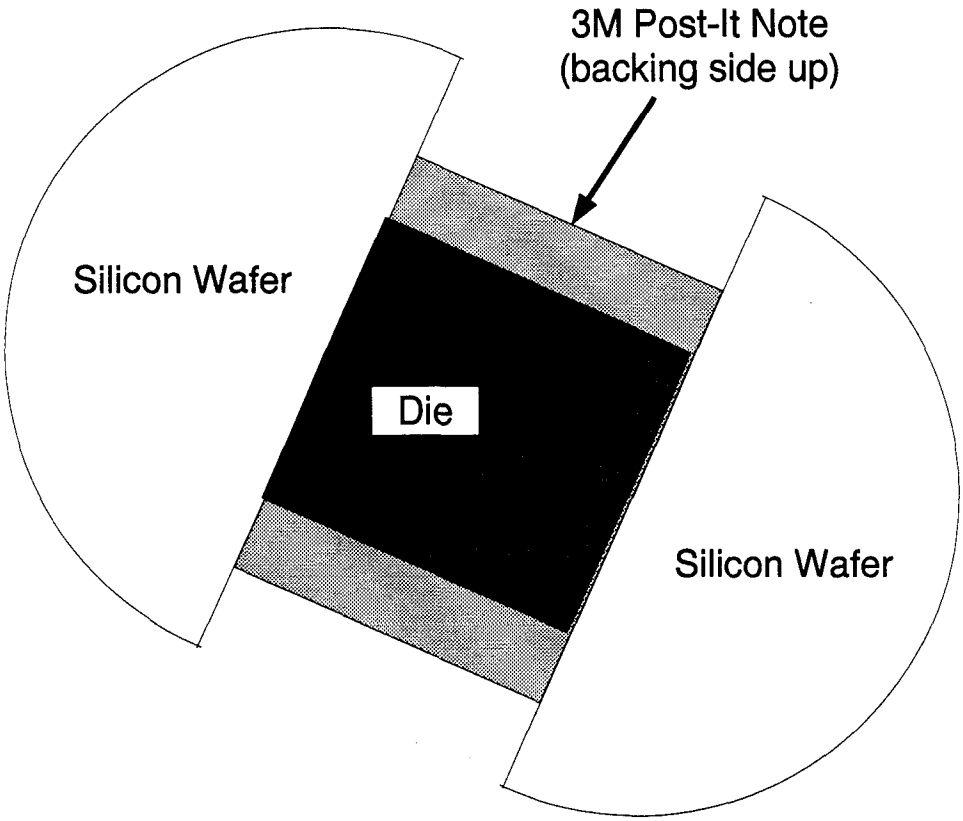

Figure 53. Die holder for mask alignment.

desired to apply multiple coatings to different devices on one chip in order to make multiple sensors for an arrayed sensing system. Three application procedures were attempted before a hybrid masking system was developed that satisfied all requirements. The three initial application procedures were direct application without a mask, chemical masking and physical masking.

5.6.1.1 Direct Application. This procedure involved applying a thin film directly on a chip without regard to masking or device isolation. In essence, a new layer was added to the chip. The problems associated with this process were numerous, including covering bond pads, shorting contacts, clogging hinges (if the thin film was rubbery) and limiting the wafer to a single film. This process was used during the initial stages to gain familiarity with the thin films on unfabricated silicon wafers.

5.6.1.2 Chemical Masking. This method, whether using positive or negative photoresist, provided the most selective deposition capabilities. Once the photoresist was applied, patterned and developed, a thin film could be readily applied only to the patterned areas. One major question this thesis did answer was whether a released MEMS device could be coated with photoresist without damage. It was found that indeed the devices were robust enough to be coated, spun, developed and layered without injury. The problem with using photoresists arose at the end, when the resist was supposed to lift off along with the film material from unpatterned areas. Acetone baths were ineffective with negative resists but had limited results with positive resists. The polymer coatings used dissolved in acetone. The metal oxides did not release properly and required rubbing with a cotton applicator or agitation in an ultrasonic bath for removal. While these techniques worked well on unreleased chips, the applicator and ultrasound readily destroyed the released devices.

5.6.1.3 Physical Masking. Masks were made by cutting holes in heavy paper and covering wafers. This method was used both to sputter oxides and to spray polymers onto wafers. Since no chemicals were used, the problem of lift-off was not an issue. The problem associated with

this procedure was similar to the direct application in that resolution was difficult to achieve. Only areas could be covered, not individual devices.

5.6.2 Hybrid Masking. The masking problems were solved by using a hybrid system of chemical and physical masks. Photoresist was applied to the chip and patterned; however, along with the device of interest being patterned, other areas such as bond pads and conductors (if exposed) were patterned as well so that upon development they were open. A physical mask was made to cover the area around the patterned devices. In this way, the resolution of chemical masking ensures that only a specific device is patterned while the physical mask ensures lift-off without damaging the chip. The photoresist was baked on as a passivation layer and left alone, even after the film was applied. Fig. 54 shows the hybrid mask process.

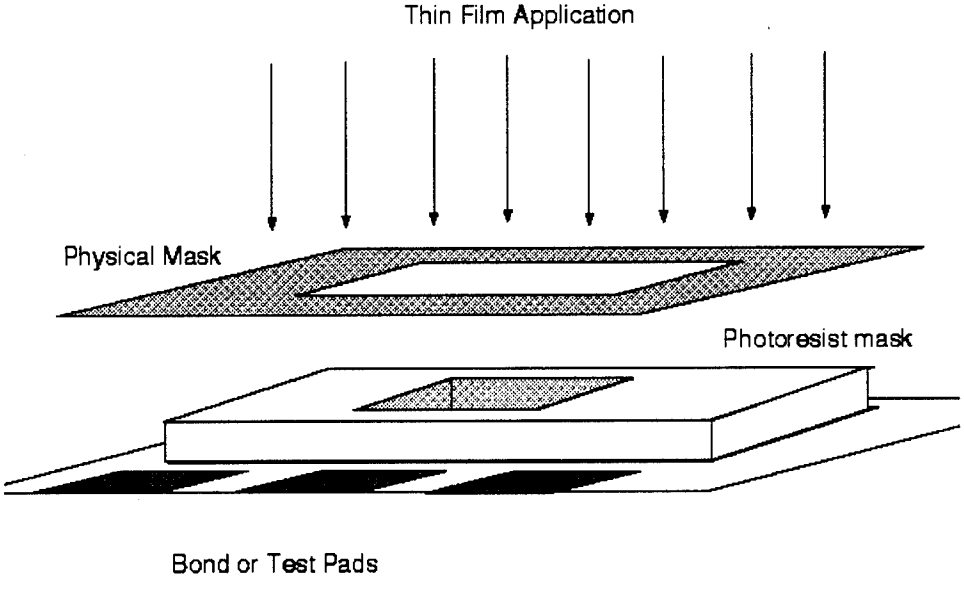

Figure 54. Hybrid mask process showing process steps (bottom to top). First, photoresist is patterned on the devices and pads. Secondly, a physical mask shields the bond pads. Finally, the thin film is applied. The physical mask is removed, but the photoresist mask can be left in place.

Using this method, different coatings were applied to individual chips without having to reapply and pattern photoresist. By moving the physical mask to different regions of the chip, different films

could be applied. The density of different coatings on a single chip is limited by the resolution of the physical mask. Only two films (PIB and PVTD) were used in this thesis due to a limitation of available coatings and working devices. Other research has shown that at least nine different areas can be covered with a physical mask on a standard MOSIS die [24].

5.7 Application Techniques

A number of thin films were found in the literature that were successful in identifying chemical products. Table 15 shows the thin films identified for use in this research, chemicals the film had been used with successfully, and the preferred application technique to the prepared device.

Table 15. Planned Thin Films and Detectable Chemicals.

	Thin Film Coating	Chemicals to be sensed	Application	Reference
1.	tin dioxide	2-propanol, methyl alcohol, toluene, chlorobenzene, acetone	sputtering	[5]
2.	iron (II) trioxide	toluene, xylene, methyl alcohol	sputtering	[75]
3.	platinum	2-propanol, trichloroethylene	sputtering	[33]
4.	copper and lead phthalocyanine	trichloroethylene, toluene, xylene, chlorobenzene, 1,1,1 trichloroethane	thermal evaporation	[24]
5.	negative photoresist	xylene, toluene, chlorobenzene	spin coating	[46]
6.	poly(isobutylene)	trichloroethylene, acetone, n-butyl acetate	air brush	[44, 56]
7.	poly(vinyl tetradecanal)	toluene, chlorobenzene, trichloroethylene, xylene, 1,1,1 trichloroethane	air brush	[56]

5.7.1 Application Processes. As shown in Table 15, a number of application techniques were required to apply a particular film. Some application techniques could be substituted such as spin coating and air brushing. Each technique is described below.

5.7.1.1 Sputtering. This technique required that the proper target material be installed in the RF sputterer. Iron trioxide was tried on MUMPS 6 devices but without success due to poor lift-off of the mask. The target was removed for other work and was not replaced in time for work on this thesis. Tin dioxide was identified as a target material and ordered; however, it did not arrive in time for this thesis. Platinum was also identified but due to time restrictions, was not applied.

5.7.1.2 Thermal Evaporation. Thermal evaporation used the same cryogenic vacuum system as the sputterer and is used at the AFIT Coop laboratory for aluminum deposition. Phthalocyanines were evaporated in the system in previous research [24]. Due to filtration problems phthalocyanines caused in the vacuum system, it was decided to leave these materials alone unless no other thin films became available.

5.7.1.3 Spin Coating. This method provided uniform and reproducible layers for any film that could be dissolved and applied as a liquid. The spin-coater speed was set based on layer thickness for the photoresist. A thin film of less than 1000 $\mathring{A}$ using HR-200 could not be obtained using the spin-coater in the laboratory. The lowest published value in the manufacturer's specifications was 7000 $\mathring{A}$ at 8000 rpms [76].

5.7.1.4 Air Brushing. An airbrush (Paasche, Model H#, New Jersey) was used to apply the dissolved polymers onto the die. The set-up for the application is shown in Fig. 55. Prior to applying the thin film to the chip, a test run was done on a clean wafer with a clear tape mask. The airbrush sprayed the wafer for 25 cycles (where one forward and one return motion is a cycle) at two seconds per cycle. The tape was removed and the thickness was measured by a profilometer. Layer buildup was assumed to be linear, so any reduction or increase of film thickness was simply a proportion of the test run. Results of the application are shown in Table 16.

Fresh chloroform was used to purge the airbrush after applications. The chip was prepared for application by patterning its masks and securing it to a 3 inch wafer with a small drop of negative

photoresist. The wafer and chip were baked at 65° for 15 minutes to harden the adhesive. Once a film was applied, the chip was removed with tweezers and packaged for testing.

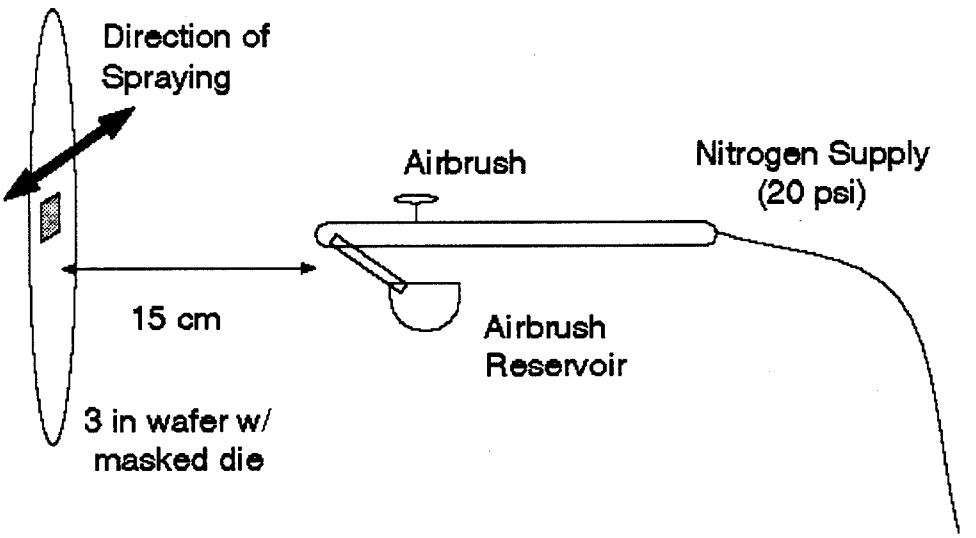

Figure 55. Airbrush film application process. A masked chip has been attached to a wafer with negative photoresist. The separation of 15 cm was kept by measuring the distance and manually sighting the brush to the wafer. Dissolved thin film was placed in a detachable reservoir cup on the airbrush and applied with nitrogen at 20 psi.

Table 16. Airbrush Application Results Based on a 25 Cycle Application. Test Thickness is thickness after 25 cycles. Actual Cycles is the number of cycles applied to a sensor chip, and Actual Thickness is the measured thickness on the sensor chip.

Thin Film	Test Thickness (Å)	Actual Cycles	Actual Thickness (Å)
PIB	3400	10	700
PVTD	4200	8	1340

VI. Experimental Design

"For, although common Snarks do no manner of harm,
Yet I feel it my duty to say
Some are Boojums- ..."

The Bellman
The Hunting of the Snark, Lewis Carroll

6.1 Introduction

This section describes the test set-ups used to evaluate the sensors both before and after a thin film had been applied. Once analyzed and processed, the sensor package must then be exposed to a chemical agent in a controlled and safe environment.

6.2 Instrumentation

A variety of test equipment was used to initially characterize the different devices and then measure actual chemical responses. The various techniques used are described below. The basic platform for testing was a micromanipulator (Model 6200, Micromanipulator Company, Inc.) using vacuum-held probes. Chips were mounted on a glass speciman slide with double-sided tape to prevent movement. The temperature of the ambient air was taken before each test with a refrigeration thermometer (Weston Model 2261, Newark, NJ); however, room temperature remained constant between 18 and 21 degrees Celsius.

6.2.1 Impedance Analysis. This test was used for moving devices such as the bridge structures to measure impedance response over frequency. A signal generator (HP 3314A Signal

Generator) was used to drive the device at discrete frequency settings while an impedance analyzer (HP 4194A Impedance Analyzer with a 16047D Test Fixture) swept frequency values through the heating element of the bridge. Data from the impedance analyzer was transferred to a PC (AT&T 486) via an 82335B Hewlett Packard Interface Bus card using HP Interactive Environment software. Instructions used to remotely control the impedance analyzer and transfer data are provided in the Appendix. The test center was connected to the analyzer's input test fixture by shielded test leads with BNC connectors and alligator clips. This test was used for Devices 7 and 8, the resonating bridge structures. The test set-up is shown in Fig. 56.

The MUMPS 9 heated chemoresistor also used the impedance analyzer, but without a function generator. A variable DC power supply was used to heat the polysilicon heater. The test set-up for this device is shown in Fig. 57.

6.2.2 I-V Parameters. This procedure measured the current as a function of applied voltage to an element in order to characterize the device's heater. This test was conducted at the micromanipulator prior to a thin film application. A variable voltage source (HP 6236B Triple Output Power Supply) was connected to an element on a device with an ammeter meter (Fluke 8600A Digital Multimeter) in series and a voltmeter (Fluke 77/BN Multimeter) in parallel to the device. Since another element was typically affected by the heating of the element being tested, an impedance analyzer (HP 4192A Low Frequency Impedance Analyzer) was used to monitor the change at a constant frequency (1000 Hz). Data was read directly from the instrument read-outs. For devices that did not overlap each other and would not be affected by localized heating, current was measured as a function of voltage without a secondary impedance measurement.

6.3 Mounting and Packaging

Once processed with an acceptable thin film coating, the dies were mounted on standard 64-pin dual in-line packages (DIPs) with a single drop of superglue (Quicktite, Loctite Corp., Cleveland, OH).

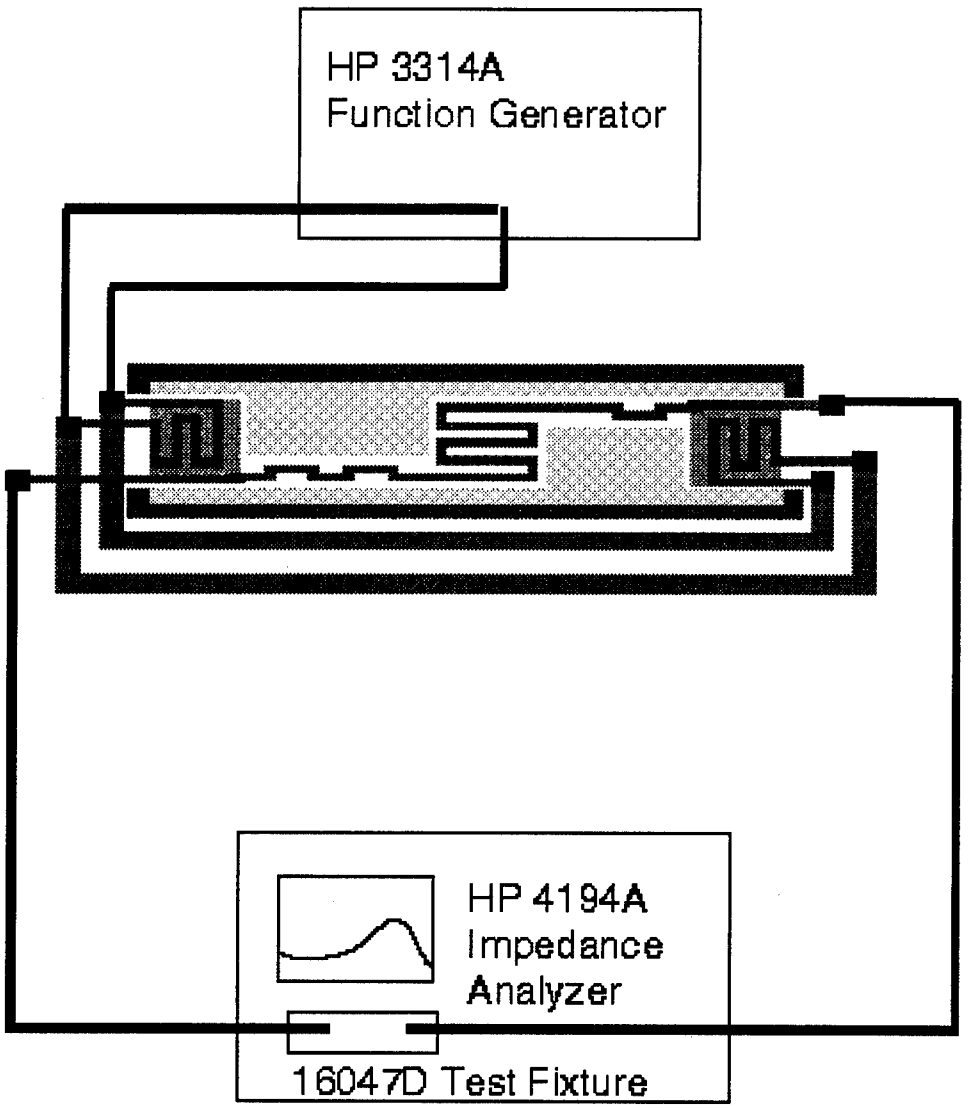

Figure 56. Resonating bridge test set-up. The frequency bandwidth used for testing was 100 Hz to 5 MHz. Both bridge devices were driven at 7.5V with 0.2V offset at frequencies varying from 1 Hz to 50 Hz.

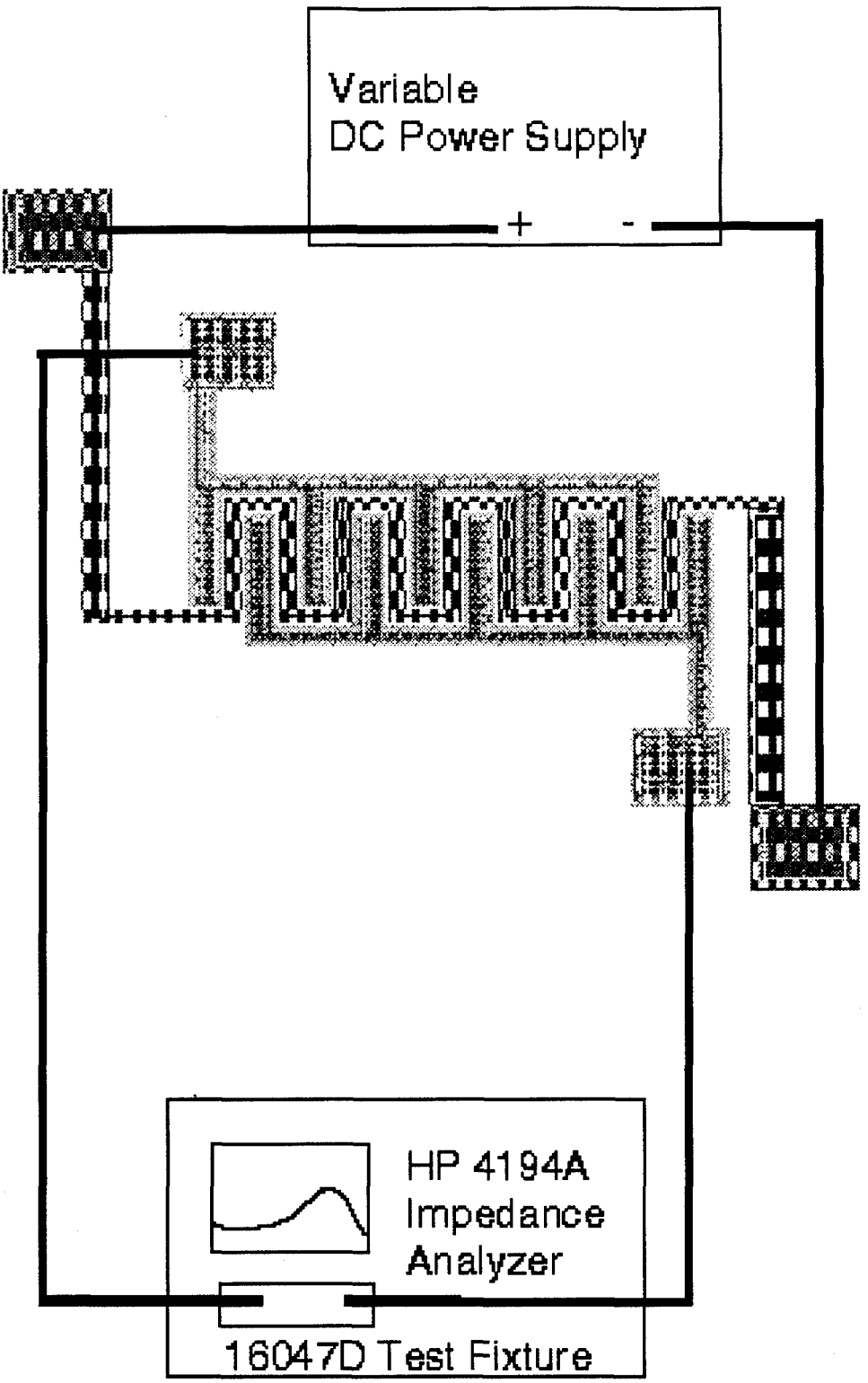

Figure 57. Heated chemoresistor test set-up. The frequency bandwidth used for testing was 14 - 18 MHz.

Pads were bonded to pins via a wire bonder (Kulicke & Saff Industries, Inc.). A completed sensor package is shown in Figure 58.

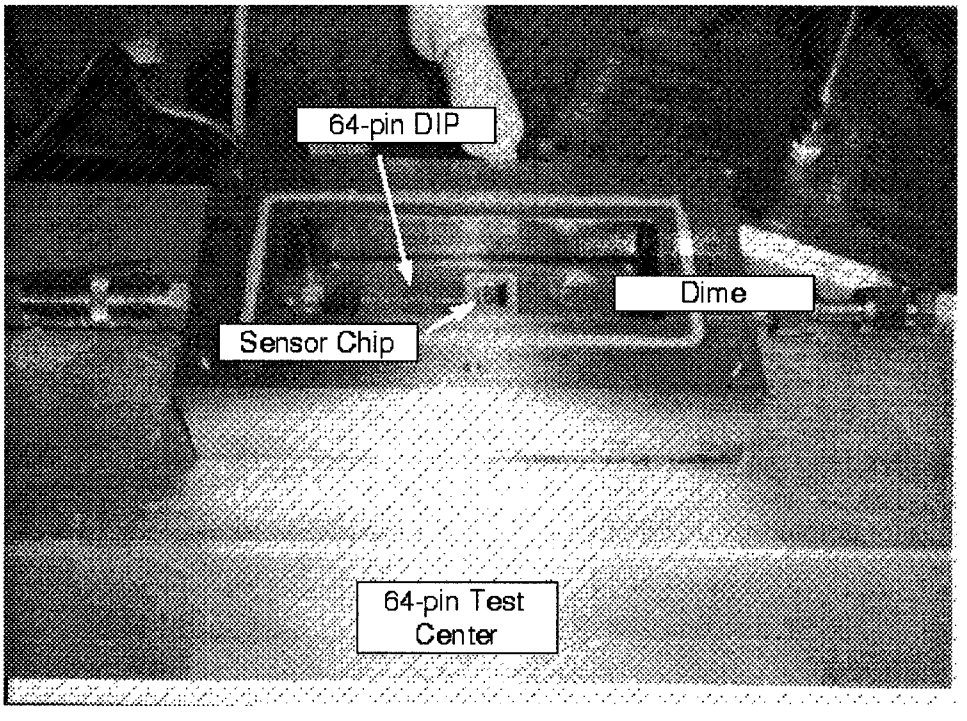

Figure 58. Sensor test package in the 64-pin test center. A dime has been added to show scale.

6.4 Gas Delivery System

A gas delivery system was constructed by modifying an existing system used for previous research [24]. A schematic diagram of the system is shown in Fig. 59, while a picture of the actual system is shown in Fig 60. The system is composed of 1/4-inch stainless steel and polyvinylchloride (PVC, Nalgene Tubing Co., Rochester, NY) pipe with 1/4-inch fittings (Swaglok Inc., Solon, OH). Flowmeters (Gilmont Instruments Co., Great Neck, NY) measured incoming carrier gas flow and outgoing purge/challenge gas flow. The gas system is shown in Fig. 59.

In addition to the piping, the system also includes a 64-pin test center that allows direct access to each of the pins on a standard 64-pin package. The test center has a removable top that allows a sensor

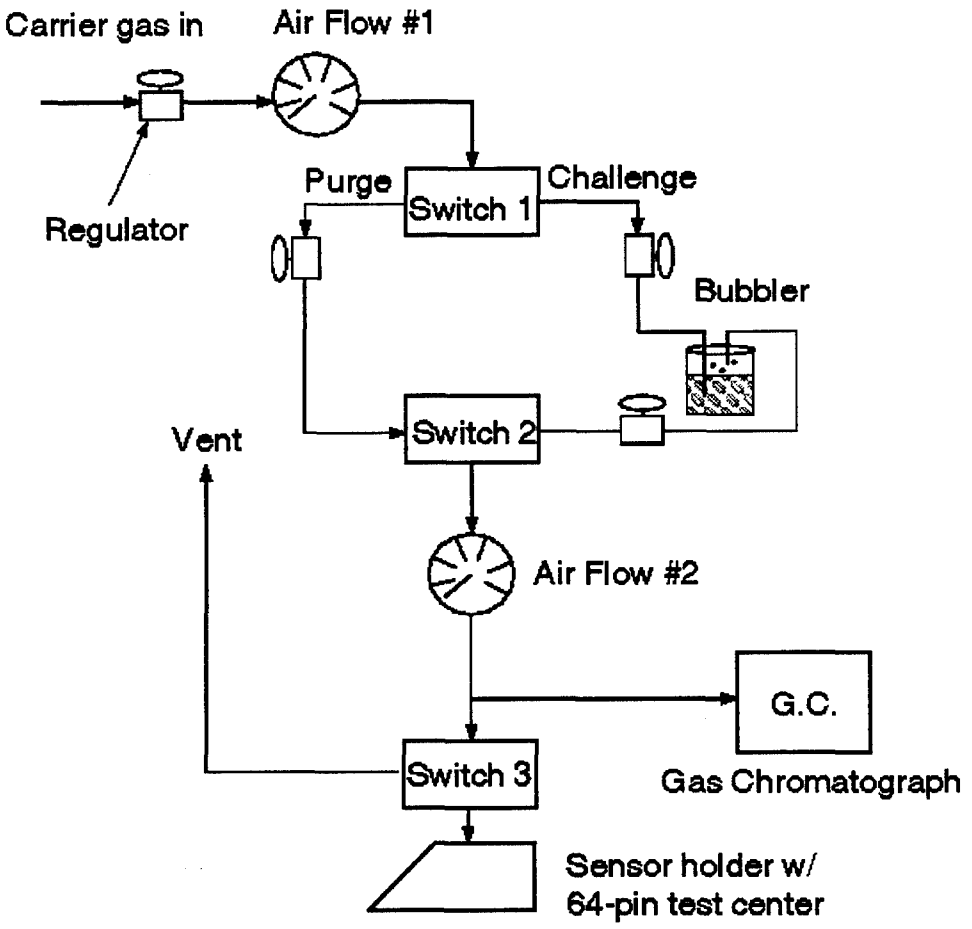

Figure 59. Layout of gas delivery system.

package to be placed in an enclosed environment and secured by a quick-release socket. Connectors are standard BNC connectors with outside shields grounded to the chassis. The test center, along with the gas delivery system, is shown in Fig. 60.

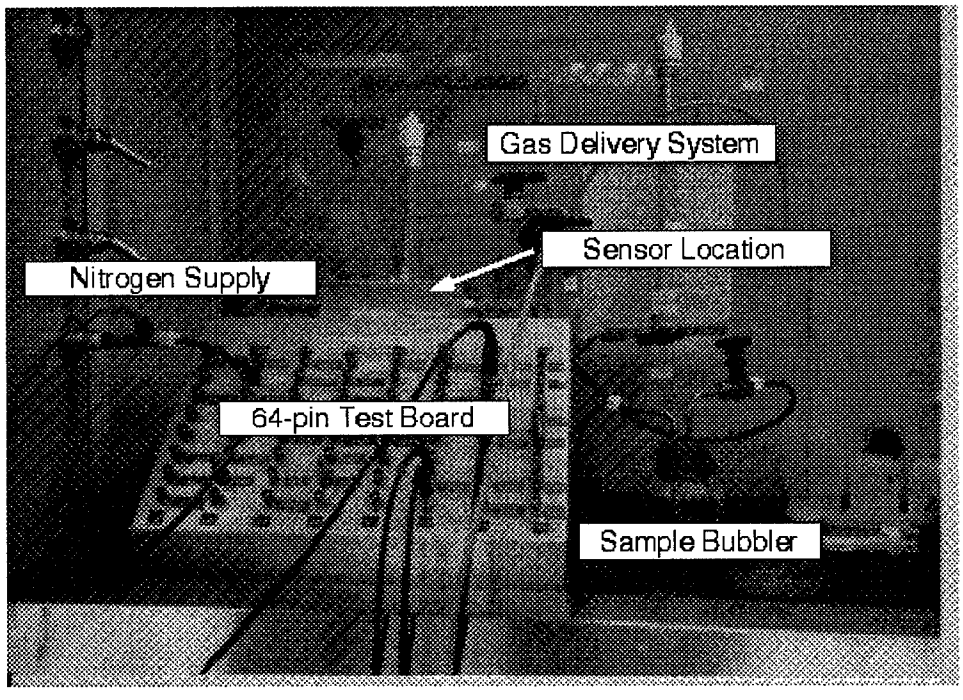

Figure 60. Actual layout of gas delivery system showing location of the 64-pin test center. Nitrogen gas is used to bubble samples and purge the system between tests.

Nitrogen (99.9% pure, 88 SUPS, Wright-Patterson AFB, OH) is used as a purge gas and carrier gas for the chemicals under investigation. Initially, pure chemicals are placed in the bubbler in order to perform proof-of-concept experiments. The chemicals tested are shown in Table 17. If the chemical was detected by a sensor, the chemical was mixed with water and then aerated. Because of the sensors used, it was found to be impractical to directly immerse the devices in a liquid; therefore, gas delivery was used. This system could easily be scaled down for a field unit and should be investigated in further research.

Table 17. Actual chemicals tested on both heated chemoresistor and resonating bridge.

	Thin Film Coating	Chemicals tested
1.	poly(isobutylene)	trichloroethylene (TCE), 1,1,1 trichloroethane (1,1,1-TCA) toluene
2.	poly(vinyl tetrachloride)	trichloroethylene (TCE), 1,1,1 trichloroethane (1,1,1-TCA) toluene
3.	negative photoresist	xylene

6.5 Data Analysis

Once collected via the HPIB card, the data was analyzed using MATLAB Version 4.2c [77]. The process of preparing the data involved taking the absolute difference between the exposed response and the purged response:

$$\Delta\Omega = |\Omega_{purge} - \Omega_{exposure}| \tag{38}$$

where $\Delta\Omega$ is the difference in impedance, Ω_{purge} is the impedance response under purge (nitrogen) conditions and $\Omega_{exposure}$ is the impedance response when the challenge gas is exposed to the sensor.

The difference vectors were filtered using a 5-increment moving average filter. A moving average filter is a discrete filter that takes a designated number of data points (in this case five), averages them, gives its position the averaged value and then increments to the next position and averages the next five values. The filter is described as

$$y[n] = \frac{1}{M_1 + M_2 + 1} \sum_{k=-M_1}^{M_2} x[n-k] \tag{39}$$

where y is the position being averaged, M_1 is the first location to begin averaging, M_2 is the last location, and x is the individual data being summed [78]. The effect of the filtering was to smooth the data as shown in Fig. 61. Data was then manipulated to produce suitable plots.

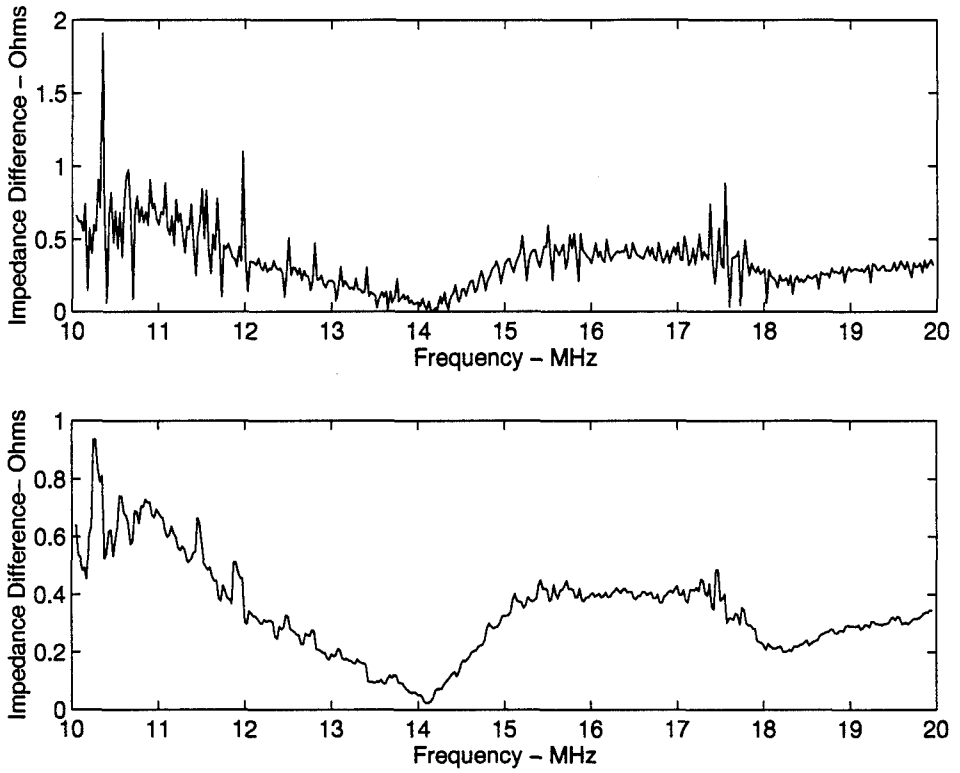

Figure 61. Effects of filtering on data. The top figure shows raw data while the bottom figure shows data filtered with a 5-increment moving filter. These plots were made from the difference response of a PIB-coated heated chemoresistor in TCA and a heated purge of 2 V.

VII. AFIT Microsensor Fabrication

7.1 Introduction

Due to aggressive testing using MUMPS 6 and CMOS devices, available test dies were quickly used up. Interim test structures were needed to refine application techniques until the next MUMPS chip (MUMPS 9) arrived. For this reason, a decision was made to fabricate basic MEMS sensor structures using in-house capability. In addition, this fabrication exercise illustrated the simplicity of MEMS device fabrication and provided AFIT with an in-house MEMS fabrication capability.

7.2 Device Description

Using knowledge gained from other devices, a bulk micromachined microsensor device was produced at the AFIT Cooperative Electronics Laboratory in Bldg 125. The device fabrication process required two oxide growths, a phosphorus diffusion and a metallization of sputtered gold. The total sensor area (TSA) and sensor area (SA) were designed to be 10000 μm^2. A boron-doped resistive element insulated by silicon dioxide would provide the embedded heater while 6 μm interdigitated gold electrodes provided the sensing mechanism. The device was designed to operate as a chemoresistor suspended over a substrate void with an insulated heater. The final device resembles Device 9, fabricated during various MOSIS CMOS runs. The completed device design is shown in Fig. 62.

7.3 Fabrication Process

Device fabrication took eight distinct fabrication steps, not including making and developing the three masks used in the process. Masks were made using the Cadence design tool on the AFIT VLSI network and followed the same steps described in Chapter 5 for printing and developing. The actual fabrication steps are:

1. Initial oxide growth.

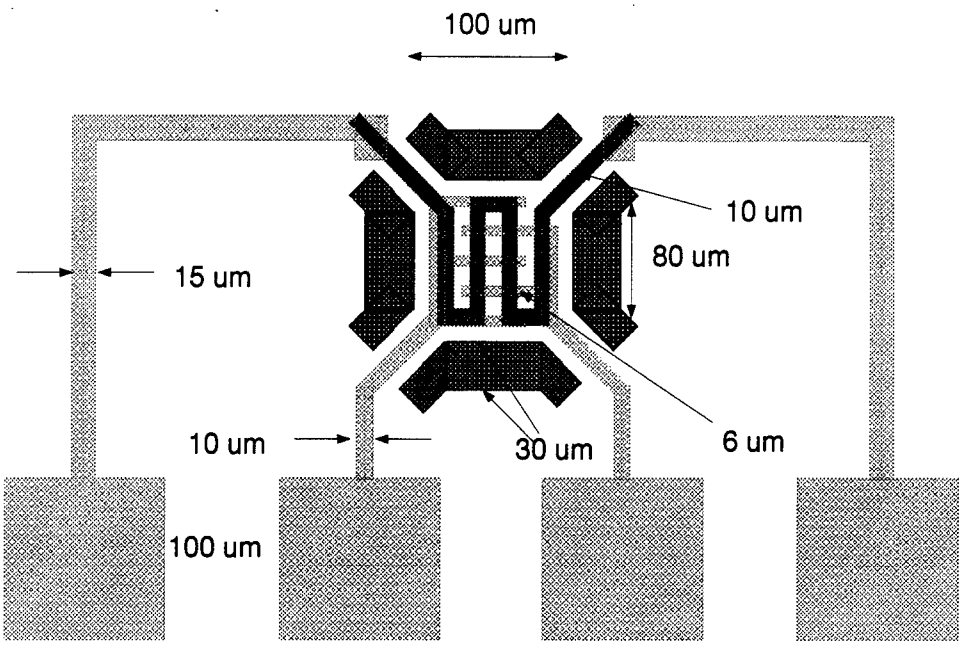

Figure 62. AFIT microsensor layout.

2. Boron diffusion patterning and initial oxide etch.

3. Boron diffusion.

4. Second oxide etch.

5. Second oxide growth.

6. Oxide open cuts patterning and third oxide etch.

7. Metallization and final patterning.

8. Metal etch and device release.

Once released, the devices can have thin films applied to their sensor areas as described in previous chapters.

7.3.1 Preprocessing. The devices were made on boron doped (p-type) silicon wafer substrates with (100) orientation. After an initial cleaning in a 3:2 H_2SO_4:H_2O_2 "piranha etch", the

surface resistivity was measured at 10.6 ohms-cm with a Veeco AP-150 Automatic Resistivity Probe (Plainview, NY).

7.3.2 Process Steps. Prior to fabrication, each step was simulated using TSUPREM-4 version 6.1. From these simulations, growth times and temperatures were set. Simulation code and graphic results of the simulation are given in the Appendix. Subprocesses such as photoresist application are described in earlier chapters.

7.3.2.1 Initial oxide growth. An oxide layer was grown on the cleaned wafers in a diffusion oven (Thermco) using steam oxidation at 1100° Celsius for 30 minutes. The resulting growth was measured at 3530 Å with a Leitz MPV-SP Film Thickness Measurement System.

7.3.2.2 Boron diffusion patterning and initial oxide etch. After the oxide growth, the wafers were cleaned again in a piranha etch and spincoated with negative photoresist (HR-200). After their soft bake, the first mask was patterned using a 0.65 minute exposure time. The exposed wafers were then developed and hard baked. Prior to patterning, a buffered etch solution was mixed and allowed to sit for two hours. The buffered etch consisted of 4:1 ammonium fluoride (NH_4F, 40% solution, Ashland Chemicals, Columbus, OH):hydrofluoric acid (HF, Mallinckrodt, Paris, KY). Wafers were etched until all unpatterned oxide was removed (approximately 1 minute 45 seconds), leaving exposed silicon.

7.3.2.3 Boron diffusion. All photoresist was removed with another piranha etch and wafers were transferred to a quartz boat with patterned sides facing boron planar diffusion sources (OI-NEG, Toledo, OH). The boat was placed in the diffusion oven at 1150° Celsius for 60 minutes. Surface resistivity was measured on an unpatterned test wafer at 0.0767 ohms-cm after diffusion. A drive-in step was not used in order to keep the dopants near the surface.

7.3.2.4 Second oxide etch. Prior to growing the insulating oxide layer over the doped regions, the patterned oxide on the wafers was etched away. Another buffered etch was mixed and allowed to settle. The wafers were then immersed in the etch bath until all oxide was etched away (approximately eight minutes). Alignment marks were still noticeable on the substrate even after this etch due to the different oxide growth rates during the boron diffusion.

7.3.2.5 Second oxide growth. Wafers were placed back in the diffusion oven for 30 minutes at 1100^{o} Celsius in a steam oxidation environment. An oxide growth of 4200 $\mathring{A}$ was measured on a test wafer.

7.3.2.6 Oxide open cuts patterning and third oxide etch. Additional oxide cuts were necessary to expose the silicon substrate during the EDP release etch and to allow metal contacts with the n-doped heater. After cleaning in a piranha etch and spincoating with negative photoresist, the wafers were patterned with the second mask. Due to alignment errors in the mask, the patterning was done sectionally, using 3M Post-It notes to cover up sections not being aligned and exposed. After developing and baking, the wafers were etched using another buffered etch solution until the substrate silicon was exposed (approximately 1 minute 45 seconds).

The entire fabrication process was modeled on TSUPREM-4. Distribution plots and text files are included in the Appendix; however, the final boron concentration distribution is shown below in Fig. 63. A critical concentration level of 2.5x10^{1}9 atoms/cm^{3} appears to have been achieved.

7.3.2.7 Metallization and final patterning. The wafers were cleaned again in a piranha etch and placed in the sputtering machine. An adhesion layer of titanium was originally applied for 20 minutes at 150W forward power/11W reflected power for a total deposition of 22 $\mathring{A}$ and a final layer of gold was deposited for 11 minutes at 150 W forward power/3W reflected power for a total deposition of 4100 $\mathring{A}$.

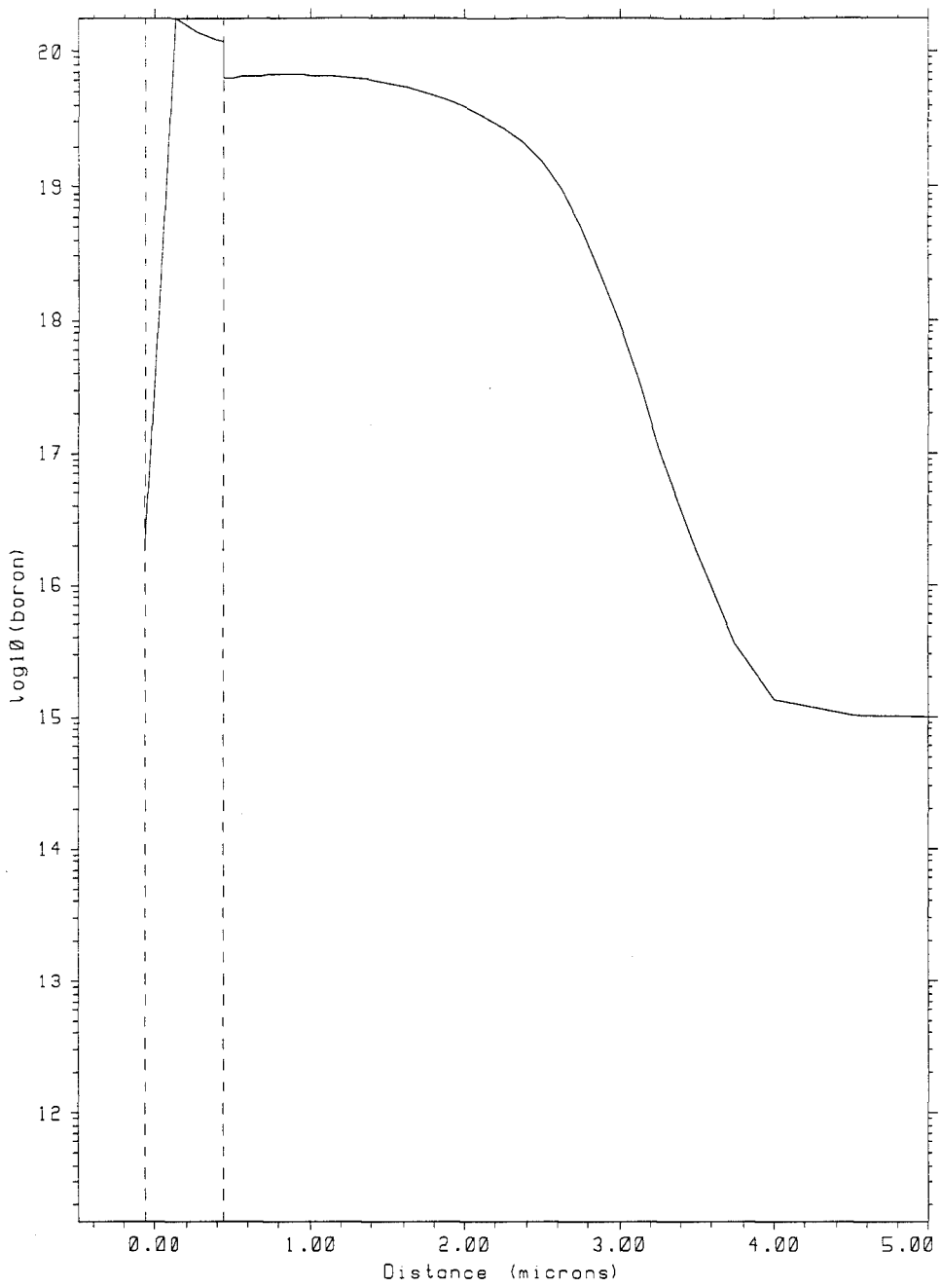

Figure 63. Final distribution of boron concentrations after fabrication as modeled on TSUPREM-4.

The plated wafers were then coated with positive photoresist (Shipley 1350 J) and an HMDS adhesion promoter. The final pattern was lithographed onto the surface and developed. The wafers were then subjected to a 3:1 hydrochloric acid (HCl):nitric acid (HNO_3) etch to remove the excess gold for approximately 20 seconds. Once rinsed, the wafers were bathed in acetone to remove the photoresist and rinsed with DIW and 2-propanol.

7.3.2.8 Metal etch and device release. After metal etch, the wafers were rinsed in DIW and 2-propanol for two minutes each before being diced into individual chips using a diamond scribe. The individual chips were then released using a standard EDP release method. Problems were encountered during the device release when the oxide open cuts had a residual field oxide that was not removed prior to the release. When this occurred, the EDP would not etch the dioxide in a reasonable time (< 60 minutes) due to the dioxide resistance. As a result, the chip would have to be removed from the etch and the dioxide removed with a diluted HF etch. The effectiveness of an EDP etch changes each time the chip is removed and the etchant is exposed to oxygen and water vapor. The longer the wafers were exposed to the etch, the more chance there was of injury to the electrodes. While the electrodes would not be eaten away, the surface adhesion between the metal and the oxide surface would deteriorate over time and the metal would float away.

A sectional view of the fabrication process is shown in Fig. 64. A profile of a released device with a thin film coating is shown in Fig. 65.

7.4 Initial Design Considerations

Prior to achieving the final design process, a number of trials using phosphorus as a dopant and varying electrode lengths were used. In addition, a potassium hydroxide (KOH) release was evaluated.

7.4.1 Phosphorus Doping. Based on the atom-density that allows heavily doped boron regions ($>2.5*10^{19}$ atoms/cm^3) to resist anisotropic etching, it was unknown whether a highly doped

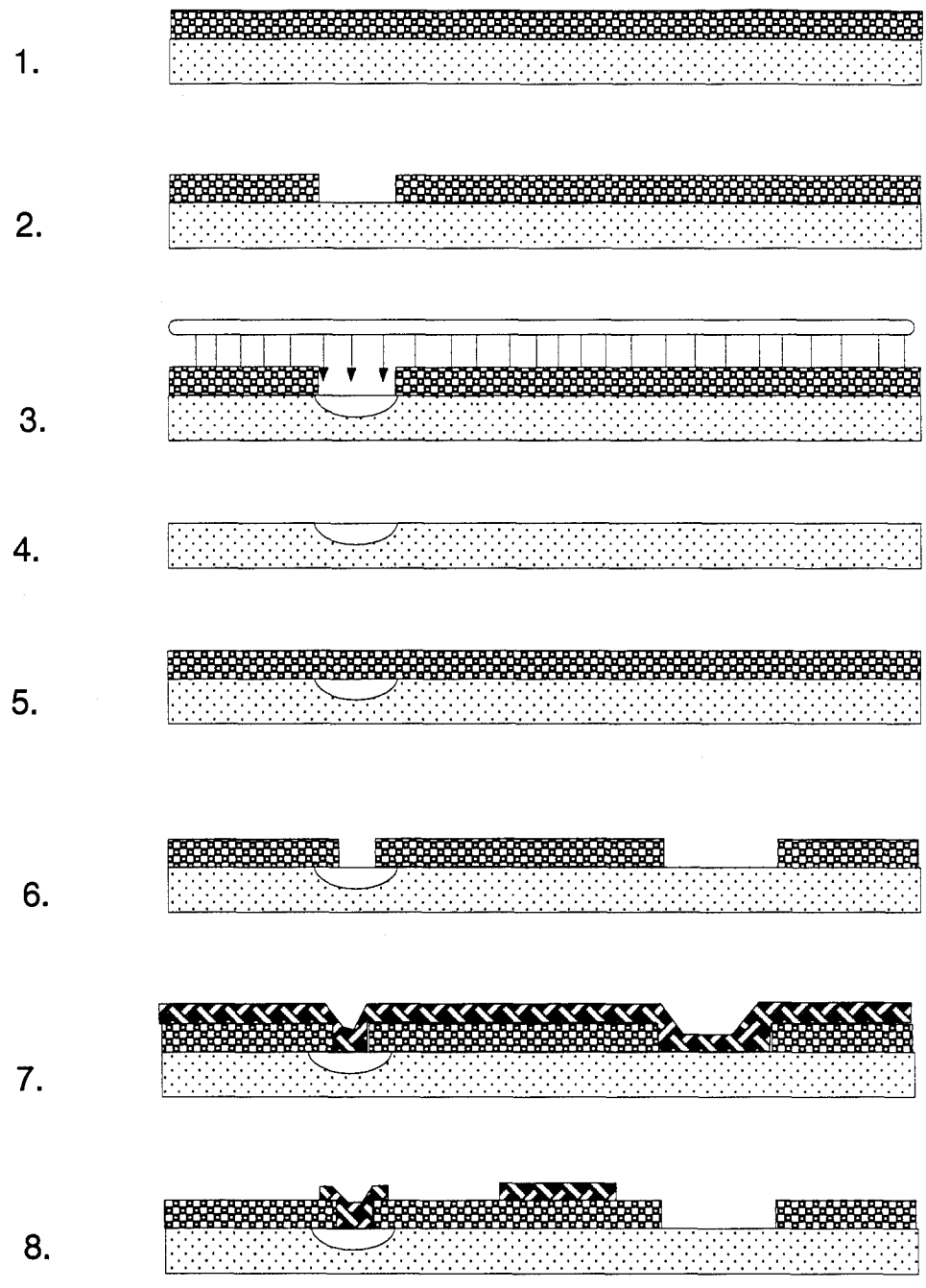

Figure 64. Cross-sectional view of the fabrication process. The initial oxide is grown (1) and etched (2). A diffusion source drives dopants into the etched area (3). The oxide is completely removed (4) and a new oxide is grown (5). Another etch is made for contacts and open cuts (6) and a metal is deposited on the surface (7). A final etch forms the electrodes and conductors (8).

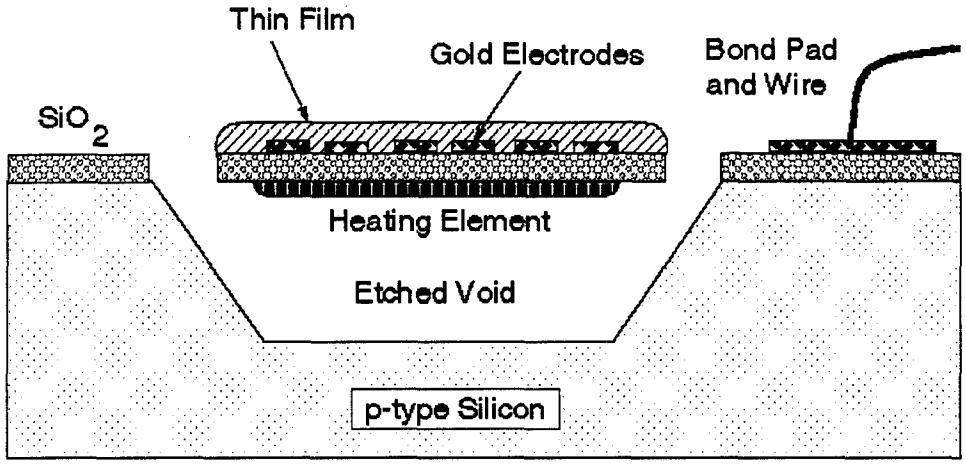

Figure 65. Cross-sectional view of a released sensor showing the embedded boron-doped heater underneath the suspended silicon dioxide sensor platform. A thin film has been applied to the sensor, covering the interdigitated gold electrodes.

phosphorus region ($>10^{15}$ atoms/cm^3) would also resist etching. A literature review revealed that the etch rate of silicon dioxide by diluted hydrofluoric acid (an isotropic etchant) increased in the presence of doped phosphorus [79]. Data on how doped silicon would react in the presence of an anisotropic etchant was unavailable but it was presumed that the etch rate would increase. The concentration was first modeled on TSUPREM-4 which showed that phosphorus diffusion could not achieve the same dopant concentration as boron. The profile is shown in Fig. 66.

To determine the effect of heavily doped phosphorus on etch rates, (100) p-type silicon wafers similar to the ones used to fabricate the microsensor were diffused with planar phosphorus sources and etched with EDP and KOH. An undoped wafer was also etched to provide a control.

In preparation for the diffusion, all wafers were cleaned in a piranha etch. The test wafers were placed in a wet oxide environment for 30 minutes at 1100^o C. A total oxide growth of 3500 $\mathring{A}$ was measured. A pattern was photolithographed on the surface and the exposed oxide was etched away using a buffered hydrofluoric acid etch (3:1 NH_3:HF) to the silicon substrate. The wafers were then cleaned again in a piranha etch and taken to the diffusion oven. Phosphorus was allowed to diffuse onto two wafers at 950^o C for 90 minutes. A surface resistivity of 1.283 Ω-cm was later measured.

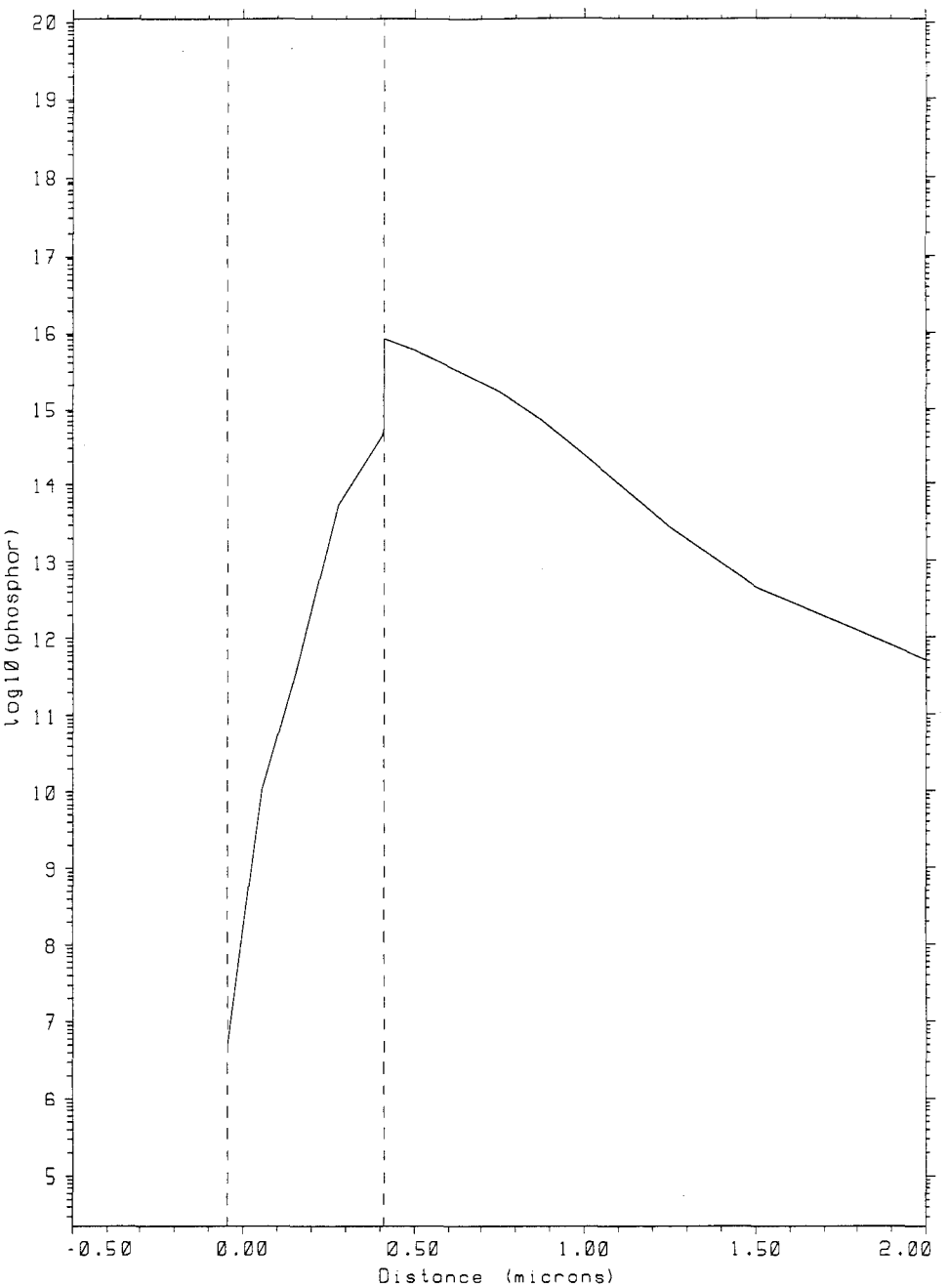

Figure 66. Phosphorus concentration profile after diffusion for 90 minutes at 950° C and a wet oxide growth at 1100° C for 30 minutes.

An EDP and a KOH etch were prepared. The doped and undoped wafers were cut with a diamond scribe and placed into each etch. The EDP etch lasted for 50 minutes at 85° C while the KOH etch lasted 15 minutes at 85° C. The results are given in Table 18 and shown in Figs. 67 and 68. While doping had no effect on a KOH release, it reduced the EDP etch rate by approximately 30%. Unfortunately, this was not enough to allow the device to release before the doped regions were eaten away.

Table 18. Etch rates of undoped silicon (Normal) and doped silicon (Phosphorus). The silicon was doped with phosphorus planar sources for 90 minutes at 950° C. The KOH etch was for 15 minutes at 85° C and the EDP etch was for 50 minutes at 85° C. Thickness refers to much silicon was etched away and how deep the resulting void was.

Etch Type	Silicon Type	Thickness (μm)	Etch Rate (μm/min)
KOH	Normal	19.65	1.31
KOH	Phosphorus	19.65	1.31
EDP	Normal	31.65	0.63
EDP	Phosphorus	22.15	.44

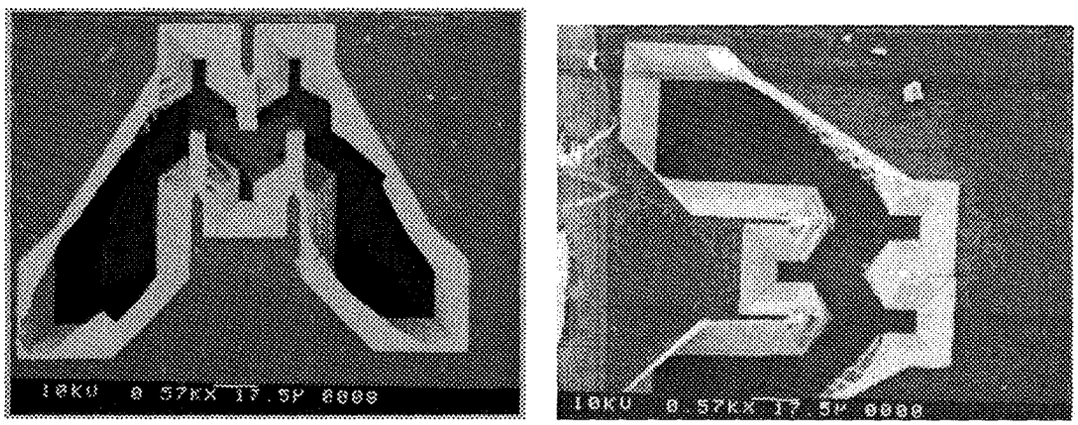

(a) (b)

Figure 67. KOH etch result on an undoped wafer (a) and a phosphorus doped wafer (b).

7.4.2 Device Release. EDP is the standard release etchant used at AFIT for bulk micromachined devices because of its relatively high selectivity between silicon dioxide and aluminum pads.

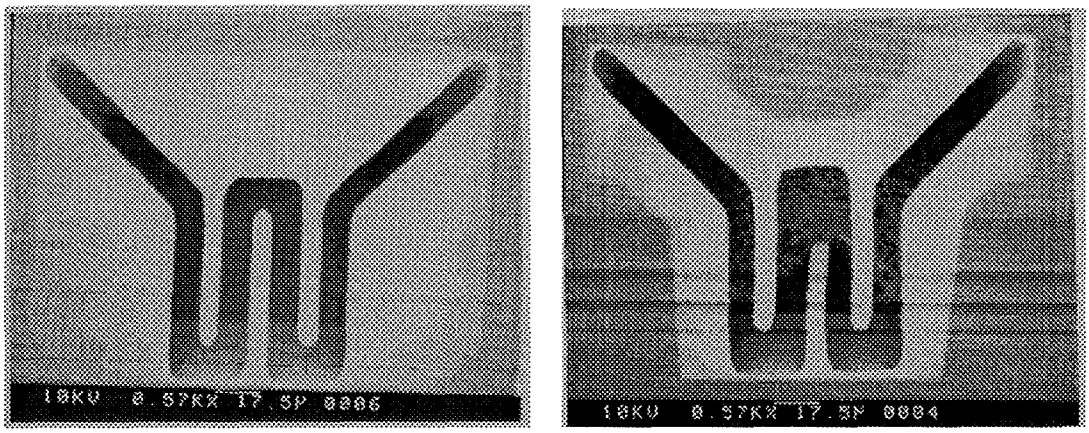

(a) (b)

Figure 68. EDP etch result on an undoped wafer (a) and a phosphorus doped wafer (b).

As mentioned before, this selectivity does not prevent the etchant from eating the aluminum, given time. Potassium hydroxide (KOH) has not been widely used because it destroys the aluminum before the device can be released. Since the AFIT microsensor uses gold, a non-reactive metal, KOH can be considered as a release etchant. Both releases were tried on a fabricated boron-doped microsensor to evaluate etch rates and selectivity between different materials. The devices were purposely misaligned during the fabrication stages to ensure that the boron-doped regions were exposed to the etchants. The results of the etches are shown in Fig. 69.

As can be seen, even though the boron-doped regions withstood both etches, the KOH etch was less selective in its etch than the EDP and ate through everything, including the silicon dioxide. EDP was chosen to release all future microsensors.

7.4.3 Electrode Size. The width and spacing between the interdigitated electrodes on the sensing area changed from 10μm wide and 10μm apart to 6μm wide and 14μm apart to account for the masking resolution. The additional separation was needed to ensure that the final etched gold would not short out between the fingers. Mask resolution error was caused mostly by poor focusing during

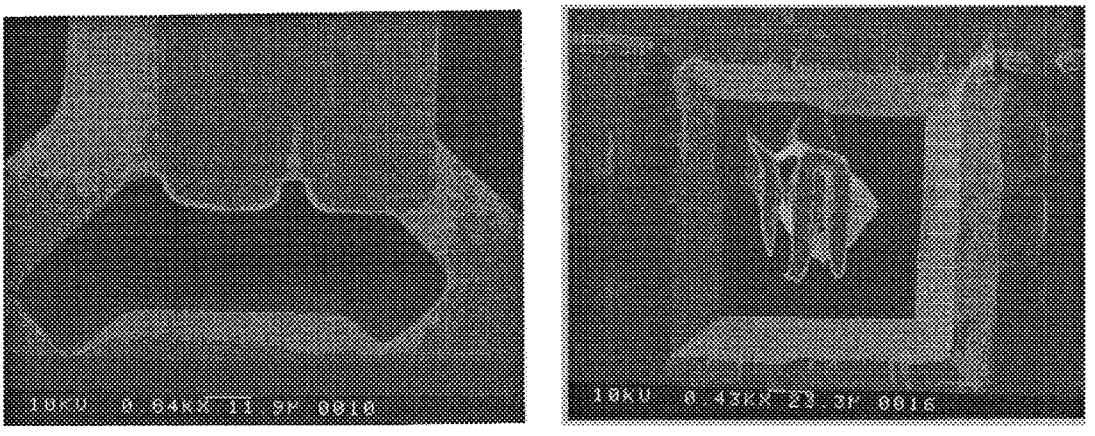

(a) (b)

Figure 69. EDP etch results after 50 minutes at 85° C (a) and KOH etch results after 15 minutes at 85° C (b).

the mask making process. Using test structures on a special mask, the best achievable resolution was 4μm.

VIII. Results

Alice laughed. "There's no use trying," she said;
"one can't believe impossible things."
"I daresay you haven't had much practice," said the Queen.
"When I was your age, I always did it for half-an-hour a day.
Why, sometimes I've believed as many as six impossible things before breakfast."

Through the Looking Glass, Lewis Carroll

8.1 Introduction

This section discusses the results of working CMOS and MUMPS designs and sensor responses to different chemicals. The final section will discuss recommendations for future research in the areas covered by this thesis.

8.2 CMOS Results

8.2.1 Fabrication Results. The single largest problem that affected the success of working CMOS (and MUMPS) devices was the design-fabrication lag time. A design for a new fabrication run had to be completed before the results of a previous run could be determined. In the CMOS runs, this time lag (and some bad luck) resulted in three designs being submitted before the first design was returned. As a result, bad designs were perpetuated. Fortunately, one design did work, as mentioned in Chapter 4.

For devices that were too large to be be released, a method was attempted to protect the aluminum pads from the EDP etchant so that the devices could be etched longer. This method involved making

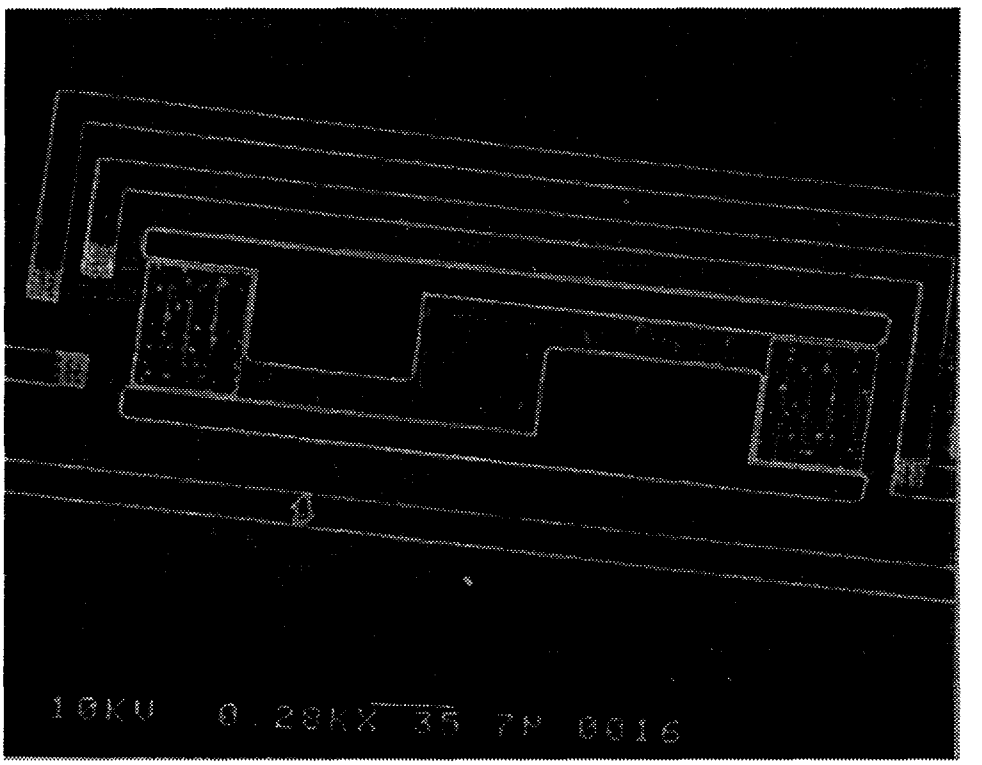

Figure 70. SEM micrograph of working resonating bridge sensor.

a photolithographic mask to cover each bond and probe pad, sputtering a titanium base and gold layer over the chip, applying photoresist, patterning and exposing the mask on the baked photoresist, and etching away the exposed gold with a 3:1 nitric acid:hydrochloric acid etch. The chip could then be etched in EDP for over 3 hours without destroying the pads. This method was attempted but not fully investigated due to the lack of extra dies and insufficient time. The results that were achieved were promising and should be investigated further.

8.2.2 Resonating Bridge DC Parameters. The individual active components of the bridge device were evaluated on an uncoated die to determine basic device parameters. The driver heaters and the sensing element, both polysilicon structures, had linear voltage-current relationships as shown in Fig. 71.

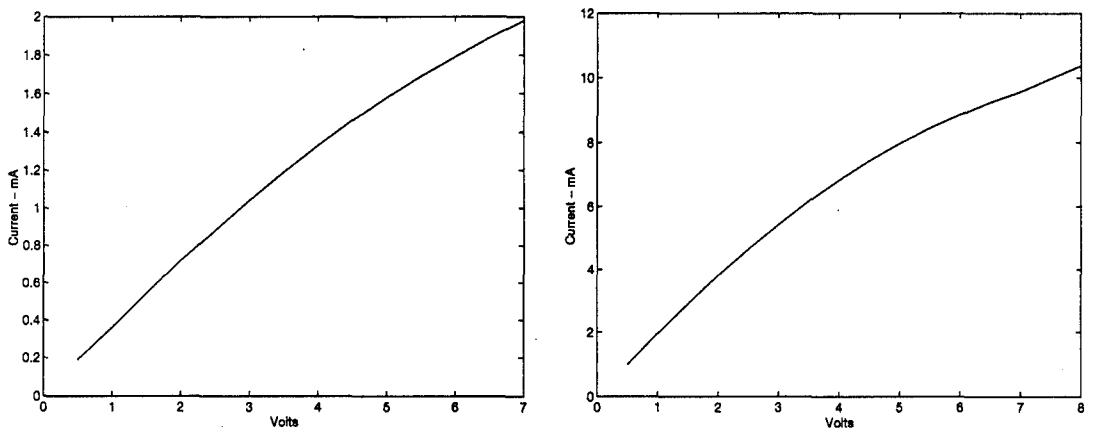

(a) (b)

Figure 71. Parameter curves for the resonating bridge device at 22° C. The polysilicon sensing element is shown in (a); its DC resistance is 2700 Ω. The driver elements are shown in (b); their combined DC resistance is 500 Ω.

8.2.3 Frequency Response. The impedance response of the bridge device was tested using the impedance analysis set-up described in Chapter 6. Measurements were taken at 1 Hz, 5 Hz, 10 Hz, 30 Hz, and 50 Hz while the device was driven at voltages of 7.5V peak to peak with a 0.2V offset. A

curious effect was noted during the frequency sweeps of the impedance as the drive frequency varied. An additional oscillation was superimposed on the low frequency (> 4 MHz) region that varied linearly with the drive frequency. Two such plots are shown in Fig. 72.

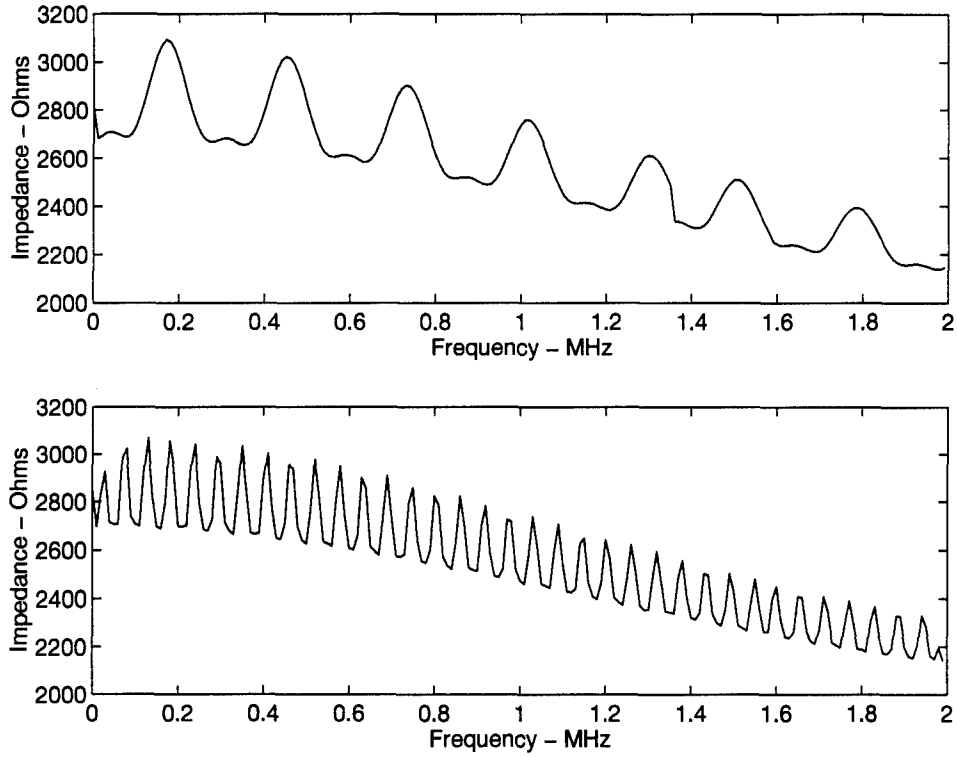

Figure 72. Superimposed oscillations on a resonating bridge device. The top device was driven at 10 Hz while the bottom device was driven at 50 Hz. The axes have been condensed for clarity.

8.2.4 Chemical Responses. Due to limitations of available dies, only one CMOS 5 chip was coated with PIB. It was tested with each chemical at drive voltages of 7.5V peak to peak with a 0.2V offset. Devices were exposed to chemicals for 2-minute durations at 0.5 liters per minute (lpm) after which time, exposure response data was taken. The devices were then purged with 4.2 lpm of nitrogen for two minutes with a 2 V bias voltage applied to the sensing element through the impedance analyzer.

8.2.4.1 Data Collection Procedure. Data was collected by letting the device come to a steady state after two minutes of uninterrupted exposure or purge. Two minutes was arbitrarily chosen as the settling time. The first measurements taken were the impedance and phase values of the impedance analyzer (see Chapter 6 for the experiment set-up) after the device had been exposed to the chemical for two minutes. The chemical was then shut off and the device was allowed to purge in pure nitrogen for two minutes. After the purge time, another data set was collected (both impedance and phase). Both sets of data (after exposure and after purge) were taken with the drive heaters operating at the same frequency. After the purge data was taken, the drive frequency was changed to the next value and the process repeated.

8.2.4.2 Data Collected. Data was collected at 1 Hz, 5 Hz, 10 Hz, and 50 Hz for TCE and 1,1,1-TCA and at 1 Hz, 5 Hz, 10 Hz, 30 Hz, and 50 Hz for toluene. Results for TCE are shown in Figs. 73 and 74. Results for 1,1,1-TCA are shown in Figs. 75 and 76. Results for toluene are shown in Figs. 77 and 78.

The device showed measurable responses to each chemical. More importantly, the varying drive frequencies evoked different responses for the same chemical, suggesting that the drive frequency could be used to provide a desorption mechanism and should be further investigated.

8.2.5 Interpretation of Results. The results obtained from the heated chemoresistor suggest that the device response is a function of the thin film and the chemical to which it was exposed. Possible explanations describing the response mechanisms are polymer degradation and physical desorption.

8.2.5.1 Polymer degradation. The first thoughts on the device responses were that the polymer may be irreversibly damaged by the heating element or exposure to different chemicals. The data does not suggest that the polymer is degrading as responses do not vary significantly enough to show that the polymer has lost its integrity and sorbing capability. There is also a gradation of response

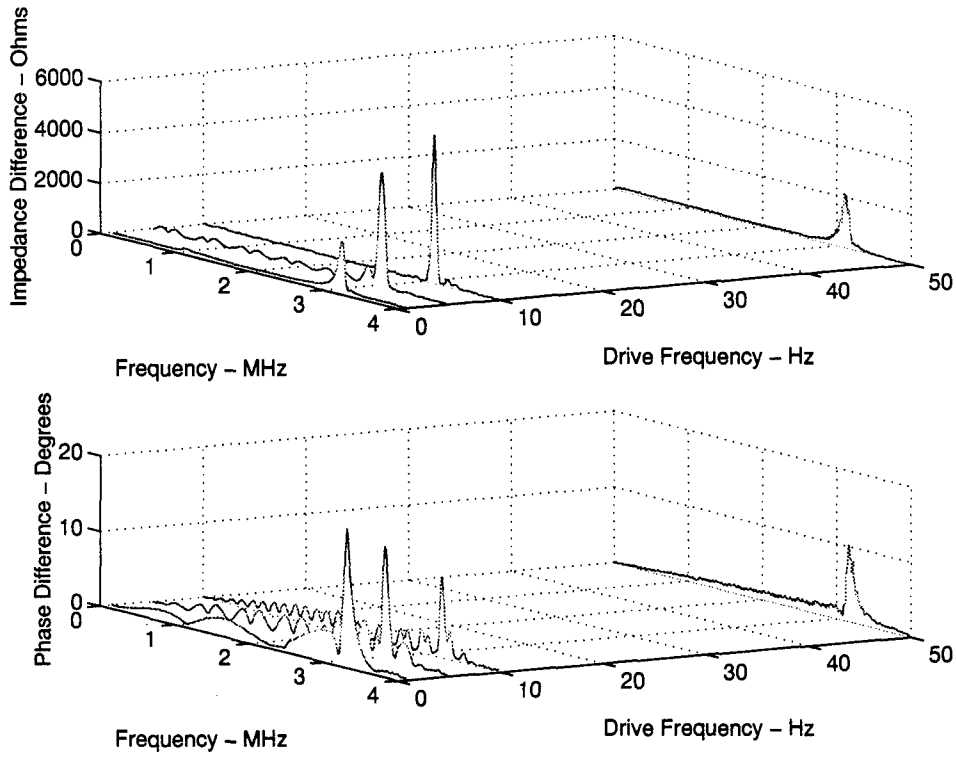

Figure 73. Resonating bridge responses to TCE. The top figure shows impedance changes over different drive frequencies while the bottom figure shows phase changes over different drive frequencies.

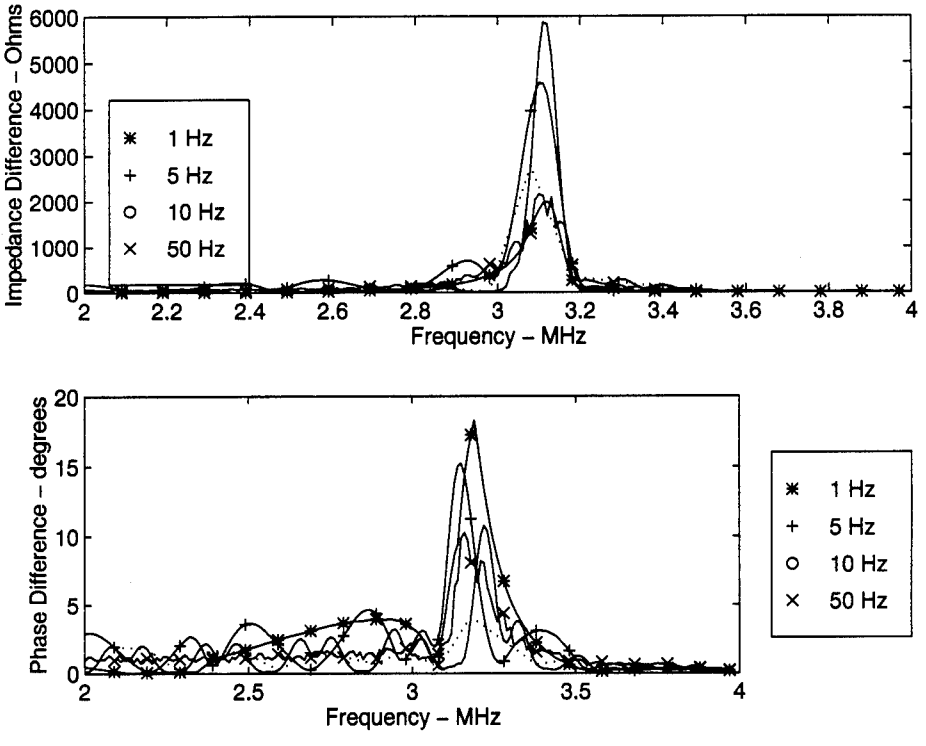

Figure 74. Resonating bridge responses to TCE within a 2 MHz bandwidth window to show more detail. The top figure shows impedance changes over different drive frequencies while the bottom figure shows phase changes over different drive frequencies.

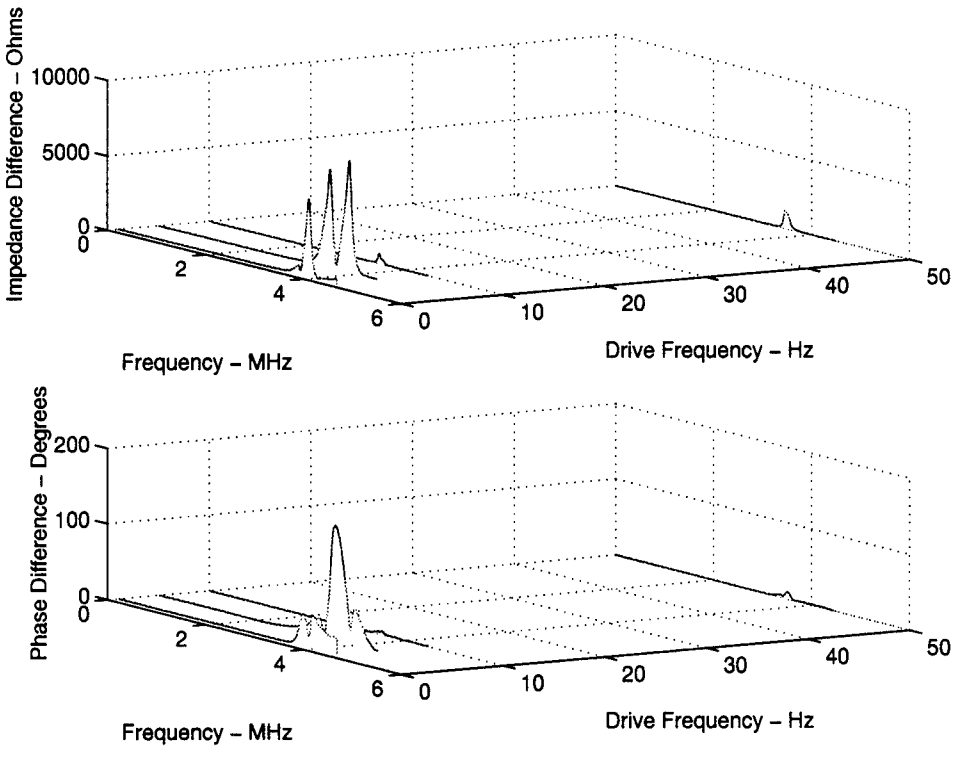

Figure 75. Resonating bridge responses to 1,1,1-TCA. The top figure shows impedance changes over different drive frequencies while the bottom figure shows phase changes over different drive frequencies.

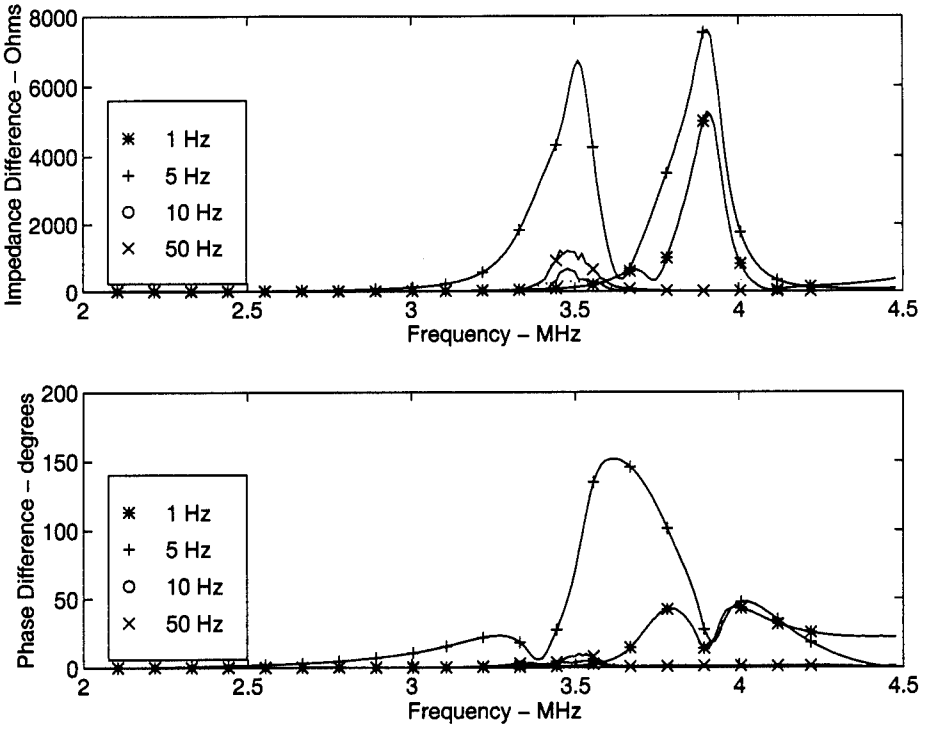

Figure 76. Resonating bridge responses to 1,1,1-TCA within a 2.5 MHz bandwidth window to show more detail. The top figure shows impedance changes over different drive frequencies while the bottom figure shows phase changes over different drive frequencies.

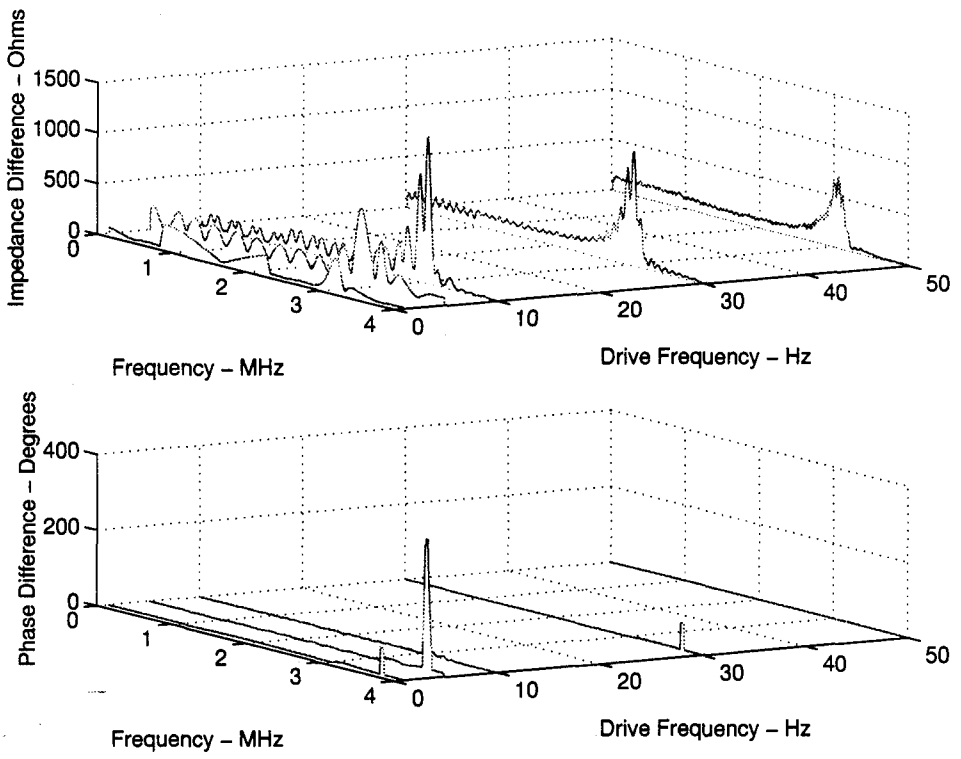

Figure 77. Resonating bridge responses to toluene. The top figure shows impedance changes over different drive frequencies while the bottom figure shows phase changes over different drive frequencies.

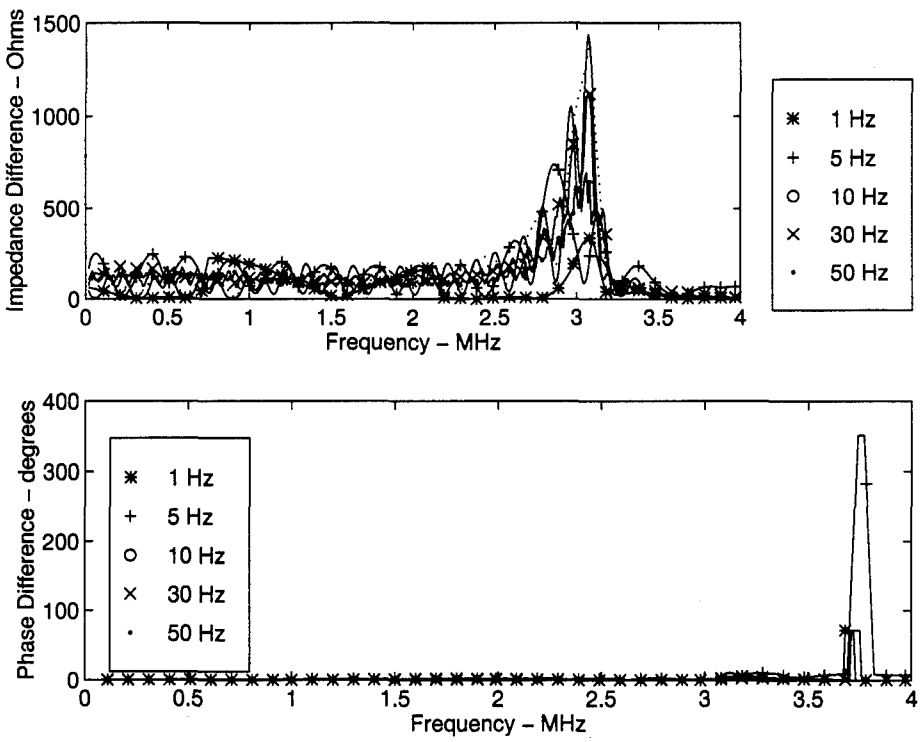

Figure 78. Resonating bridge responses to toluene within a 2 MHz bandwidth window to show more detail. The top figure shows impedance changes over different drive frequencies while the bottom figure shows phase changes over different drive frequencies.

in some chemicals suggesting that the device is desorbing chemicals as expected. Polymer degradation is not considered to be an issue for these responses.

8.2.5.2 Physical desorption. While a small bias voltage was applied to the sensing element during the purge phase, it was not enough to cause heat effects to the polymer. Any desorption occured on the device as a result of time in an inert environment or physically being thrown off the device as a result of the driving action. These mechanisms are both physical in nature and may be affected by physical parameters. One area investigated was the effect of changing the gas exposure volume from 0.5 lpm in the chemical exposure phase to 4.2 lpm in the purge phase. The devices are small enough to be affected by this pressure difference. A test of an uncoated device was made in which the the drive frequency was held constant at 10 Hz and the rate of nitrogen was varied. Nitrogen rates were varied from 0.0 to 4.0 lpm with impedance and phase data collected at each 0.5 lpm increment. The collected data is shown in Fig. 79. The standard deviation of each set (impedance and phase) was then calculated. The resulting standard deviation for each element is plotted in Fig. 80. An actual data array has also been plotted to provide scale. The largest deviation is only 14% of the actual data, suggesting that air volume does not effect the device performance significantly.

8.3 MUMPS Results

As discussed in Chapter 4, none of the devices fabricated on runs MUMPS 6 through MUMPS 8 made successful sensors and only one device, the heated chemoresistor, worked. The main problem associated with the other devices was a lack of contact between the thin film and the polysilicon electrodes. Once a metal (gold) was substituted for the polysilicon, the devices worked well. The electrostatic devices suffered from fabrication problems beyond the designer's control.

The remainder of this section will discuss the results achieved with the heated chemoresistor.

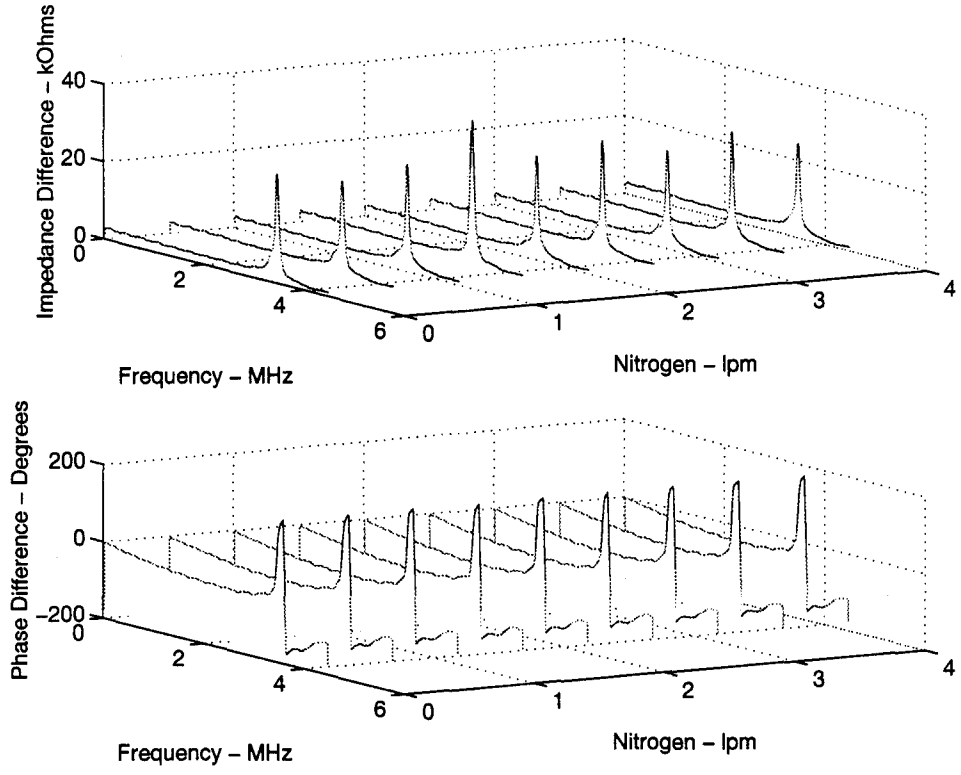

Figure 79. Effects of air volume on device operation. An uncoated bridge was driven at 10 Hz with varying volumes of nitrogen. The peak occurring in the 1.5 lpm data is most likely due to measurement error.

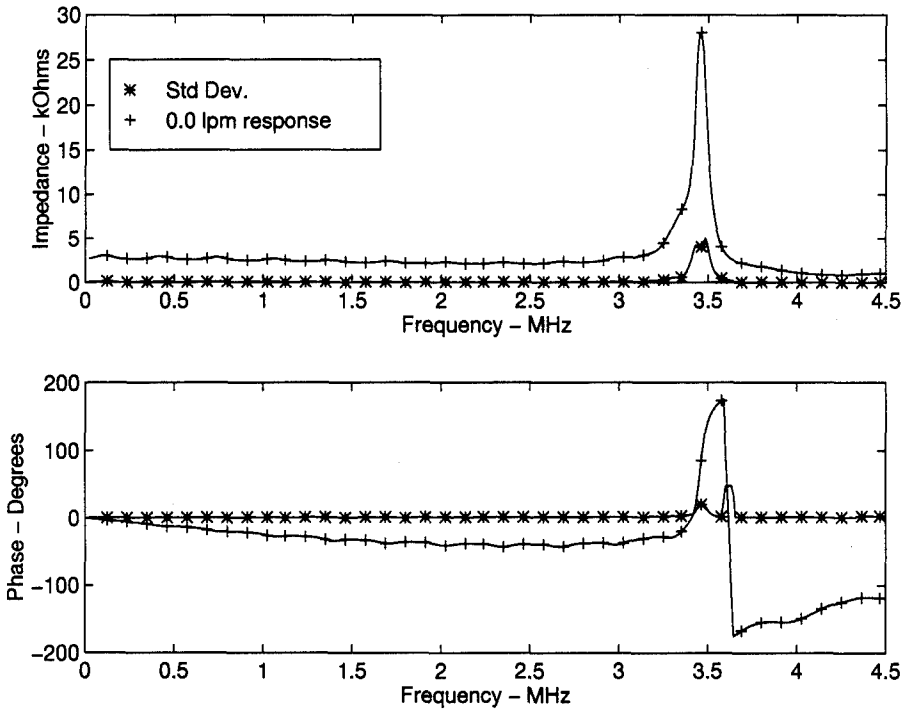

Figure 80. Standard deviation of air data. A data set has been plotted with the standard deviation curve to provide scale. This particular data plot was collected under a no gas environment (0.0 lpm).

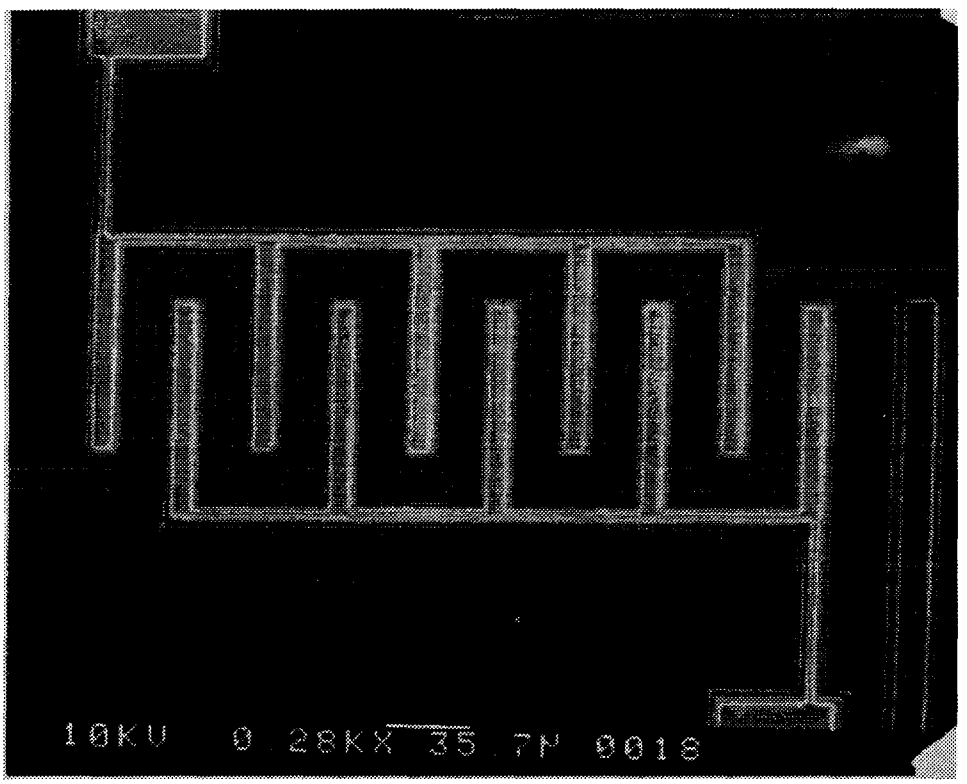

Figure 81. SEM micrograph showing close-up of the interdigitated sensing area on the heated chemoresistor.

8.3.1 DC Characteristics. The heated chemoresistor is more of a chemocapacitor in which the thin film acts as a dielectric between parallel plates. The device keeps its chemoresistor nomenclature because even though the changing nature of the film changes the impedance of the device, it does not change its resonance frequency as a variable capacitor would. The heating element is very robust, capable of glowing bright yellow under an applied voltage and withstanding over 40 VDC before burning out. The heating element was observed to heat unevenly at high voltages (< 35V) when tested under the micromanipulator. Optimization for this element is needed. Temperature profiles are unavailable due to a lack of thermal processing equipment; however, the heater's linear voltage-current relationship is shown in Fig. 82.

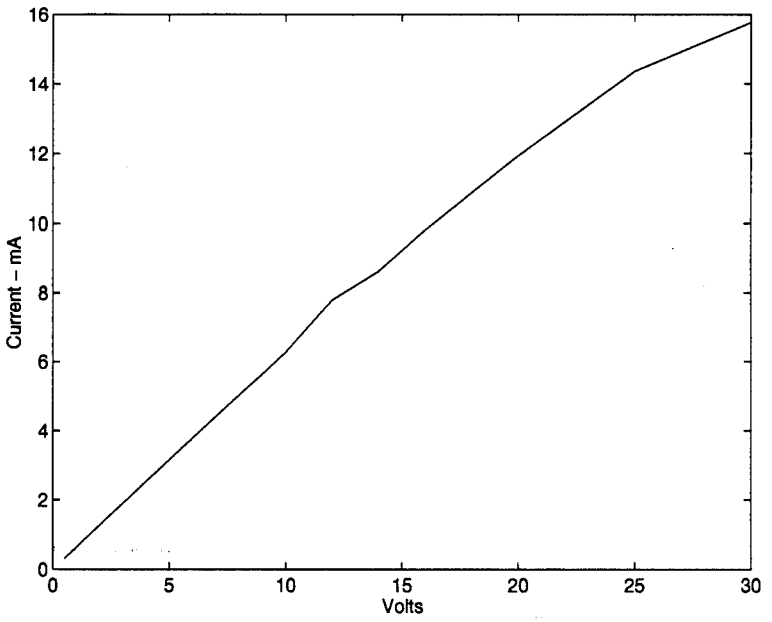

Figure 82. Heated chemoresistor's voltage current relationship at 22^o C. The DC resistance is 1320 Ω.

8.3.2 Frequency Response. Both PIB and PVTD-coated devices had similar frequency responses. A typical impedance and phase response is shown in Fig. 83. Both devices had notches in the 14-16 MHz region.

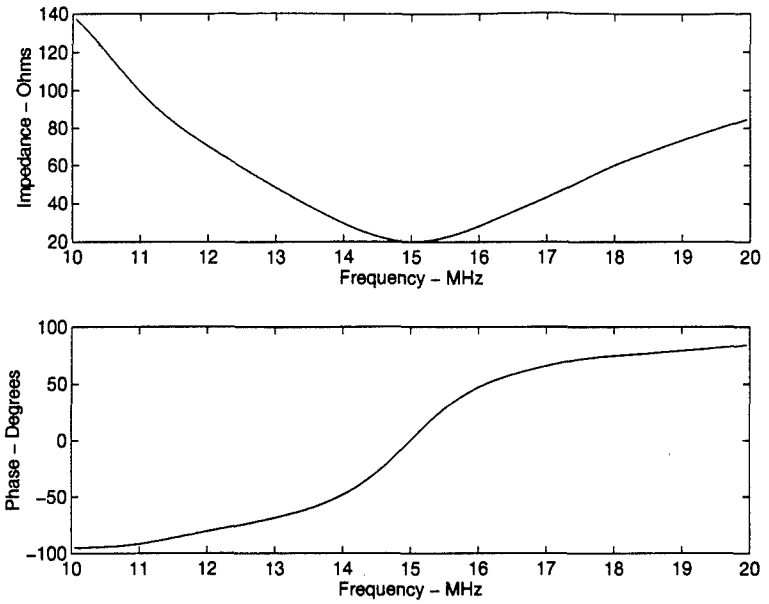

Figure 83. Frequency response of the heated chemoresistor. Impedance is shown on the top and phase is shown on the bottom. This particular device was coated with PIB.

8.3.3 Chemical Responses. Devices were exposed to chemicals for 2-minute durations at 0.5 lpm after which time, exposure response data was taken. The devices were then purged with 4.2 lpm of nitrogen for two minutes while a voltage was applied to their heaters. Purge response data was then taken after the voltage was removed. Since the thermal response of the heaters has not been characterized due to insufficient test equipment, it is assumed from Figure 82 that an increase in voltage applied to the heating element will correspond to an increase in temperature.

8.3.3.1 Data Collection Procedure. Data was collected by letting the device come to a steadystate after two minutes of uninterrupted exposure or purge. Two minutes was arbitrarily chosen as the settling time. The first measurements taken were the impedance and phase values of the impedance analyzer (see Chapter 6 for the experiment set-up) after the device had been exposed to 0.5 lpm of the chemical in a nitrogen carrier for two minutes. The chemical was then shut off, a test voltage applied to the heating element and the device purged in 4.2 lpm of nitrogen for two minutes. After

the purge time, the voltage was removed from the heating element and data sets were collected (both impedance and phase). This cycle was repeated for all voltage values applied to the heating element.

8.3.3.2 Data Analysis. Figure numbers for each device response are shown in Table 19. In addition to the device response data, a plot of the sample standard deviation of the exposure data is provided for each chemical response. This plot was generated by taking the data from the exposure data sets and computing the standard deviation at each frequency element. This test sought to ensure that the devices were consistently returning to the pre-purge condition; i.e., whether the devices were reversible. This test could also be used to determine whether significant degradation of the thin film had occurred due to chemical reaction or heating by the polysilicon element.

Table 19. Responses of Devices to Chemicals.

Chemical	PIB	PVTD
1,1,1-TCA	Fig. 84 and Fig. 85	Fig. 90 and Fig. 91
TCE	Fig. 86 and Fig. 87	Fig. 92 and Fig. 93
toluene	Fig. 88 and Fig. 89	Fig. 94 and Fig. 95

8.3.4 Interpretation of Results. The results obtained from the heated chemoresistor suggest that the device response is a function of the thin film and the chemical to which it was exposed. Possible explanations describing the response mechanisms are polymer degradation, heat-induced chemical reaction, and heat-induced diffusion barriers.

8.3.4.1 Polymer degradation. The first thoughts on the device responses were that the polymer may be irreversibly damaged by the heating element or exposure to different chemicals. The data does not suggest that the polymer is degrading as responses do not vary significantly enough to show that the polymer has lost its integrity and sorbing capability. There is also a gradation of response in some chemicals suggesting that the device is desorbing chemicals as expected. Polymer degradation is not considered to be an issue for these responses.

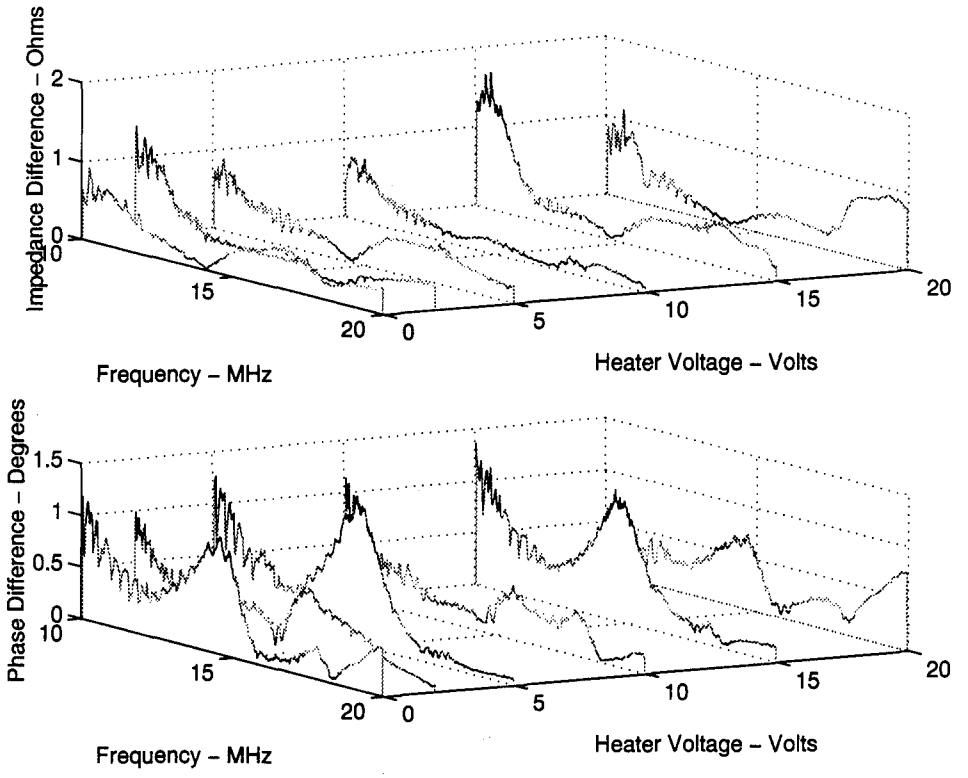

Figure 84. PIB responses to 1,1,1-TCA. The top figure shows impedance changes over different applied heating voltages while the bottom figure shows the corresponding phase changes.

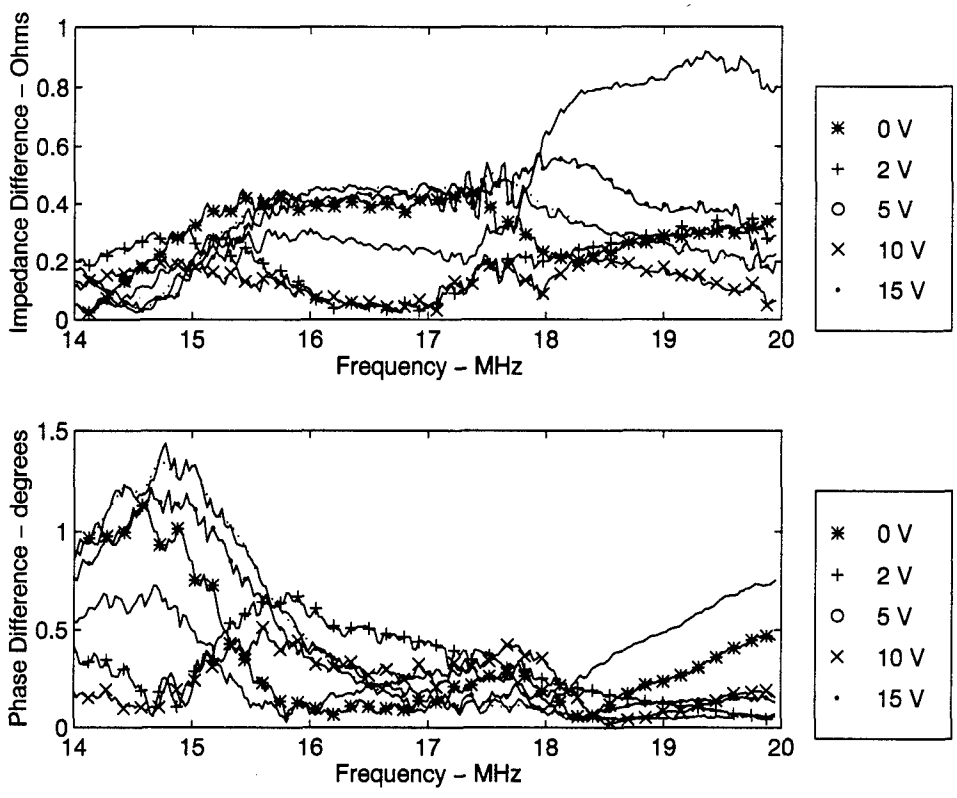

Figure 85. PIB responses to 1,1,1-TCA within a 6 MHz bandwidth window to show more detail. The top figure shows impedance changes after different heater voltages were applied while the bottom figure shows the corresponding phase changes.

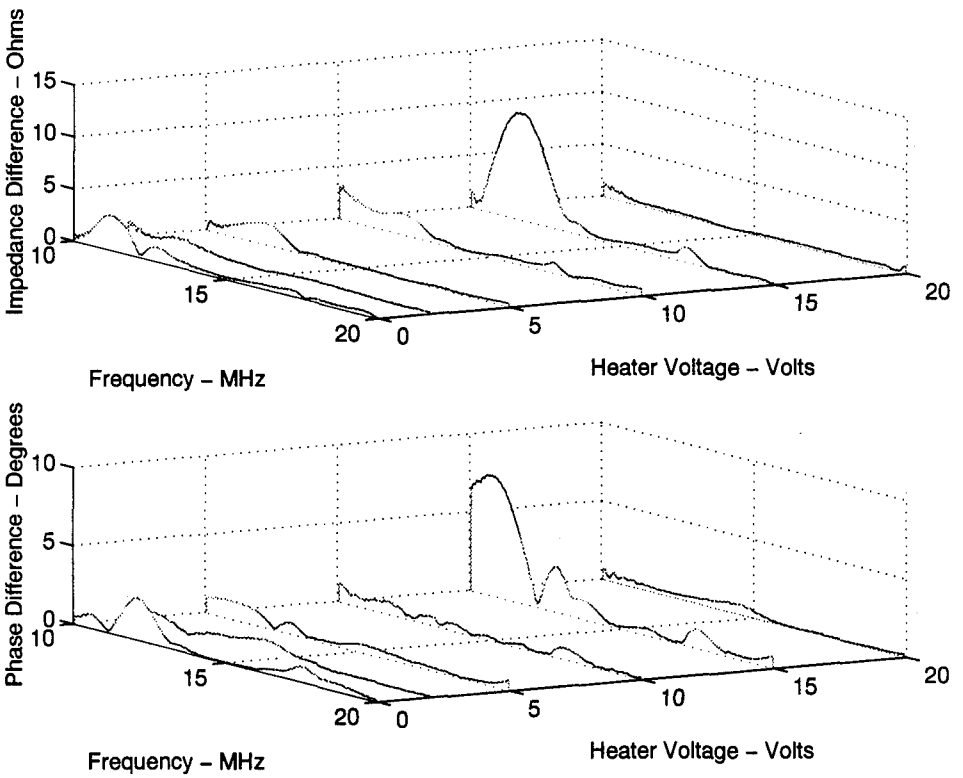

Figure 86. PIB responses to TCE. The top figure shows impedance changes over different applied heating voltages while the bottom figure shows the corresponding phase changes.

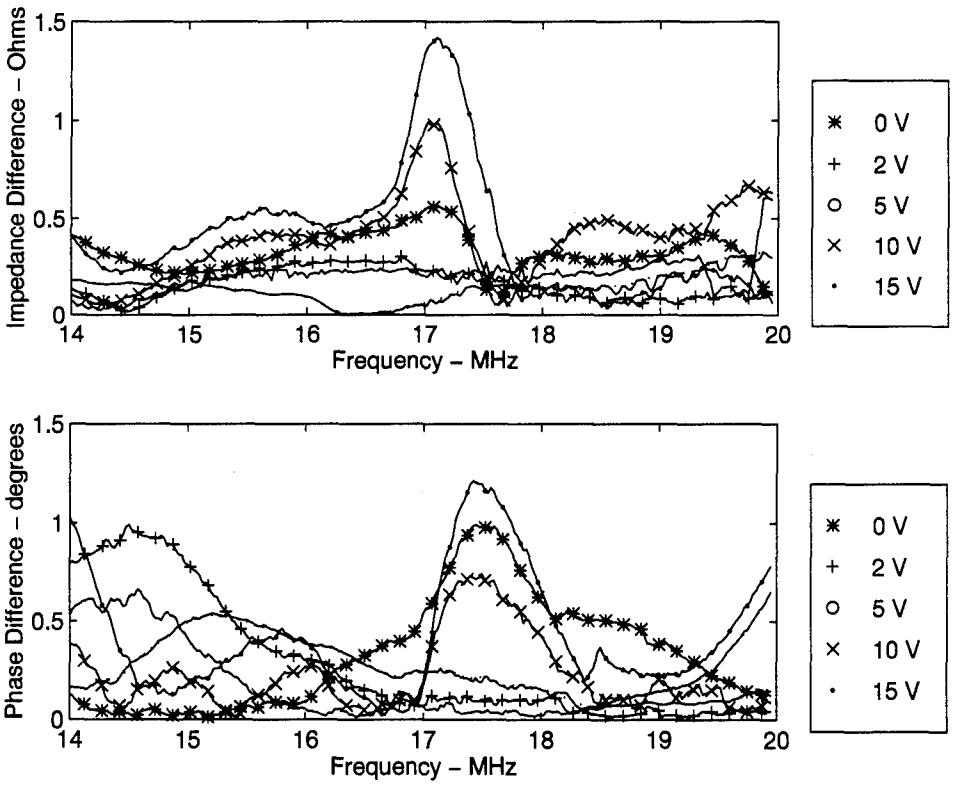

Figure 87. PIB responses to TCE within a 6 MHz bandwidth window to show more detail. The top figure shows impedance changes after different heater voltages were applied while the bottom figure shows the corresponding phase changes.

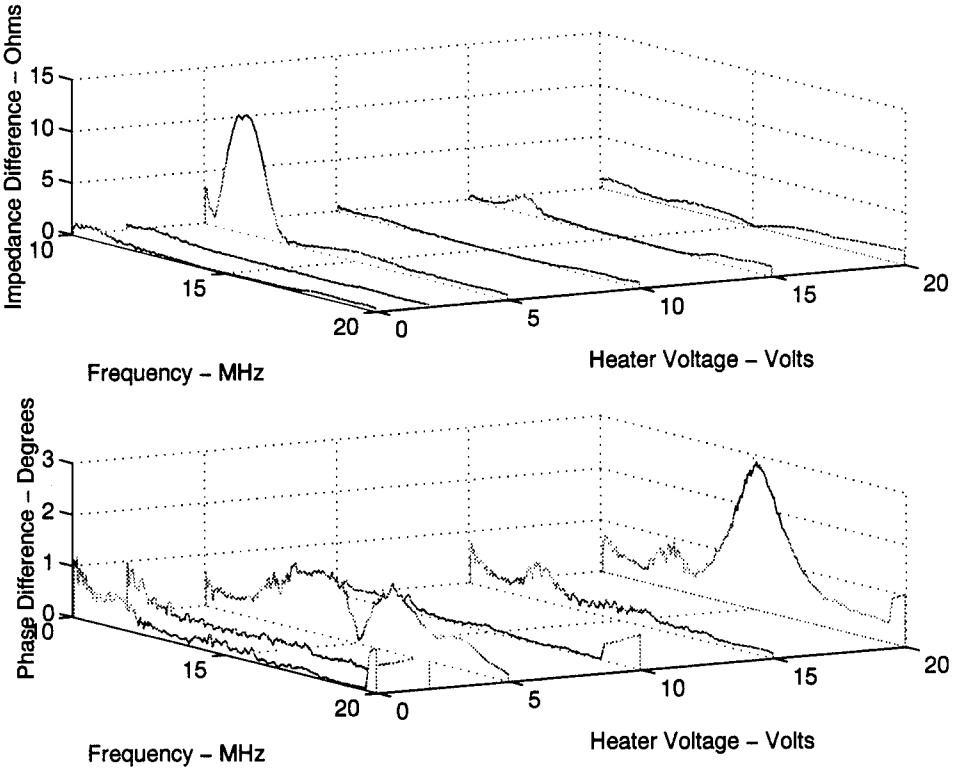

Figure 88. PIB responses to toluene. The top figure shows impedance changes over different applied heating voltages while the bottom figure shows the corresponding phase changes.

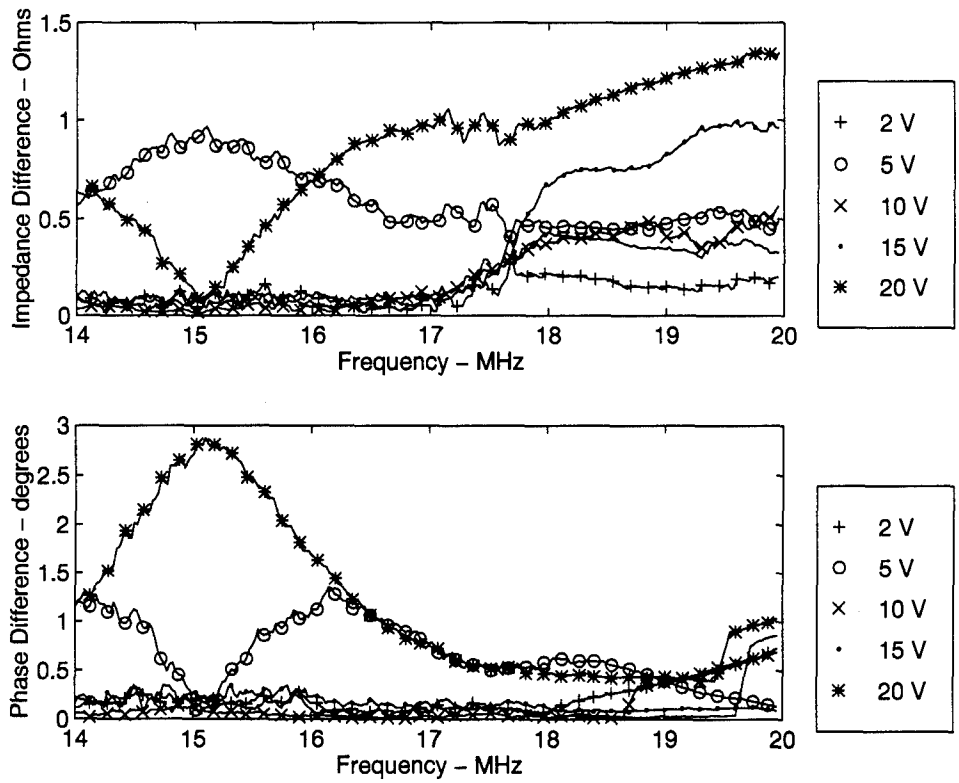

Figure 89. PIB responses to toluene within a 6 MHz bandwidth window to show more detail. The top figure shows impedance changes after different heater voltages were applied while the bottom figure shows the corresponding phase changes.

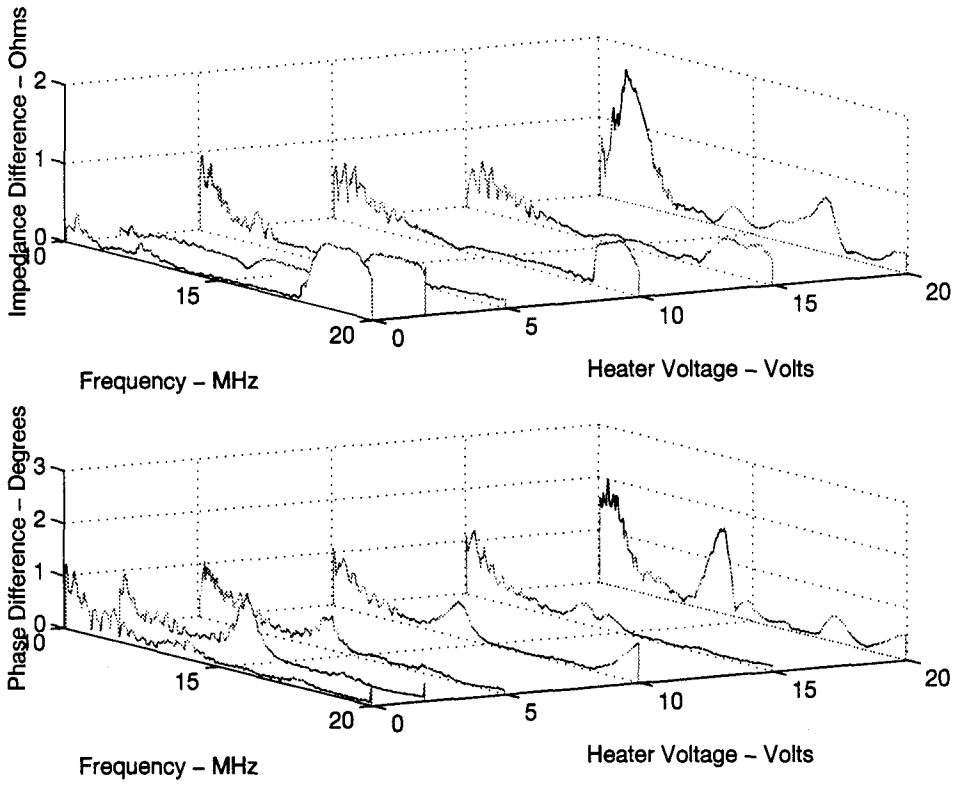

Figure 90. PVTD responses to 1,1,1-TCA. The top figure shows impedance changes over different applied heating voltages while the bottom figure shows the corresponding phase changes.

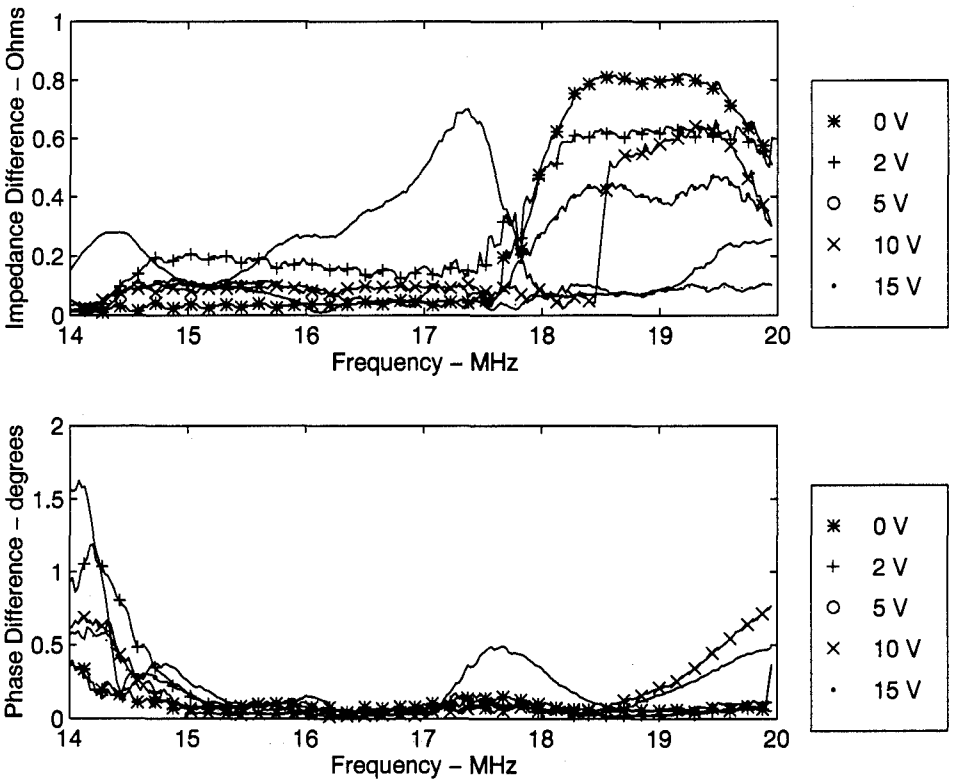

Figure 91. PVTD responses to 1,1,1-TCA within a 6 MHz bandwidth window to show more detail. The top figure shows impedance changes after different heater voltages were applied while the bottom figure shows the corresponding phase changes.

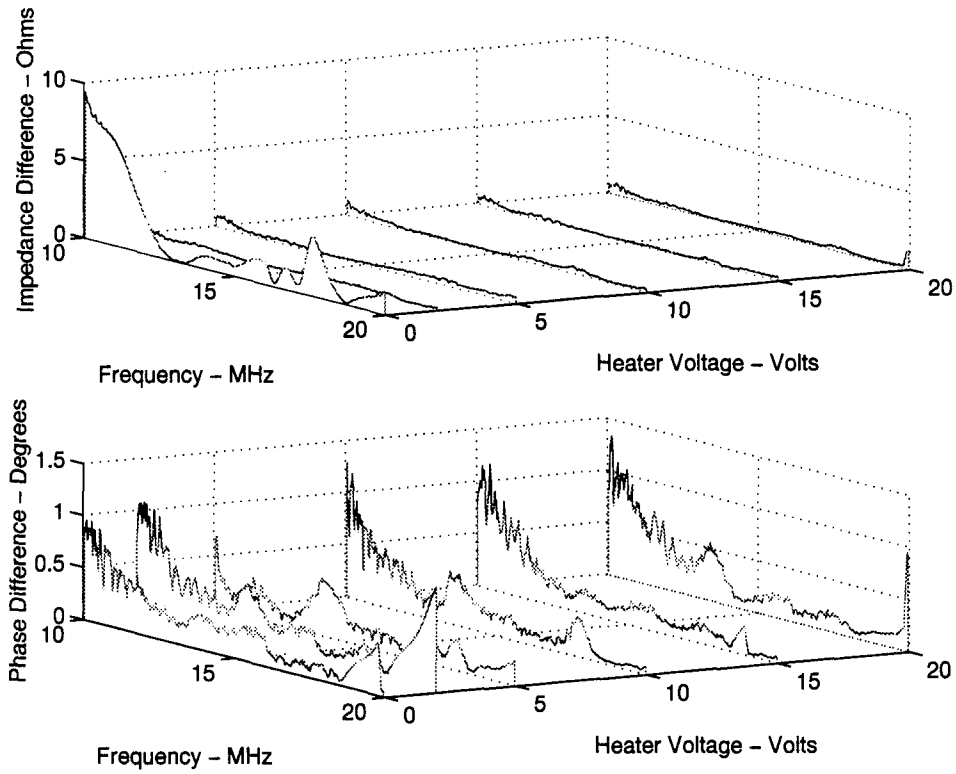

Figure 92. PVTD responses to TCE. The top figure shows impedance changes over different applied heating voltages while the bottom figure shows the corresponding phase changes.

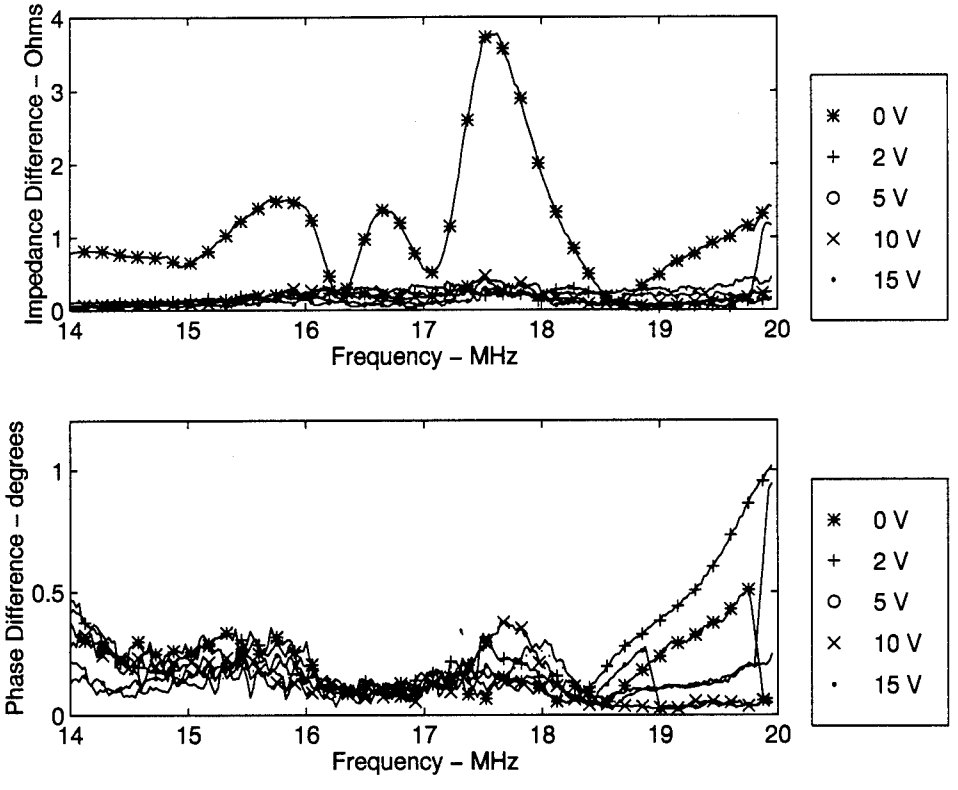

Figure 93. PVTD responses to TCE within a 6 MHz bandwidth window to show more detail. The top figure shows impedance changes after different heater voltages were applied while the bottom figure shows the corresponding phase changes. It is obvious from this graph that the 0 V purge provides the most dramatic change in the device.

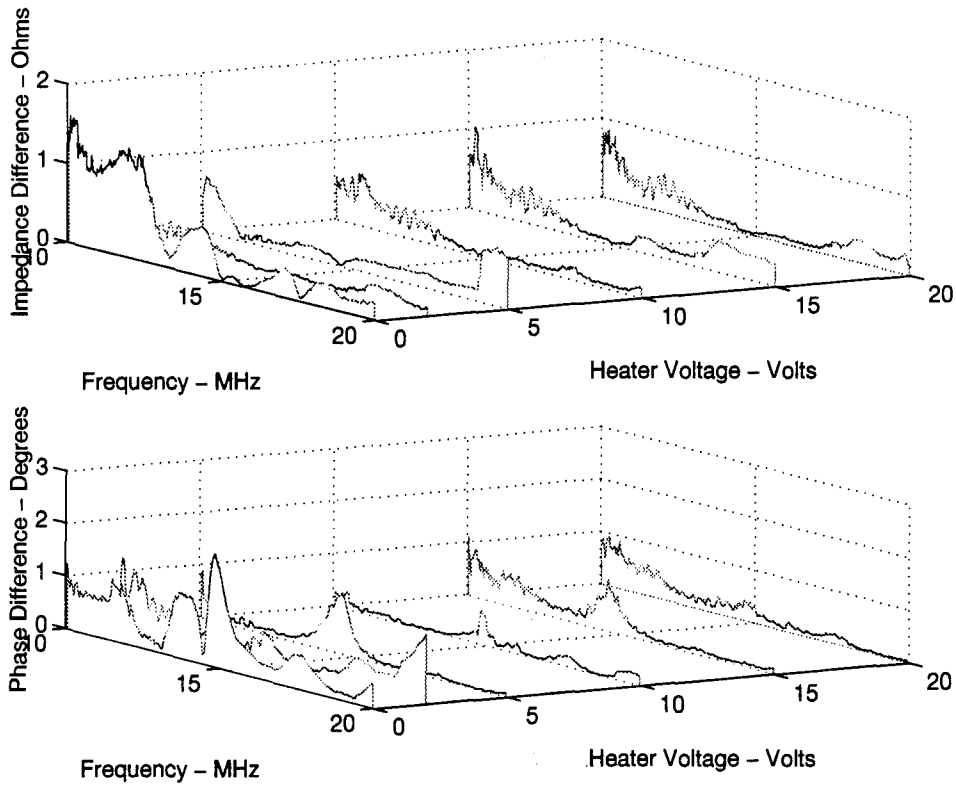

Figure 94. PVTD responses to toluene. The top figure shows impedance changes over different applied heating voltages while the bottom figure shows the corresponding phase changes.

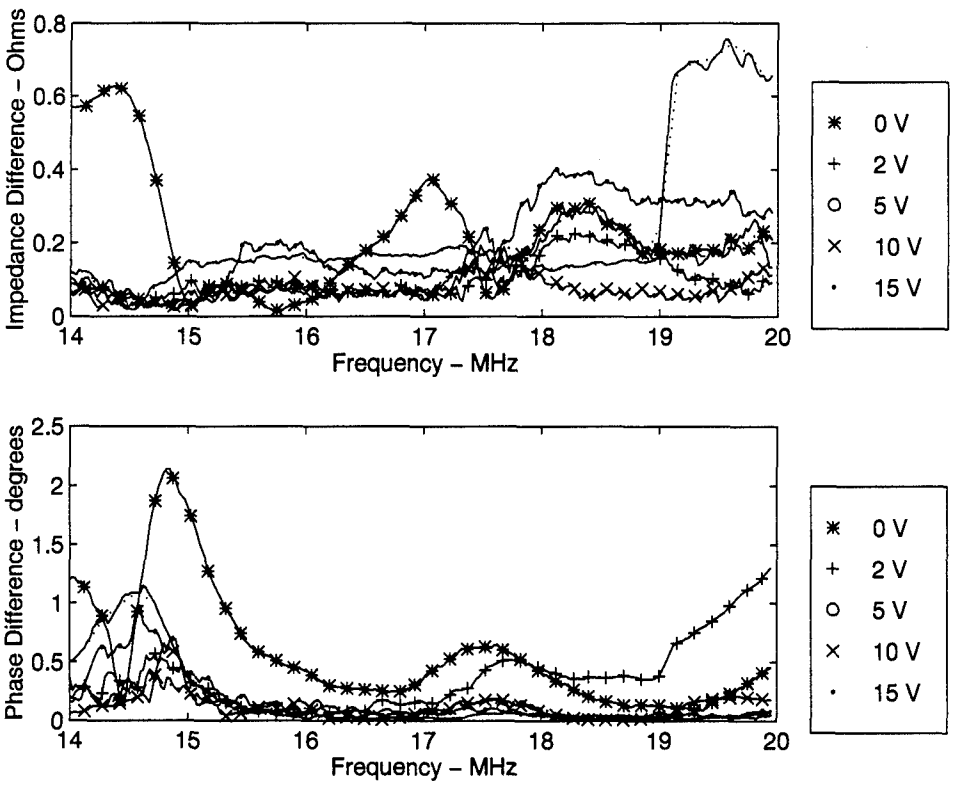

Figure 95. PVTD responses to toluene within a 6 MHz bandwidth window to show more detail. The top figure shows impedance changes after different heater voltages were applied while the bottom figure shows the corresponding phase changes.

8.3.4.2 Heat-induced Chemical Reactions. Because heat is being introduced to the system (thin film polymer with sorbed chemicals) after exposure, chemical reactions may be occurring, binding chemical molecules into the polymer surface or causing other reactions which affect the polymer's dielectric constant. If this is the case, the device may have reversability problems as total desorption will not be possible. The fact that the responses from collected data do not drift significantly disproves this theory.

8.3.4.3 Heat-Induced Diffusion Barriers. Heat may also affect the device by changing the consistency of the polymer by making it more rubbery, changing electrostatic charges or opening paths for molecular escapes. Chemicals may be trapped in the polymer based on their physical size even though they have enough energy to desorb. Heat also electrically alters the polymer, causing different responses. This was shown by testing the polymers using the same test protocol used to collect data with chemicals, but using only nitrogen for both the exposure (2 minutes at 0.5 lpm) and purge (2 minutes at 4.2 lpm with an applied heater voltage) data collection. As Figs. 96 and 97 show, the polymers will behave differently as a function of voltage applied purges.

Even though the polymers have responses in an inert environment, these responses must be compared to responses in a chemical environment. The responses are not the same, suggesting that the presence of chemicals in the polymer is affecting the electrical make-up of the dielectric, promoting or prohibiting the polymer's inherent response.

8.4 AFIT Microsensor Fabrication and Operation.

Due to time considerations, the AFIT microsensor was not coated or tested under chemical exposure. The heating element was tested; however, insufficient etching left enough oxide on the contact holes to insulate the heating element from effective contact with the gold. The surface electrodes could still have been coated and would have functioned as a chemoresistor.

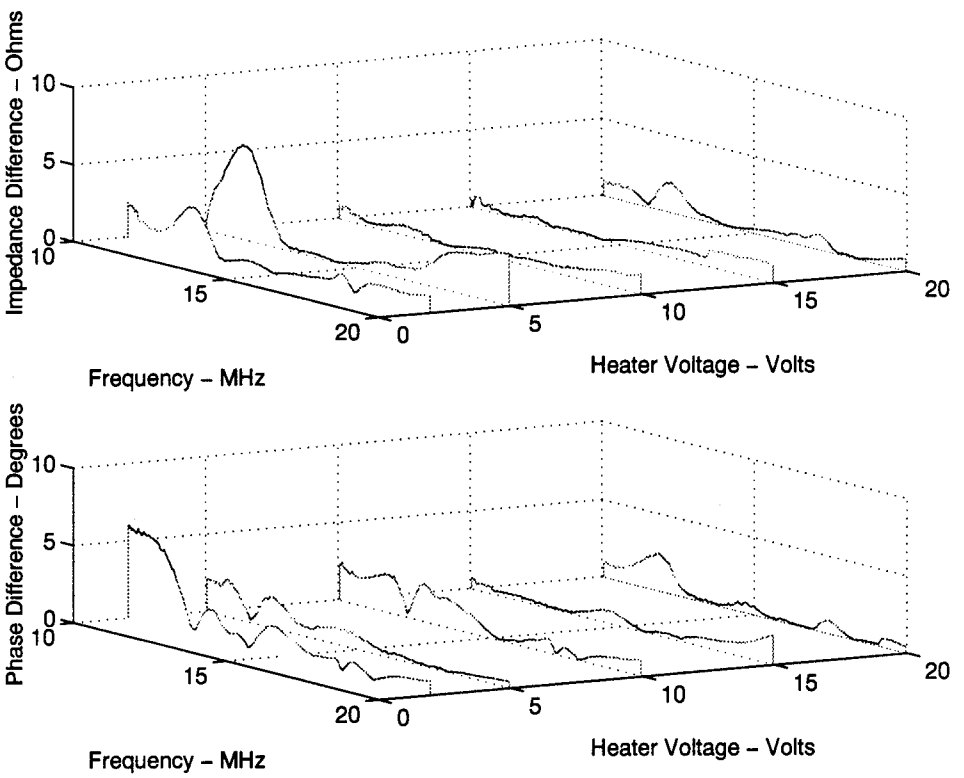

Figure 96. PIB responses in an inert environment.

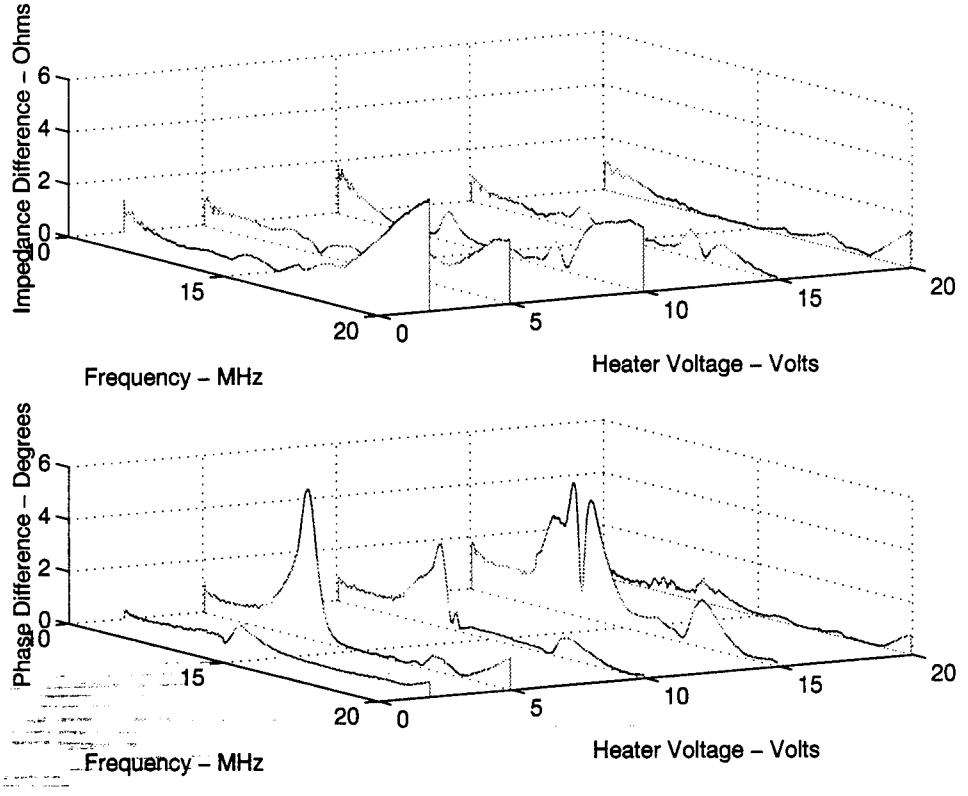

Figure 97. PVTD responses in an inert environment.

8.5 Recommendations.

A number of recommendations for follow-on study and observations made in the course of this thesis are provided below. Since this thesis required such intensive laboratory work, a special section has been included to aid future work in this area.

8.5.1 General Follow-on Research Recommendations.

8.5.1.1 Time Response Analysis. The tests and data collected from the working devices were steady-state in nature. The actual time responses of the devices when initially exposed to a chemical and during the purge phase were not analyzed due to time limitations.

8.5.1.2 Different Thin Film Coatings. While several thin films were identified for testing, only two were used. Additional devices should be fabricated and tested using other thin films, especially the metal oxides and phthalocyanines. Other polymers should also be considered in addition to the two used.

8.5.1.3 Different Chemicals. Only three chemicals were used to test the devices and all were introduced to the device at saturated levels. Different chemicals, especially common pollutant gases such as ozone (O_3), sulphur dioxide (SO_2), and nitrogen dioxide (NO_2), and chemical agent simulants such as diisopropyl methylphosphonate (DIMP) and dimethyl methylphosphonate (DMMP) should be tested. Sensitivity studies should also be conducted to determine the range and limits of detection for each chemical.

8.5.1.4 Combination Response. Challenge gases were introduced to the devices individually in order to prove the devices worked. Analysis of their steady-state response showed that features could be extracted from each device's response to successfully discriminate between TCE and

TCA. Combinations of gases should be introduced to coated devices to analyze their response and determine if enough separation exists to properly classify individual chemicals.

8.5.1.5 AFIT MEMS Capability. Although not an intentional goal, this thesis showed that AFIT has the capability to produce simple bulk micromachined devices. The potential of this process should be further investigated in light of the ruggedness of the devices and relative economy of producing them. Also, unlike outside fabrication processes where the designer has no control over fabrication processes, the designer has complete control over the process using in-house equipment.

In addition to improving the AFIT Microsensor, one possible application is in producing deformable mirrors as shown in Fig. 98. A simple heated actuator can be fabricated with a gold surface, and motion can be induced through bimorphic action between the silicon dioxide support structure and the gold layer.

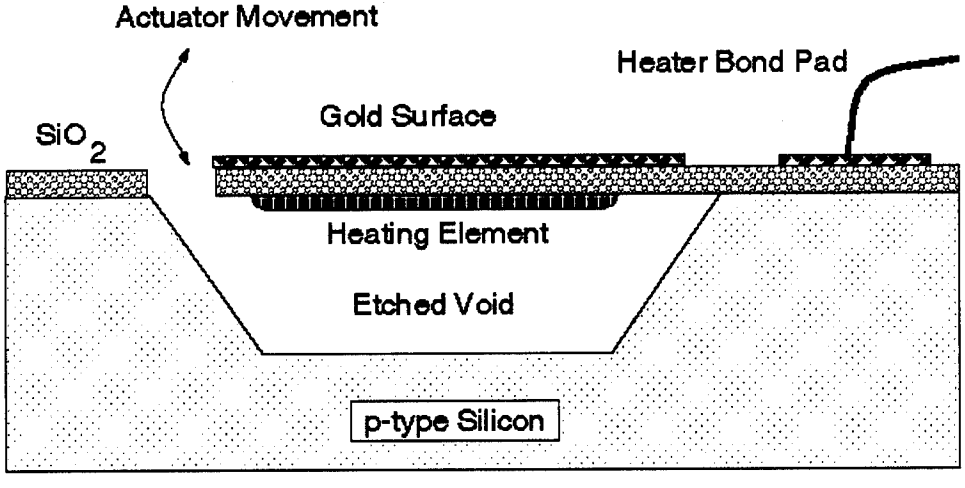

Figure 98. Profile of a deformable mirror using a heated actuator with a gold coated surface. This design could be easily produced using the fabrication process described in this thesis.

8.5.1.6 Sensor Arrays. Multiple sensors with different thin films should be incorporated with signal processing hardware to create an array sensor. Different features should be extracted

and evaluated along with various pattern recognition techniques to optimize discrimination between different chemical responses under different device environments.

8.5.2 Laboratory Recommendations.

8.5.2.1 Data Acquisition Software. A comment for AFIT in general is to train an individual on data acquisition techniques using common data acquisition software and hardware. The start-up knowledge required to learn the data gathering tools was a considerable hurdle that limited the tests that could be performed. Customer Support centers for the hardware were incapable of helping most problems and the documentation that came with the devices was difficult and often incomplete. Trial-and-error proved the most effective means to learn the system. Even more frustrating was the lack of experienced individuals at AFIT who could help set up a new experiment. Existing data collection relied on proprietary software that came with a measuring device or old software written by someone who had since graduated and was unable to provide assistance. A lab technician should be trained in IEEE-488 general purpose interface bus (GPIB) programming and be available for experimental set-up consulting, or a manual should be written that clearly explains how to program and use the card.

8.5.2.2 Thermal Imager. A thermal imaging camera should be purchased to thermally characterize MEMS devices. The Physics department currently has an instrument (Inframetrics 760 IR Image Radiometer) that has supporting lenses that have 300 μm resolution; however, they do not have the lenses themselves. Future sponsorship in the MEMS area should be encouraged to fund these lenses.

Bibliography

1. L. Gallagher, "Clean water act," in *Environmental Law Handbook* (T. Sullivan, ed.), pp. 135–168, Maryland: Government Institutes, Inc., 13th ed., 1995.
2. R. Griffin, *Principles of Air Quality Management.* CRC Press, 1994.
3. D. Skoog and D. West, *Principles of Instrumental Analysis.* Holt, Rinehart and Wilson, 2nd ed., 1980.
4. C. I. Corporation, "Toxicological profile for fuel oil (draft)," tech. rep., US Department of Health and Human Services, 1992. TP 92/19.
5. R. Cavicchi, J. Suehle, P. Chaparala, K. Kreider, M. Gaitan, and S. Semancik, "Micro-hotplate gas sensor," in *Solid-State Sensor and Actuator Workshop*, (Hilton Head), pp. 53–56, June 1994.
6. T. Oishi, M. Kaneyasu, and A. Ikegami, "Discrimination of chemical compounds and functional groups by pattern recognition using an integrated sensor," *Hybrid Circuits: Journal of the International Society for Hybrid Microelectronics*, vol. 16, pp. 19–22.
7. Q. Wu, K.-M. Lee, and C.-C. Liu, "Development of chemical sensors using microfabrication and micromachining techniques," *Sensors and Actuators B*, vol. 13-14, pp. 1–6, 1993.
8. N. Najafi, K. Wise, and J. Schwank, "A micromachined ultra-thin-film gas detector," *IEEE Trans. on E. Devices*, vol. 41, pp. 1770–1777, October 1994.
9. J. Breyzek, K. Peterson, and W. McCulley, "Micromachines on the march," *IEEE Spectrum*, pp. 20–31, May 1994.
10. L. Ristic, F. Shemansky, M. Kniffin, and H. Hughes, "Bulk micromachining technology," in *Sensor Technology and Devices*, pp. 49–93, Artech House, 1994.
11. X.-P. Wu *et al.*, "A study on deep etching of silicon using ethylenediamine-pyrocatechol-water," *Sensors and Actuators*, vol. 9, pp. 333–343, 1986.
12. "Magic version 6.4.4." Stanford University, 1990.
13. I. Cadence Design Systems, "Cadence version 4.3.3," 1992.
14. MOSIS, University of Southern California, *MOSIS Users Manual*, 1st ed., 1988.
15. 2nd Lt Briton Read, "Silicon based microactuators for telerobotic tactile stimulation," Master's thesis, Air Force Institute of Technology, Wright-Patterson AFB, OH, December 1994.
16. R. Howe, *Integrated Silicon Electromechanical Vapor Sensor.* PhD thesis, University of California Berkeley, May 1984.
17. R. Lichtenthaler, "Instrumental analysis of petroleum hydrocarbons," in *Analysis of Organic Micropollutants in Water* (G. Angeletti and A. Bjorseth, eds.), Hingham, MA: Kluwer Academic Publishers, 1984.
18. A. P. H. Association, *Standard Methods for the Examination of Water and Wastewater.* American Public Health Association, Washington DC, 1992.

19. W. Giger *et al.*, "Determination of organic water pollutants by the combined use of high-performance liquid chromatography and high-resolution gas chromatography," in *Analysis of Organic Micropollutants in Water* (G. Angeletti and A. Bjorseth, eds.), Hingham, MA: Kluwer Academic Publishers, 1984.

20. D. Dandge *et al.*, "Fiber optic chemical sensor for jet fuel," in *Chemical, Biological, and Environmental Sensors*, (Boston), pp. 132–139, SPIE, SPIE Press, Sept 1989.

21. J. Peterson, "Fiber optic chemical sensor development," in *Chemical, Biochemical, and Environmental Applications of Fibers*, (Boston), pp. 2–17, SPIE, SPIE Press, Sept 1988.

22. W. Chudyk *et al.*, "Field determination of ground water contamination using laser fluorescence and fiber optics," in *Chemical, Biological, and Environmental Sensors*, (Boston), pp. 123–129, SPIE, SPIE Press, Sept 1989.

23. S. Angel *et al.*, "Simple reversible sensor using solvatochrome dyes," in *Chemical, Biochemical, and Environmental Sensors III*, pp. 86–95, SPIE, SPIE Press, 1991.

24. 2nd Lt Neal Hauschild, "Investigation of the sensitivity, selectivity and reversibility of the chemfet to detect nitrogen dioxide, dimethyl methylphosphonate and boron trifluoride," Master's thesis, Air Force Institute of Technology, Wright-Patterson AFB, OH, December 1993.

25. G. Osbourn, J. Bartholomew, G. Frye, and A. Ricco, "Cluster-based pattern recognition using surface acoustic wave array signals," in *Solid-State Sensor and Actuator Workshop*, (Hilton Head), pp. 193–196, June 1994.

26. J. Reichert, W. Coerdt, and H. Ache, "Development of a surface acoustic wave sensor array for the detection of methanol in fuel vapor," *Sensors and Actuators B*, vol. 13-14, pp. 294–296, 1993.

27. A. Ricco *et al.*, "New materials and multidimensional cluster analysis for saw chemical sensor arrays," in *Solid-State Sensor and Actuator Workshop*, (Hilton Head), pp. 180–183, June 1994.

28. H. Lee, S. Wang, D. Smolenski, M. Viola, and E. Klusendorf, "In situ monitoring of high-temperature degraded engine oil condition with microsensors," *Sensors and Actuators B*, vol. 20, pp. 49–54, 1994.

29. J. Hunag and M. Wrighton, "Microelectrochemical multitransistor devices based on electrostatic binding of electroactive anionic metal complexes in protonated poly(4-vinylpyridine): Devices that can detect and distinguish up to three species simultaneously," *Analytic Chemistry*, vol. 65, pp. 2740–2746, 1993.

30. S. Change and D. Hicks, "Tin oxide microsensors on thin silicon membranes," in *Microsensors* (R. Muller, ed.), pp. 262–265, New York: IEEE Press, 1990.

31. G. Heiland and D. Kohl, "Problems and possibilities of oxidic and organic semiconductor gas sensors," in *Microsensors* (R. Muller, ed.), pp. 266–269, New York: IEEE Press, 1990.

32. R. Reay *et al.*, "Microfabricated electrochemical detector for capillary electrophoresis," in *Solid-State Sensor and Actuator Workshop*, (Hilton Head), pp. 229–233, June 1994.

33. M. Zanini *et al.*, "Fabrication and properties of a silicon-based high sensitivity microcalorimetric gas sensor," in *Solid-State Sensor and Actuator Workshop*, (Hilton Head), pp. 176–179, June 1994.

34. S. Terry, J. Jerman, and J. Angell, "A gas chromatographic air analyzer fabricated on a silicon wafer," *IEEE Trans. on Electron. Dev.*, vol. 26, pp. 1880–1886, Dec 1979.

35. R. Reston and E. Kolesar, "Silicon-micromachined gas chromatography system used to separate and detect ammonia and nitrogen dioxide - part 1: Design, fabrication, and integration of the gas chromatography system," *J of Microelectromechanical Systems*, vol. 3, pp. 134–140, December 1994.

36. A. Ricco, L. Kepley, R. Thomas, L. Sun, and R. Crooks, "Self-assembling monolayers on saw devices for selective chemical detection," *IEEE J of Electronic Devices*, pp. 114–117, 1992.

37. H. Wohltjen, "Mechanism of operation and design considerations for surface acoustic wave device vapor sensors," in *Microsensors* (R. Muller, ed.), pp. 274–282, New York: IEEE Press, 1990.

38. J. Gardner, *Microsensors: Principles and Applications*. Wiley and Sons, 1994.

39. Z. Khlebarov, A. Stoyanova, and D. Topalova, "Surface acoustic wave gas sensors," *Sensors and Actuators B*, vol. 8, pp. 33–40, 1992.

40. J. Grate, S. Martin, and R. White, "Acoustic wave microsensors, part 1," *Analytical Chemistry*, vol. 65, pp. 940–948, Nov 1993.

41. S. Martin, G. Frye, R. Cernosek, and S. Senturia, "Microtextured resonators for measuring liquid properties," in *Solid-State Sensor and Actuator Workshop*, (Hilton Head), pp. 229–233, June 1994.

42. J. Janata, "Chemically sensitive field effect transistors," in *Solid-State Chemical Sensors* (J. Janata and R. Huber, eds.), pp. 61–116, London: Academic Press, 1985.

43. R. Hughes, D. Moreno, M. Jenkins, and J. Rodriguez, "The response of the sandia robust wide range hydrogen sensor to h2-o2 mixtures," in *Solid-State Sensor and Actuator Workshop*, (Hilton Head), pp. 57–60, June 1994.

44. J. Smith *et al.*, "Minature shear mode resonator sensor array with integrated control electronics," Contract DE-AC04-94AL85000, Sandia National Laboratories, New Mexico, 1994.

45. R. Feynman, "There's plenty of room at the bottom," *Journal of Microelectromechanical Systems*, vol. 1, pp. 60–66, Mar 1992.

46. R. Howe and R. Muller, "Resonant-microbridge vapor sensor," in *Microsensors* (R. Muller, ed.), pp. 174–181, New York: IEEE Press, 1990.

47. D. Machin and C. Rogers, eds., *Encyclopedia of Polymer Science and Technology*, vol. 3. McGraw-Hill, 1970.

48. D. Machin and C. Rogers, eds., *Encyclopedia of Polymer Science and Technology*, vol. 12. McGraw-Hill, 1970.

49. G. Gaggiotti, A. Galdikas, S. Kaciulis, G. Mattogno, and A. Setkus, "Surface chemistry of tin oxide based gas sensors," *J. Appl. Phys.*, vol. 76, pp. 4467–4471, October 1994.

50. A. Vogel, B. Hoffmann, S. Schwiegk, and G. Wegner, "Novel langmuir-blodgett membranes for silicon-based ion sensors," *Sensors and Actuators B*, vol. 4, pp. 65–71, 1991.

51. C. Hamann *et al.*, "Lead phthalocyanine thin films for nitrogen dioxide sensors," *Sensors and Actuators B*, vol. 4, pp. 73–78, 1991.

52. R. Schwarzenbach *et al.*, *Environmental Organic Chemistry*. John Wiley and Sons, 1993.

53. S. Morrison, "Chemical sensors," in *Semiconductor Sensors* (S. Sze, ed.), pp. 383 – 414, John Wiley and Sons, 1994.

54. M. Madou and S. Morrison, *Chemical Sensing with Solid State Devices*. Academic Press, 1989.

55. J. Grate, S. Patrash, and M. Abraham, "Method for estimating polymer-coated acoustic wave vapor sensor responses," *Analytical Chemistry*, vol. 67, pp. 2162–2169, July 1 1995.

56. A. McGill, M. Abraham, and J. Grate, "Choosing polymer coatings for chemical sensors," *Chemtech*, pp. 27–37, September 1994.

57. A. Ulman, *An Introduction to Ultra-Thin Organic Films*. NY: Academic Press, 1990.

58. F. Moser and A. Thomas, *The Phthalocyanines, Volume I: Properties*. CRC Press, 1983.

59. A. Snow and W. Barger, "Phthalocyanine films in chemical sensors," in *Phthalocyanines: Properties and Applications* (C. Leznoff and A. Lever, eds.), pp. 341–393, VCH Publishers, 1989.

60. R. V. Stuart, *Vacuum Technology, Thin Films, and Sputtering*. Academic Press, Inc., 1983.

61. S. Sze, *Semiconductor Devices, Physics and Technology*. John Wiley and Sons, 1985.

62. C. Giles *et al.*, "Historical introduction," in *Langmuir-Blodgett Films* (G. Roberts, ed.), pp. 1–14, Plenum Press, 1990.

63. R. Hann, "Molecular structure and monolayer properties," in *Langmuir-Blodgett Films* (G. Roberts, ed.), pp. 17–92, Plenum Press, 1989.

64. G. Stemme, "Resonant silicon sensors," *J. of Micromech. Microeng.*, vol. 1, pp. 113–125, October 1991.

65. 2nd Lt M. Adrian Michalicek, "Design, fabrication, modelling, and testing of surface-micromachined micromirror devices," Master's thesis, Air Force Institute of Technology, Wright-Patterson AFB, OH, June 1995.

66. J. B. Marion and S. T. Thornton, *Classical Dynamics of Particles and Systems*. San Diego: Harcourt Brace Jovanovich, 3rd ed., 1988.

67. W. Hayt, *Engineering Electromagnetics*. NY: McGraw-Hill, 4th ed., 1981.

68. R. Lewis, ed., *Hawley's Condensed Chemical Dictionary*. Van Nostrand Reinhold Co., 12th ed., 1993.

69. K.-N. Tu *et al.*, *Electronic Thin Film Science for Electrical Engineers and Material Scientists*. NY: MacMillan Publishing, 1992.

70. F. MacRitchie, *Chemistry at Interfaces*. Academic Press, 1990.

71. C. Hauley, ed., *The Encyclopedia of Chemistry*. Van Nostrand Reinhold Co., 3rd ed., 1973.

72. R. Jaeger, *Introduction to Microelectronic Fabrication*, vol. V. Addison-Wesley Publishing Co., 1993.

73. Technology Modeling Associates, Inc., Palo Alto, CA, *TSUPREM-4 User's Manual*, 6 ed., December 1993.

74. B. Deal and A. Grove, "General relationship for the thermal oxidation of silicon," *J. Appl. Physics*, vol. 36, p. 3770, 1965.

75. K. Siroky, J. Jiresova, and L. Hudec, "Iron oxide thin film gas sensor," *Thin Solid Films*, vol. 245, pp. 211–214, 1994.

76. Olin Hunt Specialty Products, Inc., NJ, *Waycoat Negative Photoresist Technical Bulletin 39*, 1990.

77. The Mathworks, Inc., MA, *Matlab Reference Guide*, 1st ed., Jul 1993.

78. A. Oppenheim and R. Schafer, *Discrete-Time Signal Processing*. New Jersey: Prentice Hall, 1989.

79. L. Ristic, F. Shemansky, M. Kniffin, and H. Hughes, "Surface micromachining technology," in *Sensor Technology and Devices*, pp. 95–155, Artech House, 1994.

80. Hewlett-Packard, *Using the HPIB Interface with Microsoft Windows*, 1st ed., Dec 1991.

IX. Appendices

9.1 Appendix 1 - Masks

9.1.1 Mask Making. Photolithographic masks were used extensively in this thesis for thin film application and device fabrication. The basic steps for actually making and developing masks were described in Chapter 6. This section deals with generating the mask using the MAGIC and Cadence design tools.

1. In MAGIC, create a new cell by typing :load filename. In Cadence, create a new file and go to the Edit screen.

2. Import the desired chip design that will be masked using the :getcell command for MAGIC or the Instance command for Cadence. Expand the view to see the imported structure and the device layers. In MAGIC, the devices should have a dull color because they are not the active edit cell. Be careful that the cell is not deleted prematurely.

3. Using a layer such as Metal1 in MAGIC and Poly1 in Cadence, cover the areas desired on the designed chip. If it is known that a post-processing mask will be used and mask alignment marks have been included with the actual chip fabrication design, include the necessary alignment marks.

4. Once the mask sections have been completed, delete the imported cell and cif out the saved mask file. In MAGIC, a .cif file is cerated by typing :cif. In Cadence, go to the Main Menu toolbar and click on Translators. From there, go to CIF OUT and fill out the necessary fields. The critical fields are filename, library path, and output file name. Make sure you specify a .cif file as an output file name. The .cif files will be located in the design directory you launch the program from.

5. Using the program cif2ps (UNIX public domain software that has been revised by Lt Rob Reid), convert the .cif file into a .ps file by typing

cif2ps -m # filename.cif > filename.ps

where -m # specifies the amount of reduction (50 times is the default), filename.cif is the input .cif file and filename.ps is the output .ps file.

6. With the .ps files, print out the masks on overhead transparencies. I recommend using two copies per mask and taping them together to form a darker image.

7. In most cases, a single sheet will not be big enough and the mask will have to be broken down into sections. If this happens, include additional alignment marks on the mask to facilitate reconstruction on the backlit wall, but make sure the marks do not interfere with the rest of the chip.

9.1.2 CMOS Masks Used. Masks used on CMOS fabricated chips.

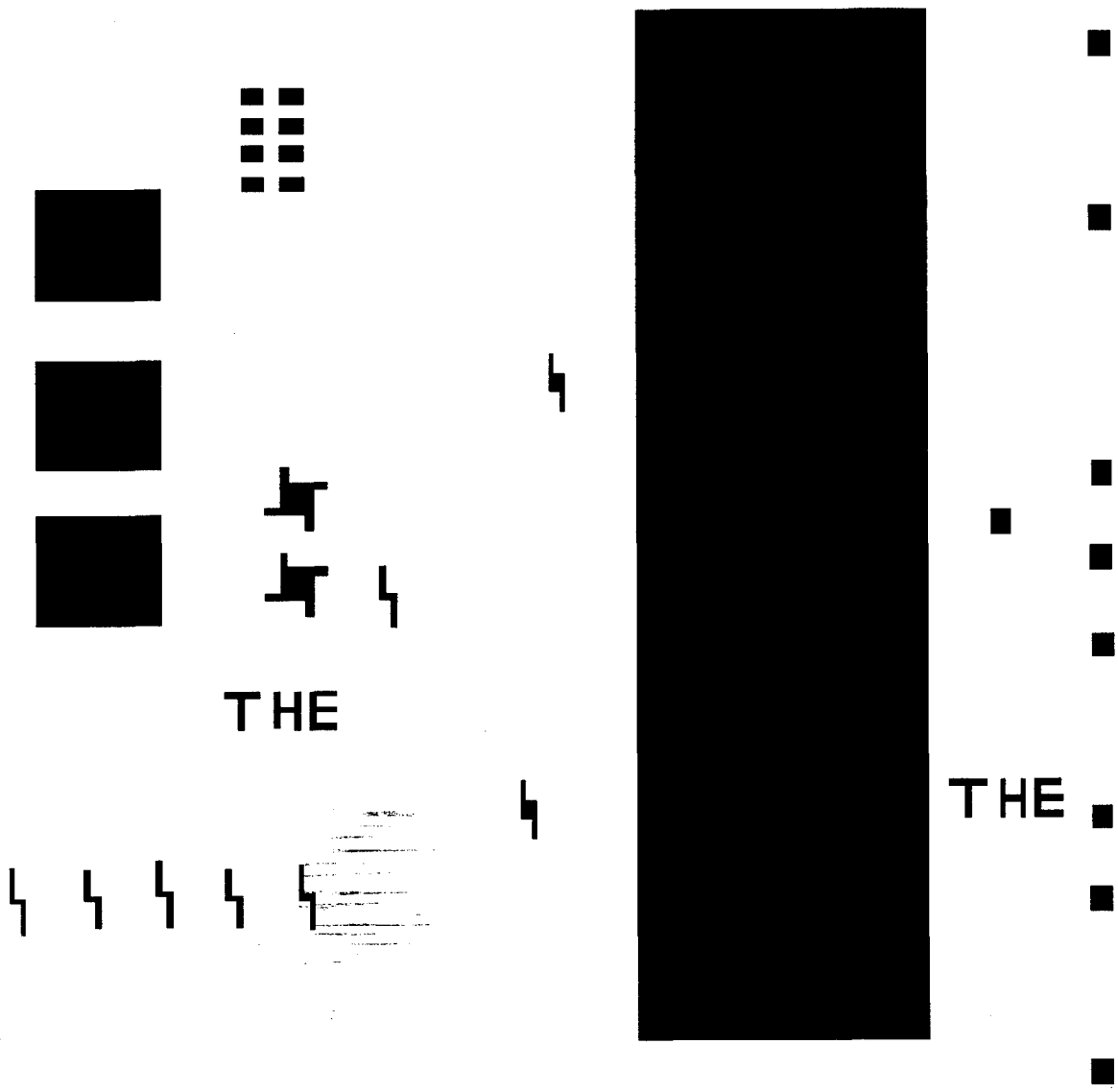

Figure 99. CMOS 4 Mask enlarged 40 times.

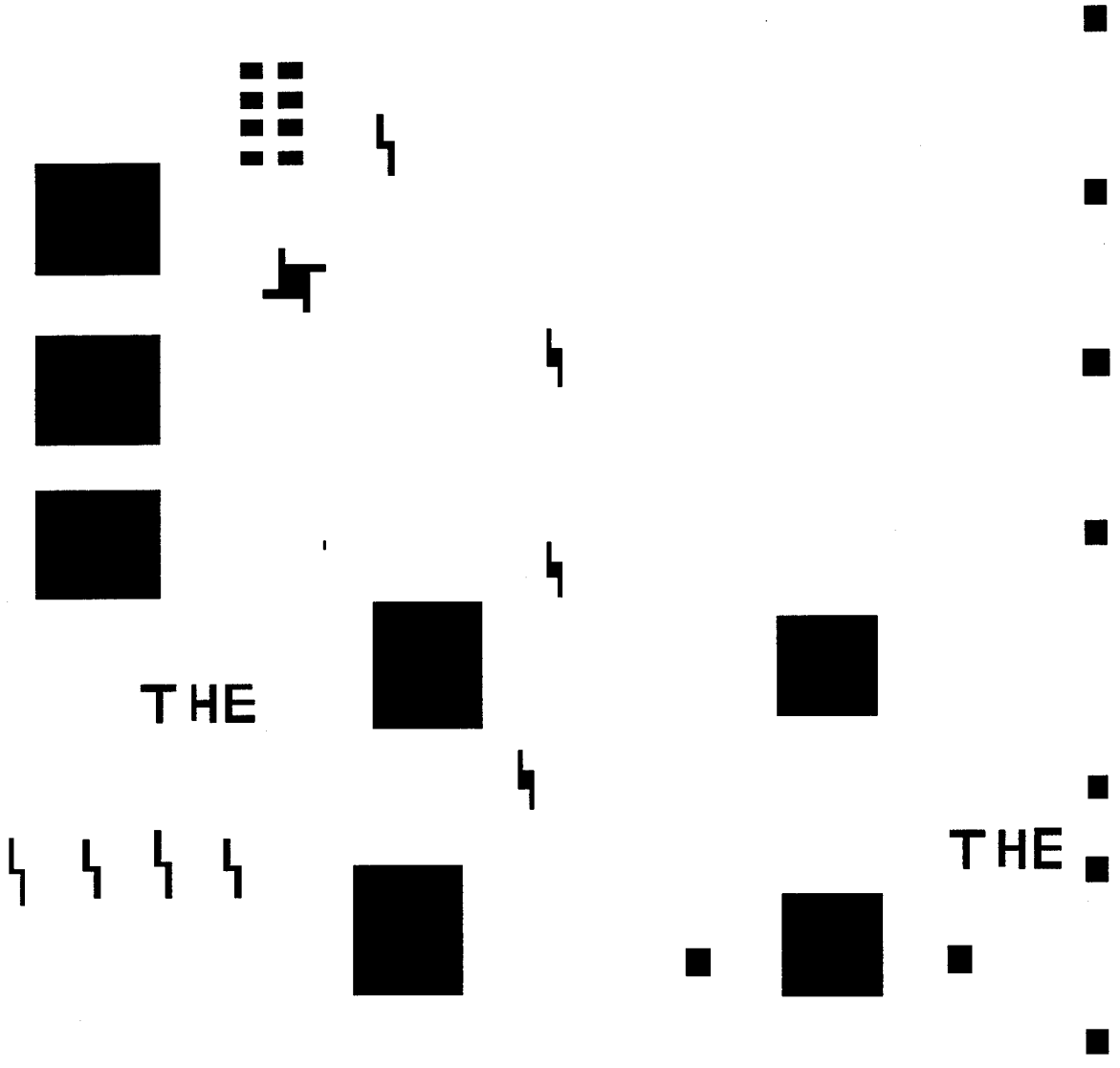

Figure 100. CMOS 5 Mask enlarged 40 times.

9.1.3 MUMPS Masks Used. Masks used on MUMPS fabricated chips.

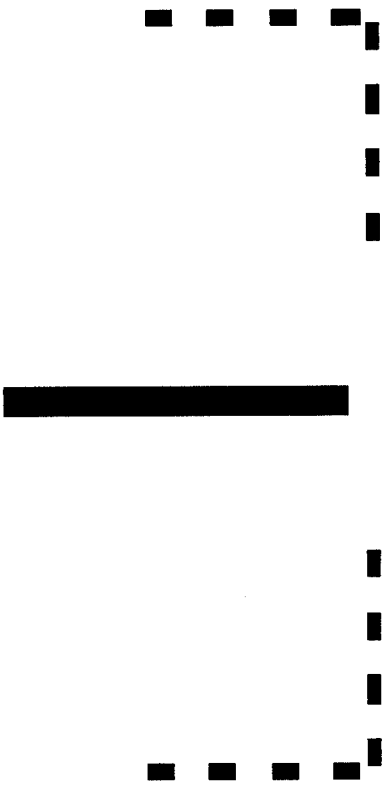

Figure 101. MUMPS 6 Mask enlarged 10 times.

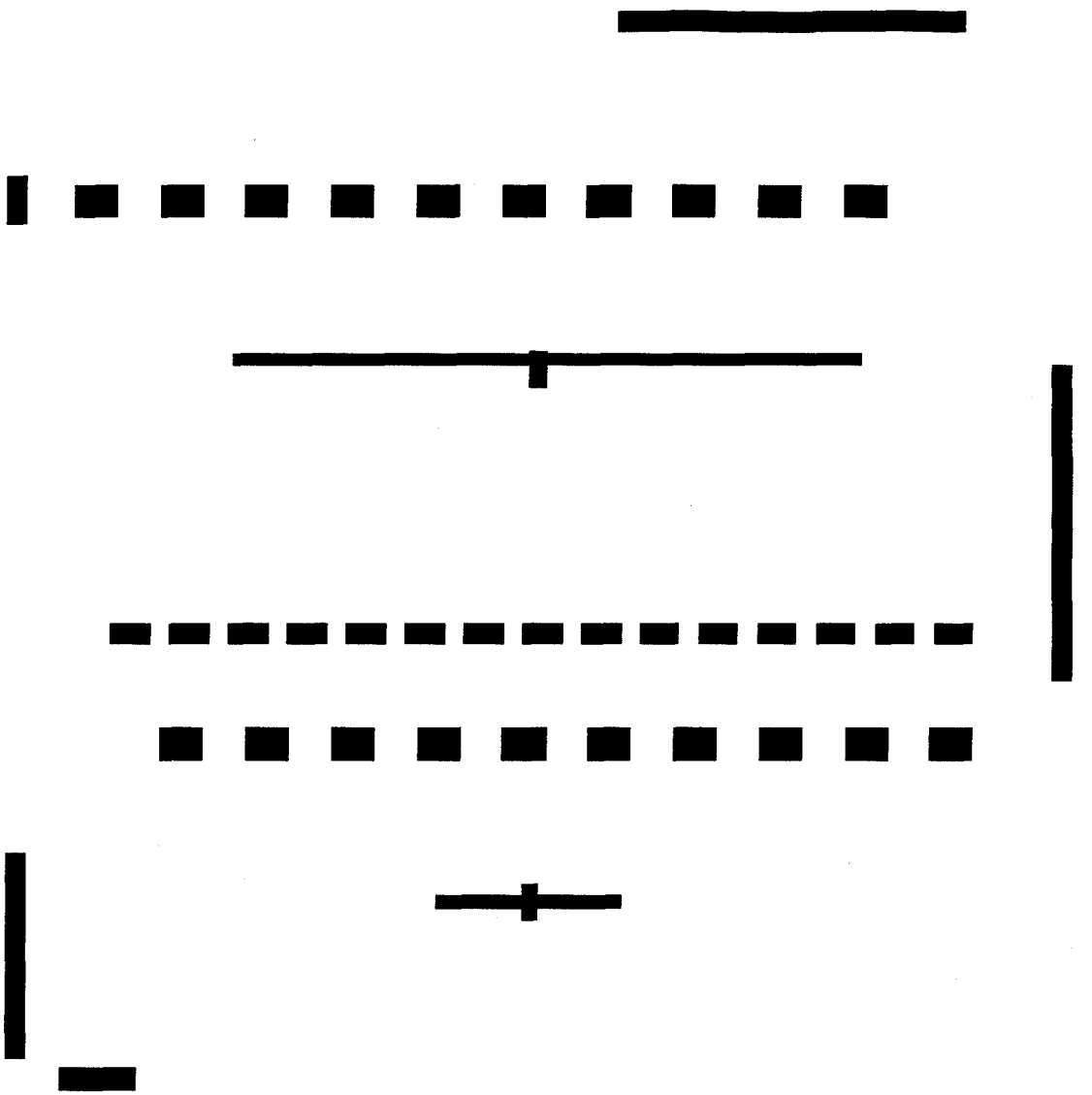

Figure 102. MUMPS 9 Mask enlarged 15 times.

9.1.4 AFIT Microsensor Fabrication Masks. Individual elements were made into 3 x 5 sheets and four sheets were aligned to form the mask pattern that was exposed on the backlit wall. The lines around each element were used as mask aligners to reconstruct the mask on the backlit wall and for successive masks during processing.

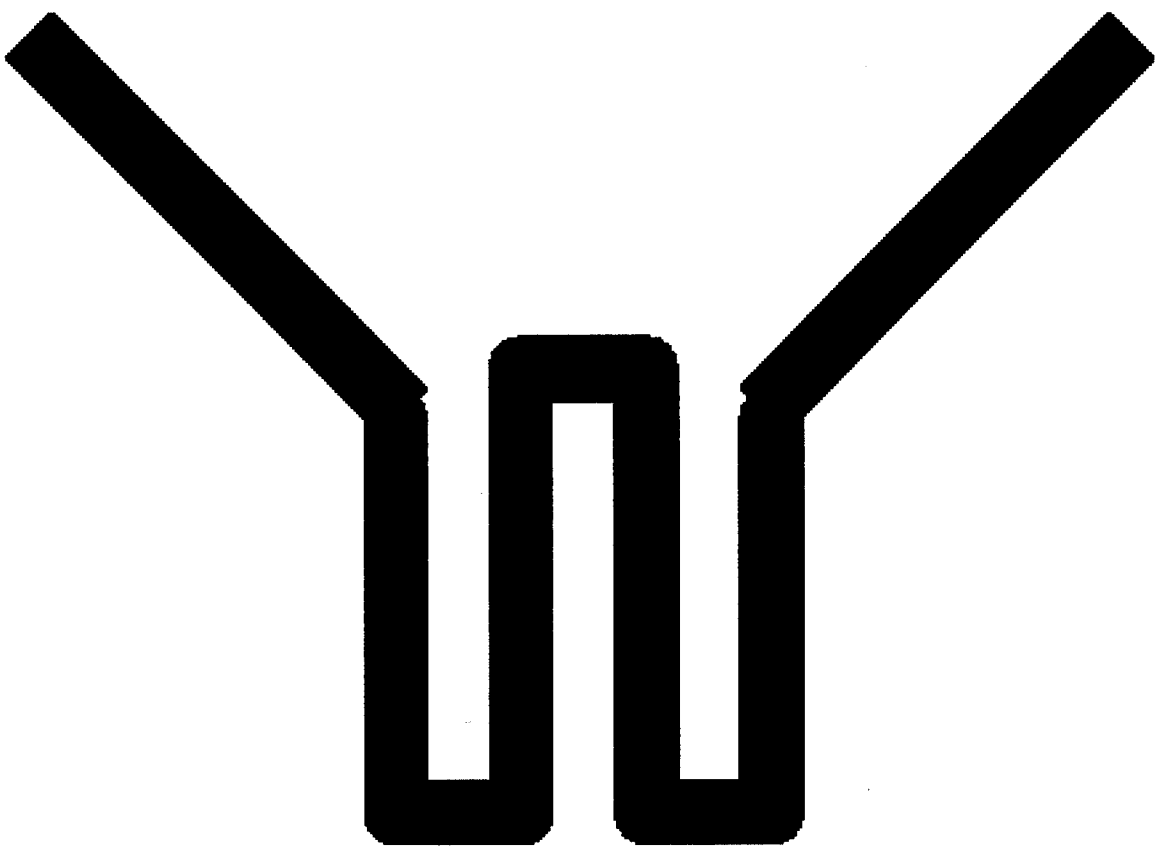

Figure 103. Mask 1: Diffusion oxide etch mask enlarged 750 times.

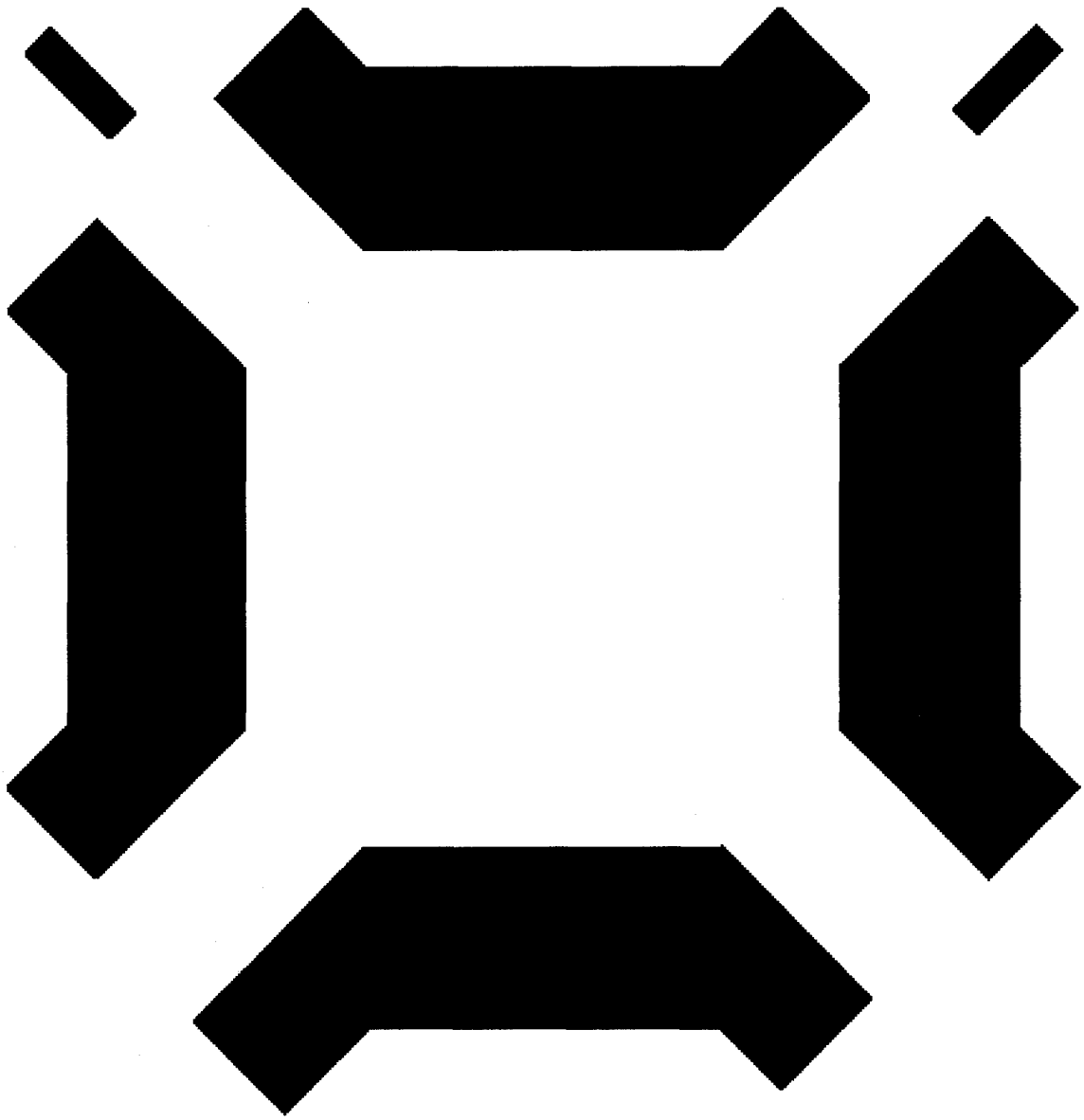

Figure 104. Mask 2: Oxide open cuts mask enlarged 750 times.

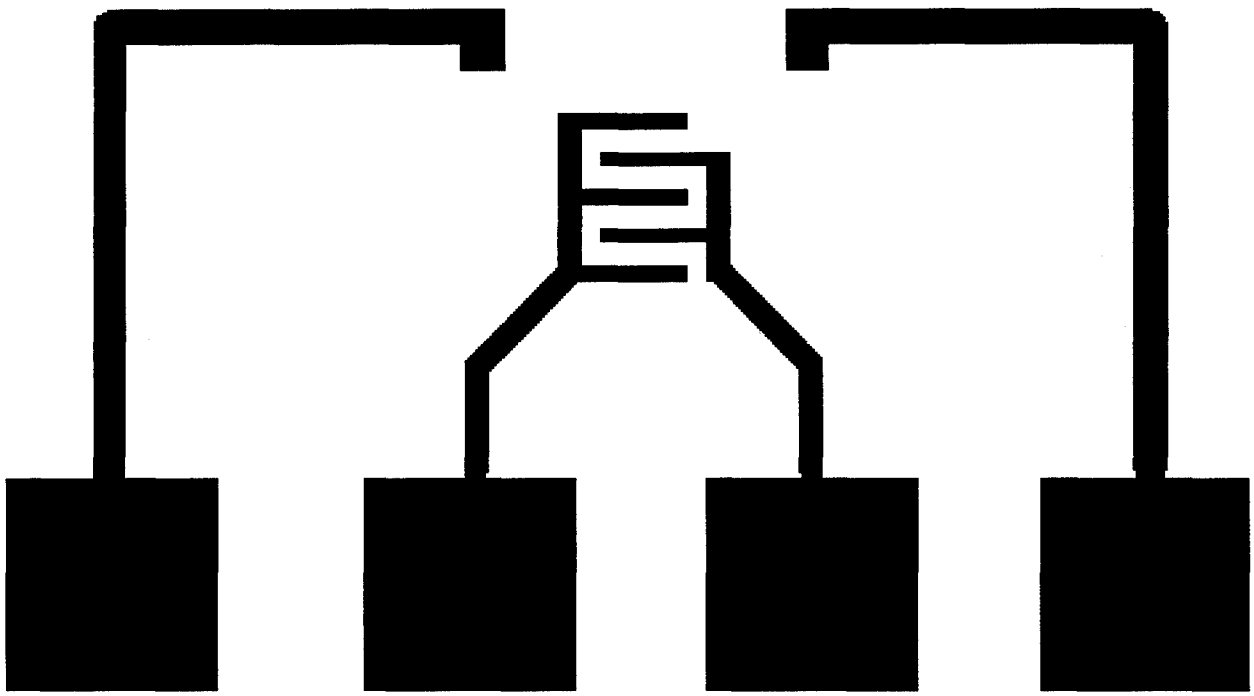

Figure 105. Mask 3: Metallization mask enlarged 250 times.

9.2 *Appendix 2 - TSUPREM-4 Source Code and Plots*

```
$Lab simulation of chip processing

line x location = 0 spacing = .5
line x location = 5 spac =.5

line y location = 0 spac = .5
line y loc = 2  spac =.5

Initialize Boron = 1E15

$Grow initial oxide
Diffusion steam time=30 temp=1100

$etch window
Etch oxide start x = 0.5 y = -0.5
Etch continue x = 1.50 y = -0.5
etch continue x = 1.5 y = .25
etch done x = 0.5 y = .25


$pre-deposition of phosphorus
Diffusion time=90 temp=1100 phosphor = 1.5E21

$etch window
Etch oxide start x = 0 y = -0.5
Etch continue x = 5.0 y = -0.5
etch continue x = 5.0 y = .25
etch done x = 0 y = .25


Diffusion time=30 temp=1100 steam

option device=ps
select z=log10(phosphor)  title=""
plot.1d x.v = 3 left=-.5
```

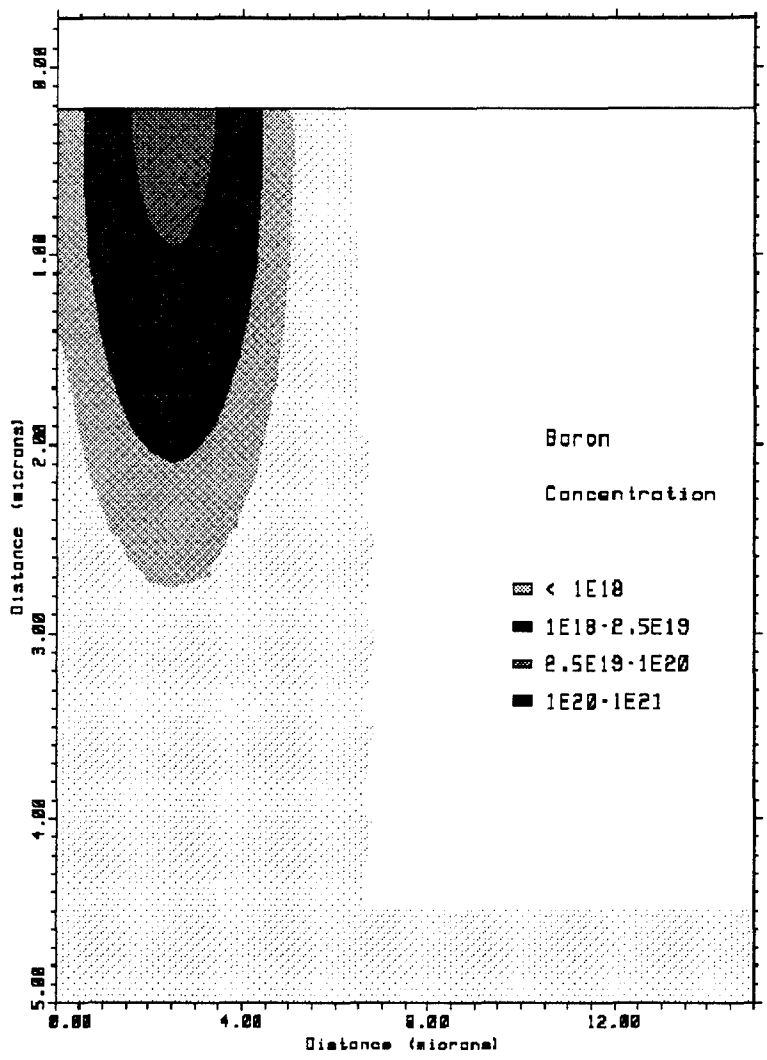

Figure 106. Boron diffusion concentrations after one hour at 1150° C and oxide etch.

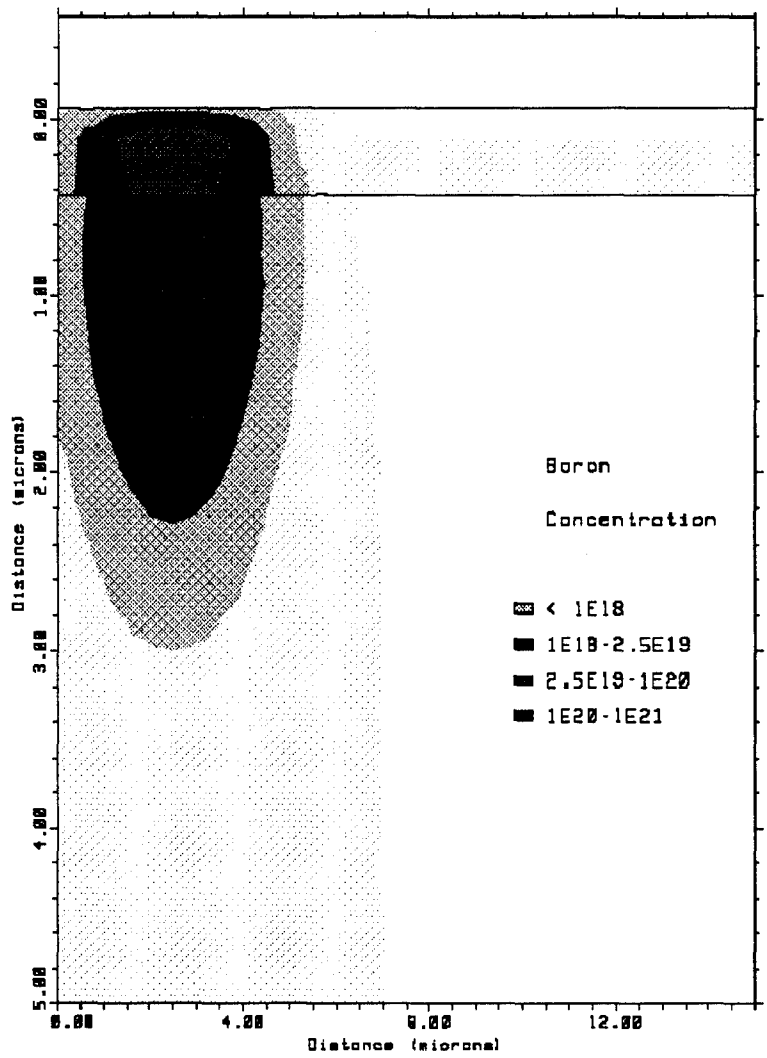

Figure 107. Boron concentrations after the second 30 minute wet oxide growth at 1100° C.

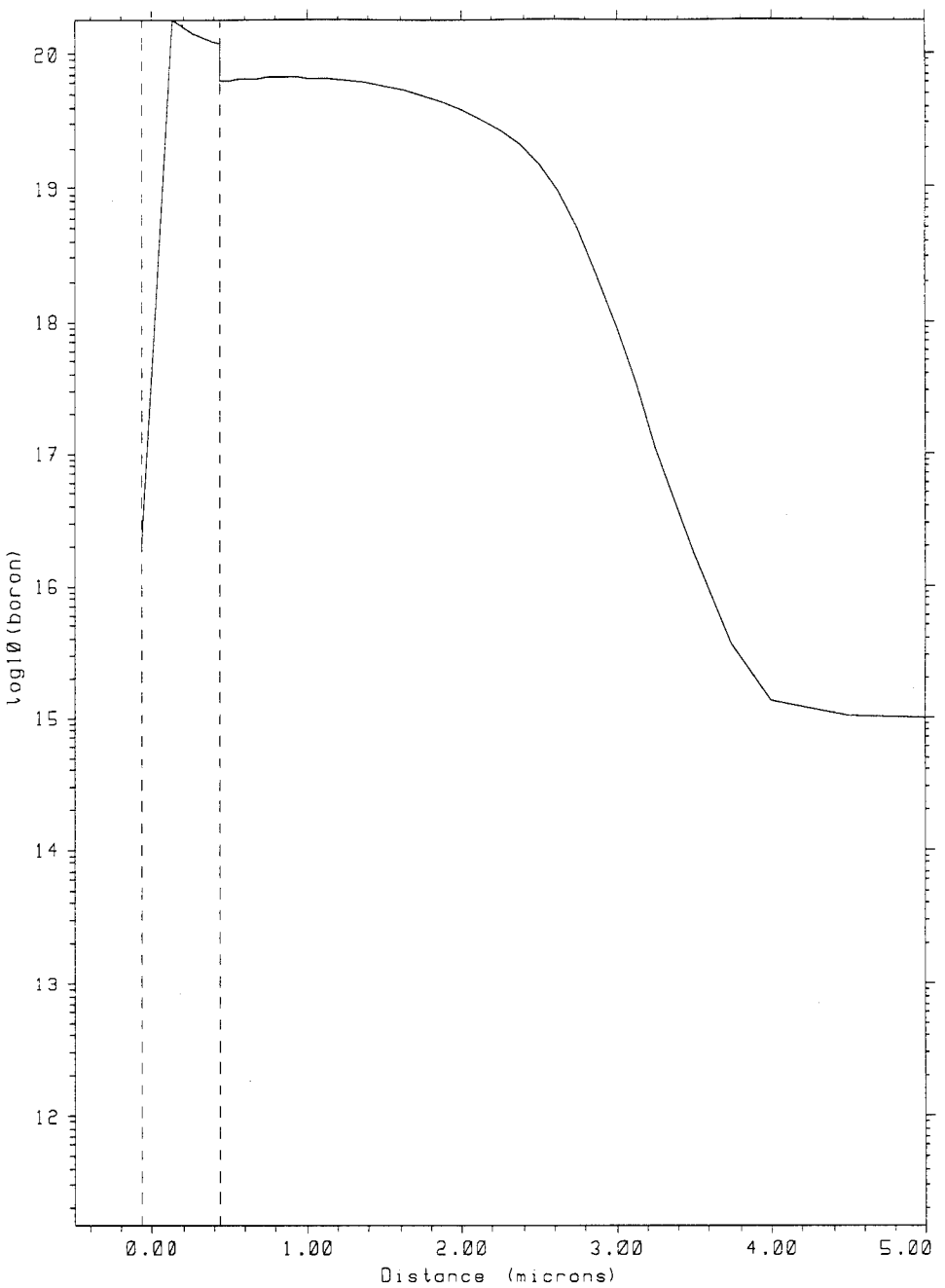

Figure 108. Final boron concentrations of a doped region.

9.3 Appendix 3 - HPIB Commands

This section summarizes screen capturing commands using an 82335B Hewlett-Packard interface bus (HPIB) and the HPIB Interface with Microsoft Windows utility [80]. This package allows easy single-command instructions to capture data and transfer it to a computer for analysis.

All commands in this section will be biased towards the HP 4194A Impedance Analyzer; however, the basic procedures of sending commands to the device and downloading data to an ASCII file are the same. Some commands, such as those requesting register data, are common to all HP test equipment with multiple array displays such as the HP 4195A Network Analyzer and the HP 4145A Parametric Analyzer. Other commands for individual equipment should be found in the operating manuals under HPIB instructions.

9.3.1 Set-Up. Each HPIB-capable device has an HPIB address that can be changed to suit an experimental set-up. The HPIB card is generally left at its preset address of 7. If the Windows Interface has not been loaded onto the computer, do so and run it.

For each device to be used, make a component file by clicking on the *Setup* menu. As long as the HPIB card is at address 7, the only fields that need to be filled are the device name and address. This tells the card where to send messages and from where to expect data.

9.3.2 Sending Commands. Commands must be sent to a device to prepare it for data transmission. The device must be told that data is requested and which data to send. Commands can also be used to remotely operate the device' but, these commands tend to be device-specific and the device manual must be consulted.

Commands are sent to the device using the *Output* menu. A single command can be sent by using the String function. Single commands are useful for capturing non-time-dependent data. To prepare the HP 4194A to send a register of data, a command must be sent to it requesting the proper register and telling the machine to prepare to send it. This is accomplished by sending $R?$ where R is the register name and ? tells the machine to put that register at the top of the stack to be transferred. Useful registers on the HP 4194A include X - the mantissa that shows the frequency scale, A - amplitude data and B - phase data. Each register holds 401 data points.

9.3.3 Receiving Data. Once the device has received instructions to send data, the data can be downloaded to a computer using the *Enter* menu. If a register contains only one value, the Number or String field can be used. For a multi-value register, send the the data directly to a text file by using the File field. The field allows a filename to be specified and whether new data should overwrite or append existing data in the file. Data is saved in row vectors which makes importing into spreadsheets a problem if the spreadsheet does not have the required number of columns. The recommended practice is to import the data in Matlab and either process the data or reformat the data into column vectors that a spreadsheet can use. One problem associated with Matlab is that all data is space and comma-separated. For negative data, the space is occupied by the negative sign and a space must be added between the comma and the sign before the data can be properly imported into Matlab. A global replace quickly rectifies this problem.

9.4 *Appendix 4 - DIP Package*

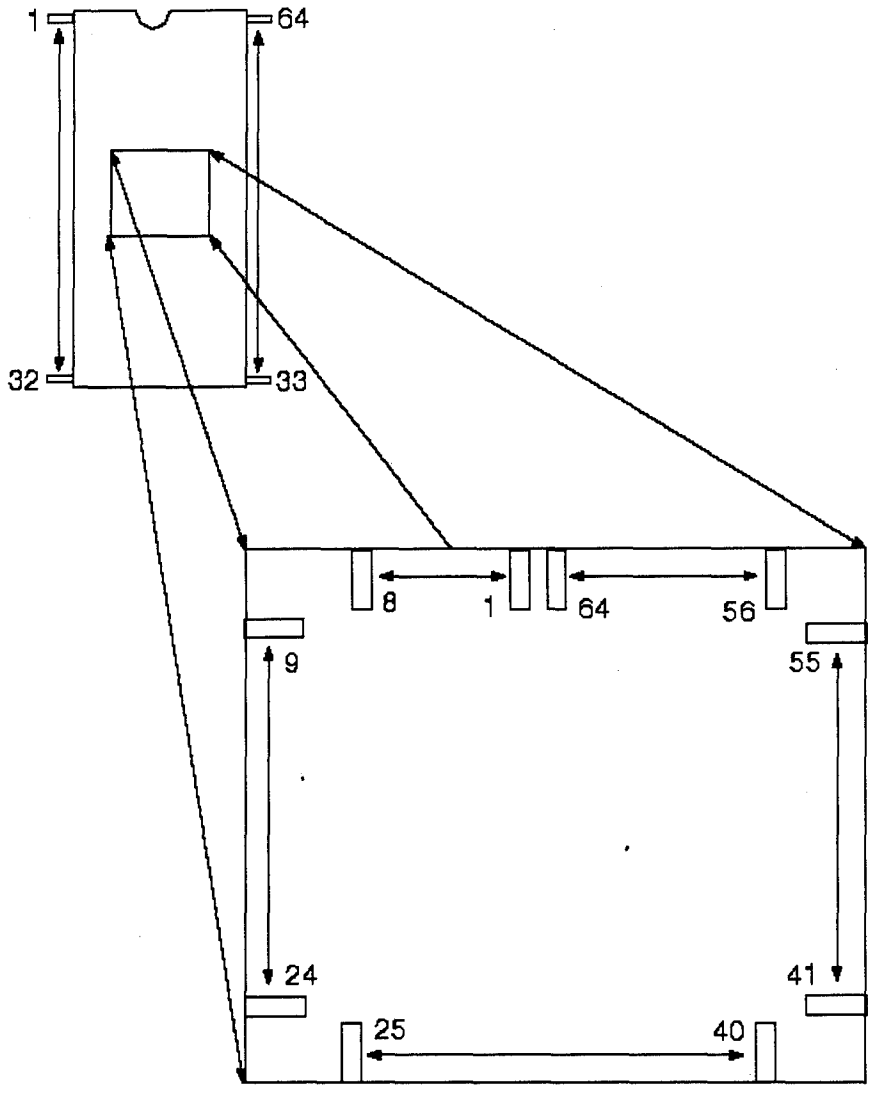

Figure 109. Pin-out for 64-pin DIP.

9.5 *Appendix 5 - MATLAB Code*

9.5.1 *Data Analysis Program.*

```
function gpib(s) %Data analyzer for PIB in 1,1,1-TCA

% This function reads a set of aquired data as a matix with each row
%representing a different data set.  Each row is assigned a variable.  Data is
%then filtered through an external moving average filter function called 'move'.
%The difference between an exposed data set and a purged data set is computed.
%Standard deviations of data elements are computed and used to calculated a
%ratio of the differnce result and the deviation called the signal:deviation
%ration (SNR).  The data is then plotted in a different formats.

%This file is representative of m-files modified for each experiment on each
%polymer coated device.  Files used for specific experiemts are
%PIB in TCE - gpib1.m, PIB in toluene - gpib2.m, PVTD in 1,1,1-TCA - gpvtd.m,
%PVTD in TCE - gpvtd1.m, PVTD in toluene - gpvtd2.m.

%By Capt Brian Freeman, Nov 1995.

load tcapib.dat % load up desired data set first

x=tcapib(1,:)/1000000;   % convert to MHz for scale

%%%%%%%%%%%%% assign arrays

a1=tcapib(2,:); %w/o
b1=tcapib(3,:);

a2=tcapib(5,:); %w/ TCA
b2=tcapib(6,:);

a3=tcapib(7,:); %w/o 2V
b3=tcapib(8,:);

a4=tcapib(9,:); %w/ TCA
b4=tcapib(10,:);

a5=tcapib(11,:); %w/o 5V
b5=tcapib(12,:);

a6=tcapib(13,:); %w/ TCA
b6=tcapib(14,:);

a7=tcapib(15,:); %w/o 10V
b7=tcapib(16,:);
```

```
a8=tcapib(17,:); %w/ TCA
b8=tcapib(18,:);

a9=tcapib(21,:); %w/o 15V
b9=tcapib(22,:);

a10=tcapib(23,:); %w/ TCA
b10=tcapib(24,:);

a11=tcapib(25,:); %w/o 20V
b11=tcapib(26,:);

%%%%%%%%%%%%%%%%%%%%%%%%%%%%%%%%  compute differences
da0=abs(a1-a2);
db0=abs(b1-b2);

da2=abs(a3-a2);
db2=abs(b3-b2);

da5=abs(a5-a4);
db5=abs(b5-b4);

da10=abs(a7-a6);
db10=abs(b7-b6);

da15=abs(a9-a8);
db15=abs(b8-b9);

da20=abs(a10-a11);
db20=abs(b10-b11);

%%%%%%%%%%%%%%%% Moving average filter %%%%%%%%%%%
x = move(x);   %update x array

da011=da0;

da0 = move(da0);
da2 = move(da2);
da5 = move(da5);
da10 = move(da10);
da15= move(da15);
da20 = move(da20);
```

```
db0 = move(db0);
db2 = move(db2);
db5 = move(db5);
db10 = move(db10);
db15= move(db15);
db20 = move(db20);

j=1;
n = length(x);
for i = 1:n
 if x(i) >=14

x1(j) = x(i);

da01(j) = da0(i);
da21(j) = da2(i);
da51(j) = da5(i);
da101(j) = da10(i);
da151(j) = da15(i);
da201(j) = da20(i);

db01(j) = db0(i);
db21(j) = db2(i);
db51(j) = db5(i);
db101(j) = db10(i);
db151(j) = db15(i);
db201(j) = db20(i);

j = j +1;
end; % if-then
end % for i
%%%%%%%%%%%%%  put legends in graphs %%%%%%%%%%%
for j = 1:40 % set number of legend points
k = ceil(j * 5.9); %set const to mult. by
x2(j) = x1(k);

da02(j) = da01(k);
da22(j) = da21(k);
da52(j) = da51(k);
da102(j) = da101(k);
da152(j) = da151(k);
da202(j) = da201(k);
```

```
db02(j) = db01(k);
db22(j) = db21(k);
db52(j) = db51(k);
db102(j) = db101(k);
db152(j) = db151(k);
db202(j) = db201(k);

end;
%%%%%%%%%%%%%% pre-filter plots
clf
axis([10,20,0,2])

subplot(2,1,1)
plot(x,da011(1:397))
xlabel('Frequency - MHz')
ylabel('Impedance Difference - Ohms')

subplot(2,1,2)
plot(x,da0)
xlabel('Frequency - MHz')
ylabel('Impedance Difference- Ohms')

%print -deps tcapibfilt
%pause

%%%%%%%%%%%%%% typical response plots
clf

subplot(2,1,1)
plot(x,move(a1))
xlabel('Frequency - MHz')
ylabel('Impedance - Ohms')

subplot(2,1,2)
plot(x,move(b1))
xlabel('Frequency - MHz')
ylabel('Phase - Degrees')

%print -deps tcapibtyp
%pause

%%%%%%%%%%%%%% sample statistics
clf
```

```
%% find sample standard deviations of exposure data
sa = [move(a2); move(a4); move(a6); move(a8); move(a10)];
deva = std(sa);

sb = [move(b2); move(b4); move(b6); move(b8); move(b10)];
devb = std(sb);

[minsda,isda] = min(deva); % find min. deviation
[minsdb,isdb] = min(devb);

snra0 = da0(isda)/minsda; %compute signal:deviation ratios
snra2 = da2(isda)/minsda;
snra5 = da5(isda)/minsda;
snra10 = da10(isda)/minsda;
snra15 = da15(isda)/minsda;
snra20 = da20(isda)/minsda;

[minsda x(isda)] %display SDRs
[0 2 5 10 15 20;
snra0 snra2 snra5 snra10 snra15 snra20]

snrb0 = db0(isdb)/minsdb;
snrb2 = db2(isdb)/minsdb;
snrb5 = db5(isdb)/minsdb;
snrb10 = db10(isdb)/minsdb;
snrb15 = db15(isdb)/minsdb;
snrb20 = db20(isdb)/minsdb;

[minsdb x(isdb)]
[0 2 5 10 15 20;
snrb0 snrb2 snrb5 snrb10 snrb15 snrb20]

%pause

subplot(2,1,1)
plot(x,deva)
xlabel('Frequency - MHz')
ylabel('Impedance - Ohms')

subplot(2,1,2)
plot(x,devb)
xlabel('Frequency - MHz')
ylabel('Phase - Degrees')
```

```
%print -deps tcapibstat
pause

%%%%%%%%%%%%%% plot difference arrays

clf
subplot(2,1,1)
plot(x1,da01,x1,da21,x1,da51,x1,da101,x1,da151,x1,da201)
xlabel('Frequency - MHz')
ylabel('Impedance Difference - Ohms')
legend('0 V', '2 V', '5 V','10 V', '15 V','20 V',0)


hold %% for legends
plot(x2,da02,'*',x2,da22,'+',x2,da52,':',x2,da102,'x',x2,da152,'.')
xlabel('Frequency - MHz')
ylabel('Impedance Difference - Ohms')
legend('*','0 V', '+','2 V', 'o','5 V', 'x','10 V', '.','15 V',0)

subplot(2,1,2)
plot(x1,db01,x1,db21,x1,db51,x1,db101,x1,db151,x1,db201)
xlabel('Frequency - MHz')
ylabel('Phase Difference - degrees')
legend('0 V', '2 V', '5 V','10 V', '15 V','20 V',0)

hold % for legends
plot(x2,db02,'*',x2,db22,'+',x2,db52,':',x2,db102,'x',x2,db152,'.')
xlabel('Frequency - MHz')
ylabel('Phase Difference - degrees')
legend('*','0 V', '+','2 V', 'o','5 V', 'x','10 V', '.','15 V',0)

%print pibtca -deps

pause

%%%%%%%% 3-D plots %%%%%%%%%%
v = [0 2 5 10 15 20];

atca = [da0; da2; da5; da10; da15; da20];
btca = [db0; db2; db5; db10; db15; db20];
```

```
subplot(2,1,1)
colormap(hsv);
waterfall(x,v,atca)
view(60,30)
grid
xlabel('Frequency - MHz')
ylabel('Heater Voltage - Volts')
zlabel('Impedance Difference - Ohms')

%pause

subplot(2,1,2)
colormap(hsv);
waterfall(x,v,btca)
view(60,30)
grid
xlabel('Frequency - MHz')
ylabel('Heater Voltage - Volts')
zlabel('Phase Difference - Degrees')
%print -deps pibtca3d
```

9.5.2 *Moving Average Filter.*

```
function x = move(x)

% Moving average filter.  Input requires data array.
% Uses 5 element averaging.
%Filtered array loses 4 data points due to averaging.
n=length(x);

f1 = x(1:n-4);
f2 = x(2:n-3);
f3 = x(3:n-2);
f4 = x(4:n-1);
f5 = x(5:n);

x = (f1 + f2 + f3 + f4 + f5)/5;
```

9.6 *Fabricated CMOS Die*

The following pictures of completed dies were furnished by MOSIS. These chips were part of the bulkmicromachined research conducted. MUMPS did not provide similar photos for their chips.

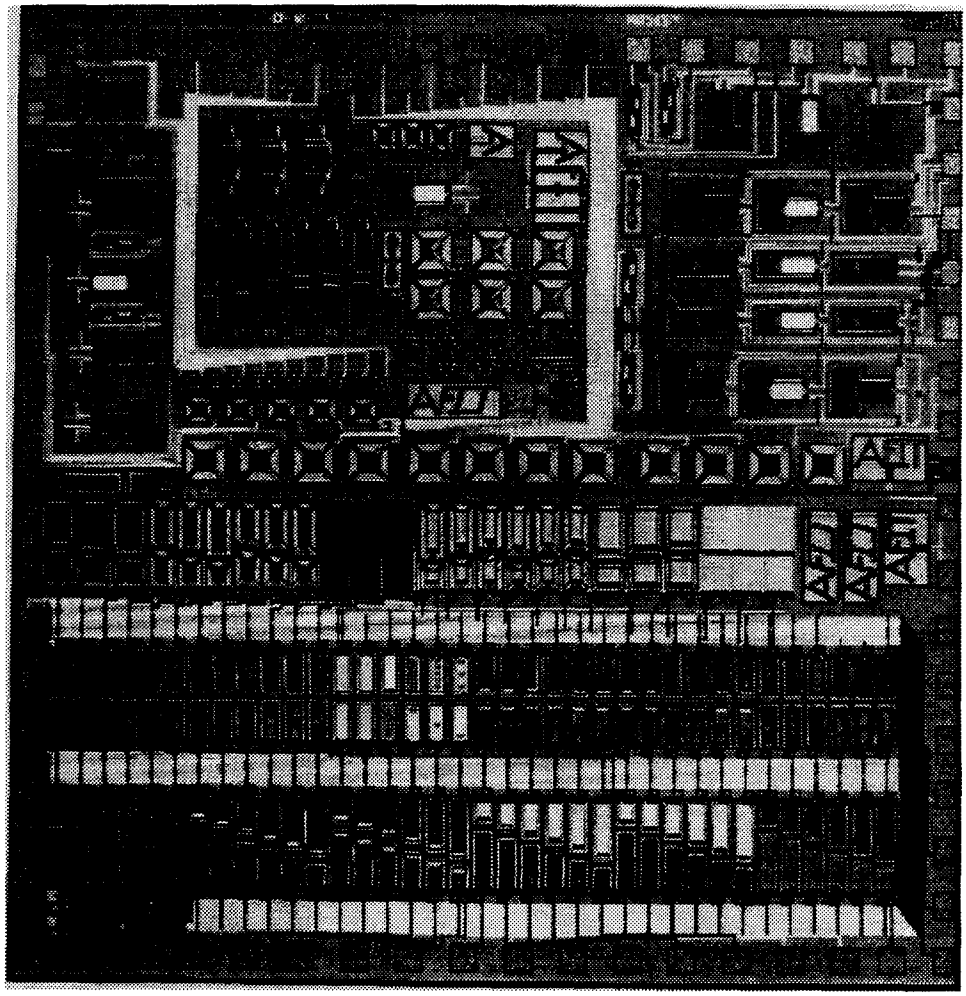

Figure 110. CMOS 3 die. This die contains many test structures not associated with this thesis. Devices used in this thesis are located on the upper right-hand corner.

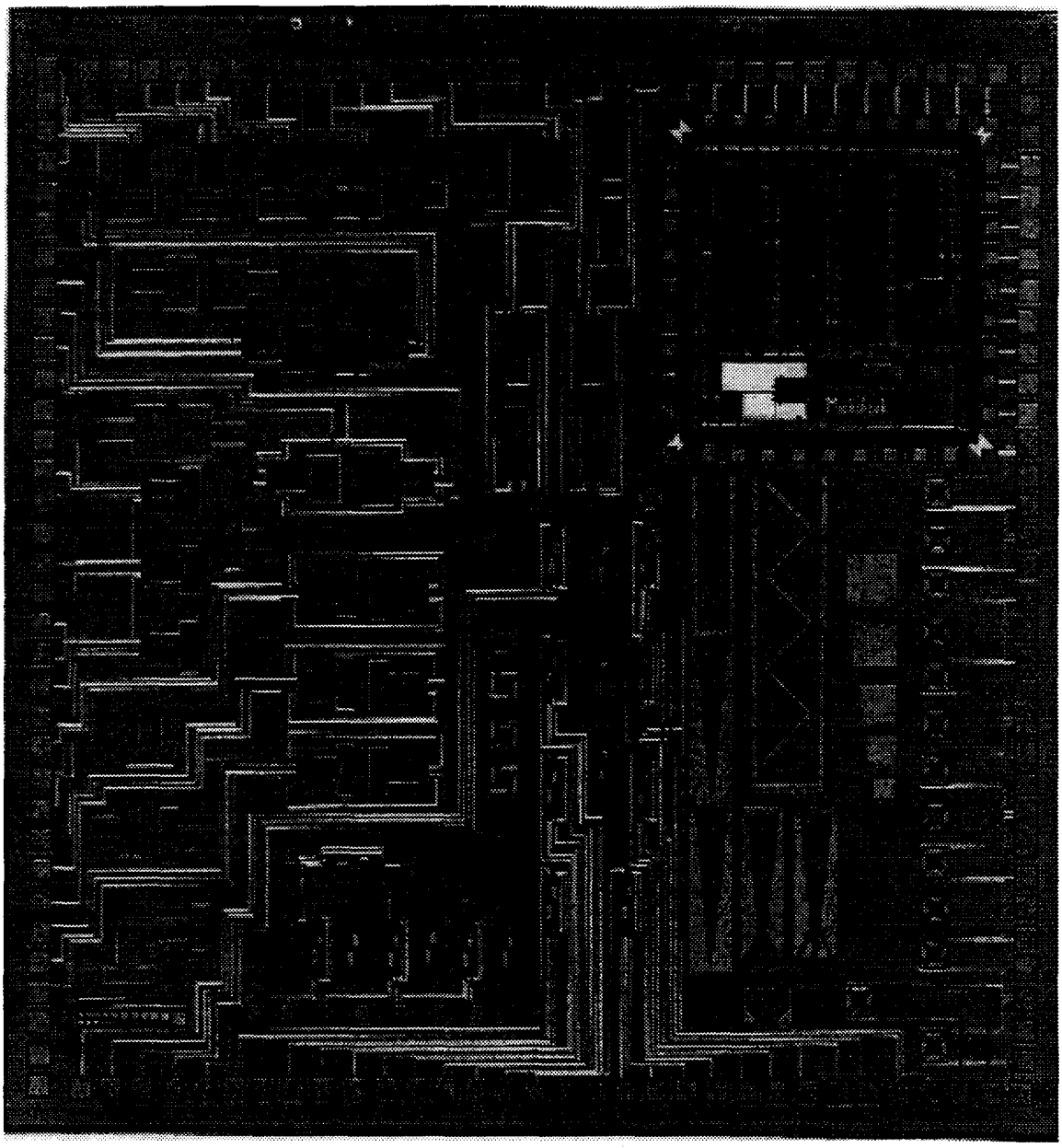

Figure 111. CMOS 4 die. This die contains devices not associated with the thesis, but these devices are limited to the upper right-hand corner.

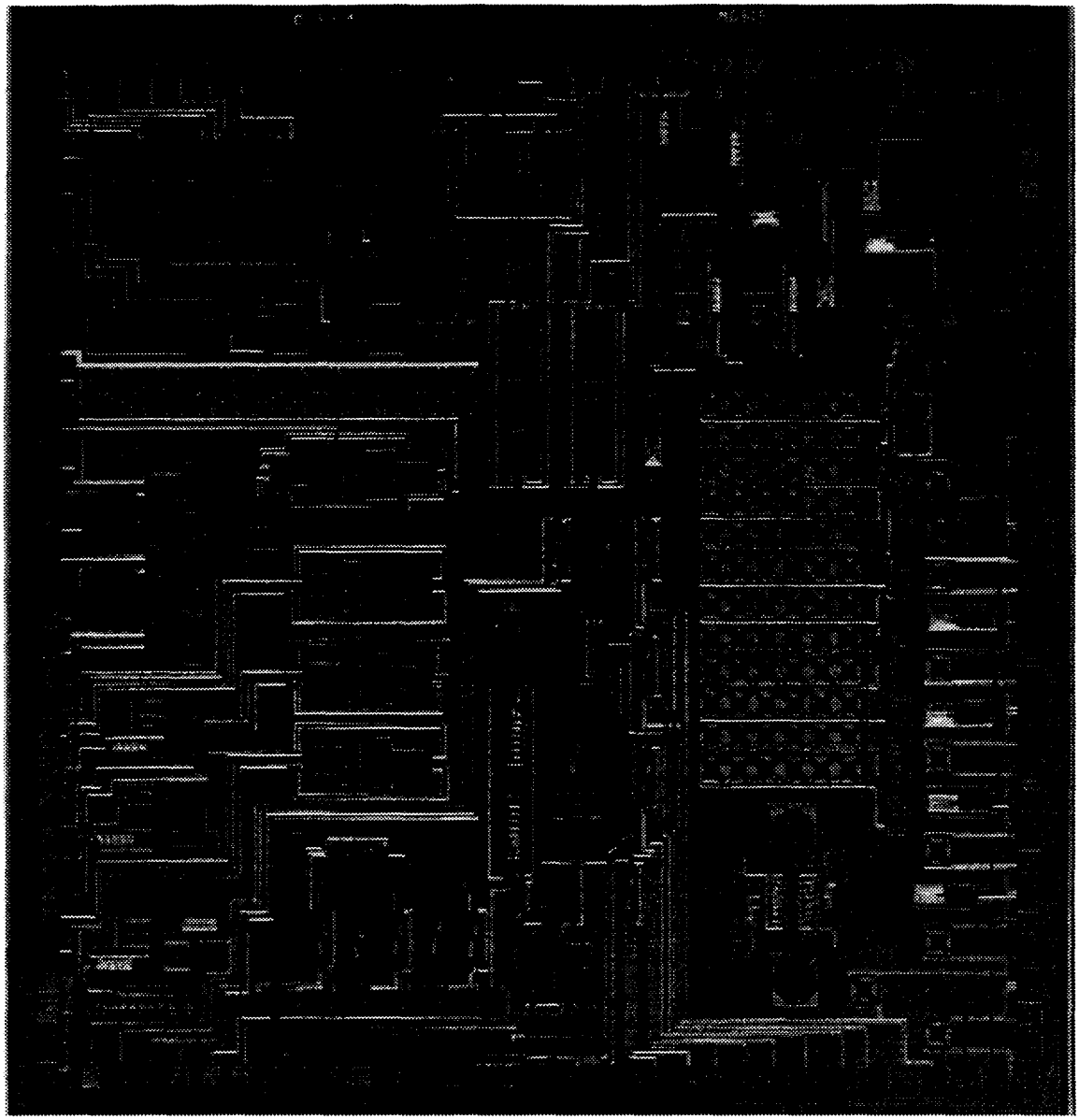

Figure 112. CMOS 5 die. This die contains devices not associated with the thesis. Thesis related devices are scattered throughout the chip. The resonating bridge designs on this chip were tested successfully with PIB in TCE, 1,1,1-TCA, and toluene.

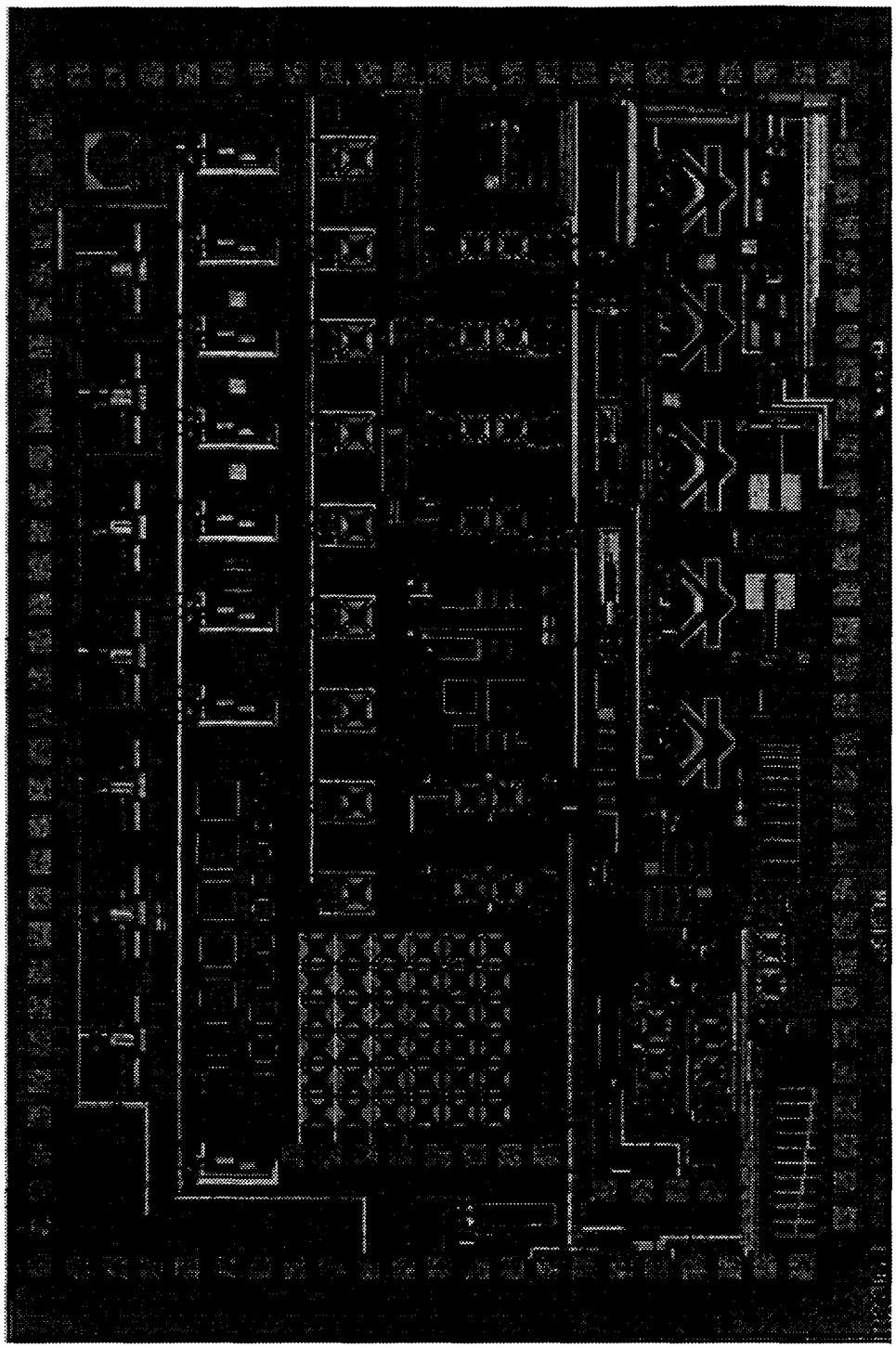

Figure 113. CMOS 6 die. This is the final MOSIS design fabricated, which arrived too late for testing. The die contains many devices not associated with the thesis. Thesis related devices are scattered throughout the chip.

Vita

Capt Brian S. Freeman [redacted]7. Things rapidly deteriorated from there. After graduating from Alfred-Almond Central School, Almond, NY, in 1985, he received an Air Force ROTC scholarship to Worcester Polytechnic Institute, Worcester, MA and graduated in 1989 with a Bachelor's of Science degree in Electrical Engineering, with distinction. Receiving his commission as a Second Lieutenant in the USAF, he was assigned to the 92nd Civil Engineering Squadron at Fairchild AFB, WA as an electrical engineer. From there, Capt Freeman went overseas to England where he was assigned to the 20th Civil Engineering Squadron at RAF Upper Heyford. From October 1991 to May 1994, Capt Freeman held a series of positions in the Engineering Flight, eventually becoming Chief of the Environmental Flight. In September 1993, Capt Freeman was deployed to Joint Task Force Provide Promise (Forward) in the Former Republic of Yugoslavia in support of the UN Protection Forces peacekeeping operation as the headquarter's staff engineer until January 1994. After attending the Air Force Institute of Technology for a Master's degree in Environmental and Engineering Management, Capt Freeman will be assigned to the Aeronautical Systems Center's Environmental Management directorate at Wright-Patterson AFB.

Capt Freeman is married with two cats, a Professional Engineer in the State of Ohio, an avid fencer, bad poet, beer gourmand, music aficionado and can play a mean tenor sax. He currently lives in Beavercreek, OH, but his heart is in Oxfordshire, England.

[redacted]

REPORT DOCUMENTATION PAGE

Form Approved
OMB No. 0704-0188

1. AGENCY USE ONLY (Leave blank)	2. REPORT DATE	3. REPORT TYPE AND DATES COVERED
	December 1995	Master's Thesis

4. TITLE AND SUBTITLE
Design, Fabrication, Processing, and Testing of Micro-electro-mechanical Chemical Sensors

5. FUNDING NUMBERS

6. AUTHOR(S)
Brian S. Freeman
Captain, USAF

7. PERFORMING ORGANIZATION NAME(S) AND ADDRESS(ES)
Air Force Institute of Technology, WPAFB OH 45433-6583

8. PERFORMING ORGANIZATION REPORT NUMBER
AFIT/GEE/ENG/95D-01

9. SPONSORING / MONITORING AGENCY NAME(S) AND ADDRESS(ES)
Phillips Laboratory, Kirkland AFB, NM

10. SPONSORING / MONITORING AGENCY REPORT NUMBER

11. SUPPLEMENTARY NOTES

12a. DISTRIBUTION / AVAILABILITY STATEMENT
Approved for public release; Distribution Unlimited

12b. DISTRIBUTION CODE

13. ABSTRACT (Maximum 200 words)

This research evaluated the effectiveness of commercial micro-electro-mechanical system (MEMS) fabrication processes for chemical microsensors using thin film (< 1000Å) coatings as chemical sorbing media. The two processes used were MUMPS at MCNC for surface micromachined sensors and MOSIS for bulk micromachined sensors. Electrostatic, bimorphic, and conductive sensing strategies were tried over eight different fabrication runs and 29 designs. Due to fabrication problems, only two designs successfully provided measurable responses when coated with polymers and exposed to saturated 1,1,1-TCA, TCE and toluene vapor. Two different polymers, poly(isobutylene) and poly(vinyl tetrachloride) were applied to released devices using an air brush. A new masking technique was developed to isolate the desired device for thin film coating while protecting surface bond pads. Results showed that each polymer has different affinities to each chemical, providing features that could be extracted for later discrimination. In addition, a process was created to make bulk micromachined microsensors and MEMS devices using AFIT facilities.

14. SUBJECT TERMS
micromechanical, MEM, MEMS, MUMPS, MOSIS, microsensor, thin film sensor, thin film application, mass sensor, thermal desorption, frequency desorption, bulk micromachining, surface micromachining

15. NUMBER OF PAGES
204

16. PRICE CODE

17. SECURITY CLASSIFICATION OF REPORT	18. SECURITY CLASSIFICATION OF THIS PAGE	19. SECURITY CLASSIFICATION OF ABSTRACT	20. LIMITATION OF ABSTRACT
UNCLASSIFIED	UNCLASSIFIED	UNCLASSIFIED	UL

GENERAL INSTRUCTIONS FOR COMPLETING SF 298

The Report Documentation Page (RDP) is used in announcing and cataloging reports. It is important that this information be consistent with the rest of the report, particularly the cover and title page. Instructions for filling in each block of the form follow. It is important to *stay within the lines* to meet *optical scanning requirements*.

Block 1. Agency Use Only *(Leave blank)*.

Block 2. Report Date. Full publication date including day, month, and year, if available (e.g. 1 Jan 88). Must cite at least the year.

Block 3. Type of Report and Dates Covered. State whether report is interim, final, etc. If applicable, enter inclusive report dates (e.g. 10 Jun 87 - 30 Jun 88).

Block 4. Title and Subtitle. A title is taken from the part of the report that provides the most meaningful and complete information. When a report is prepared in more than one volume, repeat the primary title, add volume number, and include subtitle for the specific volume. On classified documents enter the title classification in parentheses.

Block 5. Funding Numbers. To include contract and grant numbers; may include program element number(s), project number(s), task number(s), and work unit number(s). Use the following labels:

C	- Contract	PR	- Project
G	- Grant	TA	- Task
PE	- Program Element	WU	- Work Unit Accession No.

Block 6. Author(s). Name(s) of person(s) responsible for writing the report, performing the research, or credited with the content of the report. If editor or compiler, this should follow the name(s).

Block 7. Performing Organization Name(s) and Address(es). Self-explanatory.

Block 8. Performing Organization Report Number. Enter the unique alphanumeric report number(s) assigned by the organization performing the report.

Block 9. Sponsoring/Monitoring Agency Name(s) and Address(es). Self-explanatory.

Block 10. Sponsoring/Monitoring Agency Report Number. *(If known)*

Block 11. Supplementary Notes. Enter information not included elsewhere such as: Prepared in cooperation with...; Trans. of...; To be published in.... When a report is revised, include a statement whether the new report supersedes or supplements the older report.

Block 12a. Distribution/Availability Statement. Denotes public availability or limitations. Cite any availability to the public. Enter additional limitations or special markings in all capitals (e.g. NOFORN, REL, ITAR).

- DOD - See DoDD 5230.24, "Distribution Statements on Technical Documents."
- DOE - See authorities.
- NASA - See Handbook NHB 2200.2.
- NTIS - Leave blank.

Block 12b. Distribution Code.

- DOD - Leave blank.
- DOE - Enter DOE distribution categories from the Standard Distribution for Unclassified Scientific and Technical Reports.
- NASA - Leave blank.
- NTIS - Leave blank.

Block 13. Abstract. Include a brief *(Maximum 200 words)* factual summary of the most significant information contained in the report.

Block 14. Subject Terms. Keywords or phrases identifying major subjects in the report.

Block 15. Number of Pages. Enter the total number of pages.

Block 16. Price Code. Enter appropriate price code *(NTIS only)*.

Blocks 17. - 19. Security Classifications. Self-explanatory. Enter U.S. Security Classification in accordance with U.S. Security Regulations (i.e., UNCLASSIFIED). If form contains classified information, stamp classification on the top and bottom of the page.

Block 20. Limitation of Abstract. This block must be completed to assign a limitation to the abstract. Enter either UL (unlimited) or SAR (same as report). An entry in this block is necessary if the abstract is to be limited. If blank, the abstract is assumed to be unlimited.